Real-Time Energy Management and Transient Power Control for Fuel Cell Electrified Vehicles

by

Kai Wu

A dissertation submitted in partial fulfillment
of the requirements for the degree of
Doctor of Philosophy
(Mechanical Engineering)
in The University of Michigan
2019

Doctoral Committee:

Professor Jing Sun, Chair
Doctor Tulga Ersal
Professor Ilya Kolmanovsky
Professor Huei Peng

Kai Wu

kevinwu@umich.edu

ORCID iD: 0000-0002-5694-4815

To Xiaosu Liu, for making my heart smile.

And to my parents, for their endless support and faith.

ACKNOWLEDGEMENTS

First of all, I would like to express my sincere gratitude to my advisor, Professor Jing Sun for the continuous support of my Ph.D study and related research, for her patience, motivation, and immense knowledge. She always has the highest standards and most strict requirements on my research. Her guidance has helped me throughout my research career and writing of this thesis. I could not have imagined having a better advisor and mentor for my Ph.D study. Besides my advisor, I am also grateful to the members of my committee, Professor Ilya Kolmanovsky, Professor Huei Peng and Dr. Tulga Ersal for their patience and constructive suggestions.

I would like to extend my most sincere gratitude towards the Ford Motor Company. With a special mention to Mr. Ming Kuang, who provided me an opportunity to join his team as an intern, and access the laboratory and research facilities. Without his precious support, it would not have been possible to conduct my research. I am also grateful for the following Ford staff: Dr. Miloš Milačić, Dr. Alhadi Albousefi, Dr. Benjamin Pence, Marin Assaliyski, and Dr. Handian Chen. It was fantastic to have the opportunity to work with these talented researchers and engineers.

I would also like to acknowledge the Ford Motor Company for providing the Ford-University of Michigan Alliance Project funding to support my research.

In particular, I am grateful to Professor Jeffery Cook for enlightening me to pursue a career in research and providing me with an independent study opportunity at his lab. I miss our interesting and long-lasting conversations.

I would like to thank my fellow colleagues from RACE lab: Dr. Zhenzhong Jia,

Dr. Caihao Weng, Dr. Qiu Zeng, Dr. Richard Choroszucha, Dr. Mohammad Reza Amini, Dr. Jun Hou, Dr. Ziyou Song, Dr. Dongsik Chang, Hao Wang, Nick Yang for all the stimulating discussions. I also would like to thank my friends: Dr. Xiaowu Zhang, Dr. Tianyou Guo, Dr. Ziheng Pan, Dr. Chaozhe He, Xin Ding, Zheng Liu, Wei Du for accepting nothing less than excellence from me.

And finally, last but by no means least, I would like to thank my family: my parents, Peinian Wu and Aihua Wang, for supporting me spiritually throughout my student life. I cannot overcome all the difficulties without your encouragement. And my love, Xiaosu (Shirley) Liu. You came to me like the dawn through the night. You make me want to be a better man.

TABLE OF CONTENTS

LIST OF FIGURES

Figure

LIST OF TABLES

Table

LIST OF ABBREVIATIONS

A-PMP Adaptive Pontryagin's Minimum Principle

APMP-MPC Adaptive Pontryagin's Minimum Principle - Model Predictive Control

APMP-Pre APMP with a Pre-compensator

BEV Battery Electric Vehicle

BOP Balance of Plant

CAN Controller Area Network

DP Dynamic Programming

ECMS Equivalent Consumption Minimization Strategy

EUDC Extra-Urban Driving Cycle

EV Electric Vehicle

Exp Exponential Varying

FCS Fuel Cell System

FCV Fuel Cell Vehicle

FT Frozen Time

FTP-4 Federal Test Procedure 4

FTP-75 Federal Test Procedure 75

GDE Gas Diffusion Electrode

GDL Gas Diffusion Layer

GHG Greenhouse Gas

HEV Hybrid Electric Vehicle

HIL Hardware in the Loop

HWFET Highway Fuel Economy Test

ICE Internal Combustion Engine

IM240 Inspection and Maintenance Driving Cycle

IHWY India Highway Driving Cycle

ITS Intelligent Transportation System

LA92 California Unified Cycle

MNHA Manhattan Bus Cycle

MPC Model Predictive Control

MPGe Miles Per Gallon Gasoline Equivalent

NYCC New York City Cycle

OER Oxygen Excess Ratio

PEMFC Proton Exchange Membrane Fuel Cell

PHEV Plug-in Hybrid Electric Vehicle

PMP Pontryagin's Minimum Principle

RL Reinforcement Learning

RNN Recursive Neural Network

SC03 Supplemental Federal Test Procedure-1

SDP Stochastic Dynamic Programming

SOC State of Charge

TPBVP Two-Point Boundary Value Problem

UDDS Urban Dynamometer Driving Schedule

US06 Supplemental Federal Test Procedure

ABSTRACT

Automotive OEMs have responded to energy and environmental concerns with mass-produced Hybrid Electric Vehicles (HEVs), Plug-in Hybrid Electric Vehicles (PHEVs), and Battery Electric Vehicles (BEVs) that satisfy various customers demands. While the sales volume of these vehicles continues to climb, OEMs recognize that Fuel Cell Vehicles (FCVs) could be the ultimate solution to electrification of personal transportation. Thus, they have forged ahead with developing commercial FCV technologies. However, several challenges exist in bringing Fuel Cell technology to mass production. Aside from steep costs, energy management for achieving total optimal system efficiency in real-time and under all driving conditions is still under development. There is room for improvement in controlling the transient power balance between the Fuel Cell System (FCS), high voltage battery, and driver demand, calling for a systematic framework and new tools to understand and address the FCS dynamic effects. This dissertation is devoted to providing a comprehensive framework for analyzing the dynamic effects of FCS on optimal energy management applications, and developing a hierarchical control framework for real-time energy management.

Dynamic characteristics of a Proton Exchange Membrane Fuel Cell (PEMFC) system can impact fuel economy and load following performance of an FCV, especially if these dynamics are not considered when designing the top-level energy management strategy. To quantify the effects of FCS dynamics on optimal energy management, Dynamic Programming (DP) is adopted in this dissertation to derive optimal power split strategies at two levels: Level 1, where the FCS dynamics are ignored; and Level 2, where the FCS dynamics are incorporated. Analysis is performed to quantify the

differences between these two strategies to understand the effects of FCS dynamics. The results show that ignoring slow FCS dynamics in DP can lead to several problems, including deteriorated power tracking, violation of charge sustaining performance, and loss of fuel economy.

For the FCVs with fast power dynamics, an optimization-oriented supervisory controller based on Pontryagin's Minimum Principle (PMP) is proposed. The Adaptive-PMP (A-PMP) method inherits the advantages of model-based optimization to formulate a Hamiltonian and convert the trajectory optimization problem into pointwise-in-time optimization problem, where the co-state value is estimated and adapted based on average power and total travel time. A-PMP is evaluated on a high fidelity FCV powertrain model. Comparing to the default baseline energy management method, A-PMP yields better performance in fuel economy. Furthermore, a preliminary vehicle test shows up to 5.9% of improvement in fuel economy over an OEM's rule-based strategy.

For the FCVs with slow power dynamics, an online energy management algorithm is proposed to mitigate the dynamic effects of FCS while maintaining a near-optimal fuel economy. The A-PMP-Model Predictive Control (APMP-MPC) scheme includes a top level power planning controller (A-PMP) and an intermediate level controller (MPC) to handle FCS transient dynamics. The proposed APMP-MPC is tested on an FCV powertrain model with simplified FCS dynamics. Simulation results demonstrate improvements in fuel economy on representative driving cycles under the assumption of prescient load information. Moreover, the effects of load prediction error on the APMP-MPC fuel economy performance are evaluated. Requirements on load prediction are identified to maintain the effectiveness of the proposed APMP-MPC algorithm for FCVs energy management. Finally, the sensitivity of the prediction error on fuel economy is shown to be attenuated by incorporating a rate limiter.

CHAPTER I

Introduction

1.1 Background and Motivation

Vehicle electrification is the key element of a broad portfolio for building a competitive, secure, and sustainable clean energy economy. To address the need for sustainable energy and a healthy environment, the development and application of electrified vehicles have been surging worldwide (Fig. 1.1). Electrified vehicles, such as Plug-in Hybrid Electric Vehicles (PHEVs) or Hybrid Electric Vehicles (HEVs) that use Internal Combustion Engines (ICEs) as the primary power source and high power batteries as the supplemental power source, have demonstrated better overall vehicle fuel economy compared to conventional vehicles [1, 2]. In addition to these fuel efficient vehicles, pure Battery Electric Vehicles (BEVs) that use batteries as the sole power source also play an important role in vehicle electrification [3, 4]. However, as PHEVs and HEVs still rely on traditional ICE and Electric Vehicles (EVs) are limited by charging rates and driving range, the need for clean, sustainable, and mass produced vehicles has never been greater. FCVs are considered as one of the promising solutions to electrification of personal transportation [5, 6]. FCVs use hydrogen, which is considered as zero-carbon fuel, that can be produced from renewable resources [7]. To reduce Greenhouse Gas (GHG) emissions by 80 percent of 2005 levels in the transportation sector, FCVs have the potential to dominate 50% of the

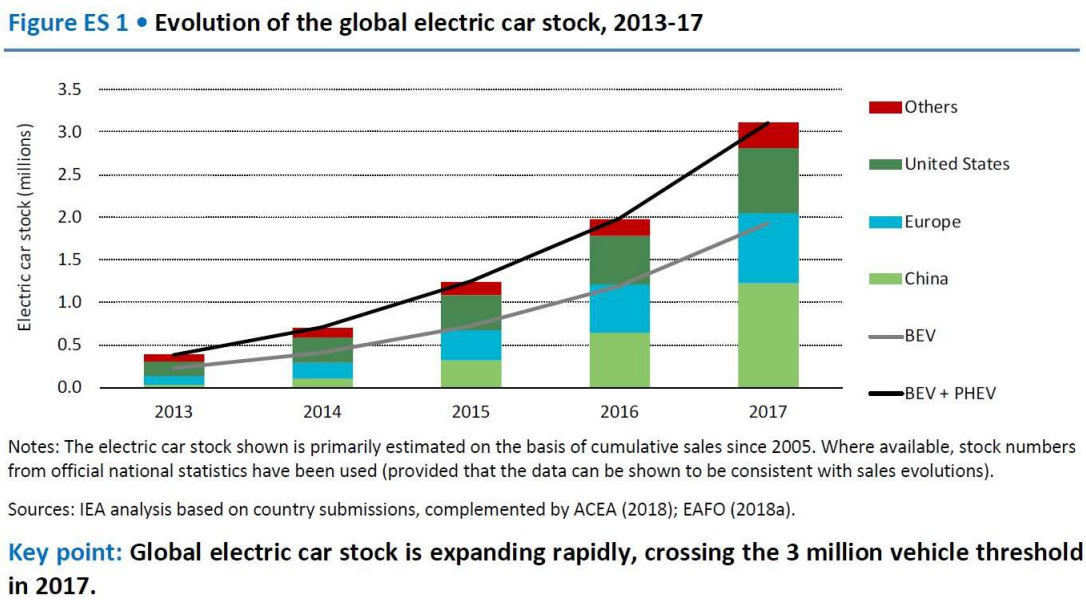

Figure 1.1: Evolution of the global electric car stock, 2013-2017 [8].

automotive market by 2050, which is shown in Fig. 1.2.

FCVs use fuel cell stacks as power generation units, which convert chemical energy into electrical energy through an electrochemical process. Among all the fuel cell types, the Proton Exchange Membrane Fuel Cell (PEMFC) is the primary candidate (Fig. 1.3) for FCVs because of its low cost, fast dynamic response capability (compared to other fuel cell technologies), and technology maturity [7, 10]. Despite these advantages, PEMFCs have limitations compared to conventional internal combustion engines, critical among which are slow dynamic properties [11]. These limitations are constraining because pushing a PEMFC to meet fast load change demands could affect the service life of an FCV. To address these limitations, most FCVs developed by automotive manufacturers are of hybrid type, for which a battery pack or other energy storage devices are integrated to complement the fuel cell operation, making FCV an HEV. To meet the stringent performance and reliability requirements of an HEV for diverse driving scenarios, a system level energy management strategy is needed to coordinate the subsystems involved and optimize system efficiency while maintaining safety, drivability and performance in terms of other vehicle attributes

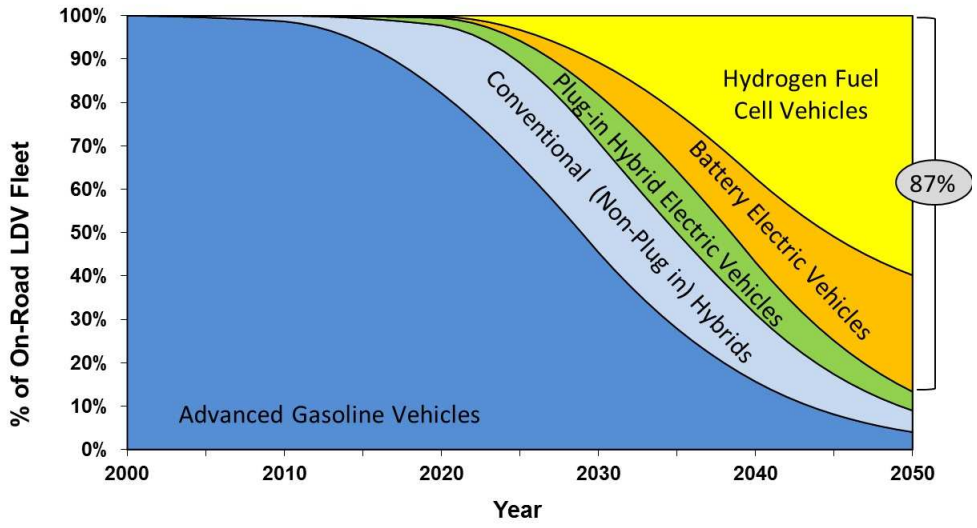

Figure 1.2: On road passenger car scenario required to reach 2050 goal [9].

[12]. Even though system level energy management strategy is well-explored for traditional HEVs, there are special challenges for FCVs: the slow transient response of the Fuel Cell System (FCS) to the change in power requests imposes a major performance limitation on drivability and fuel efficiency [14], and most likely will require predictive functions in the control strategy to mitigate the potential delays. Thus, the goal of this dissertation is to address the fundamentals of the energy management and transient power controls in fuel cell electrified powertrain applications, and to develop advanced controls that enable optimal system energy efficiency and robust powertrain operations.

1.2 General Background on FCVs

A typical fuel cell powertrain comprises an FCS, an electric energy storage system, such as a lithium-ion battery pack and an electric drivetrain, as shown in Fig. 1.4. Since the fuel cell powertrain only has electric path, it can be treated as a series HEVs. The FCS generates electricity on board for propulsion, directly impacting energy management and power balancing between supply and demand.

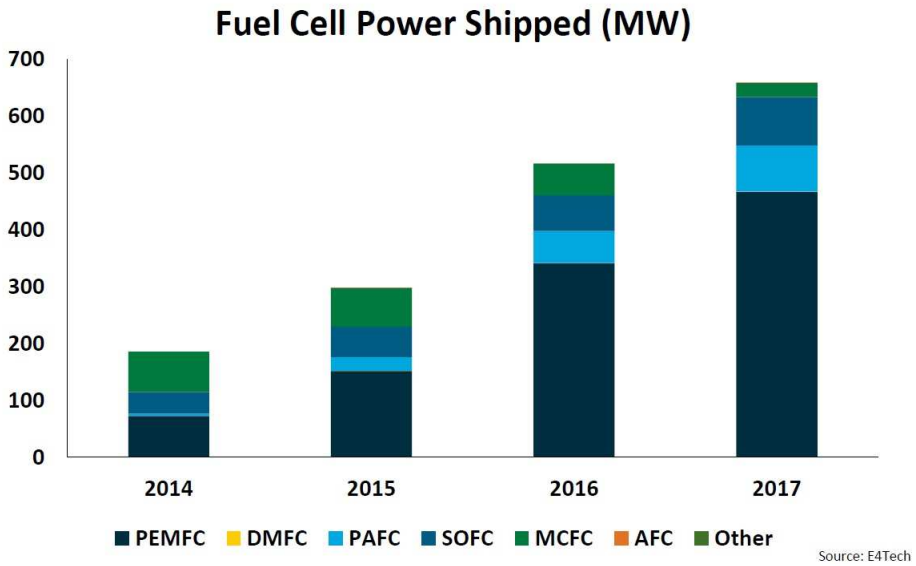

Figure 1.3: Global fuel cell power shipped growth by fuel cell types [13].

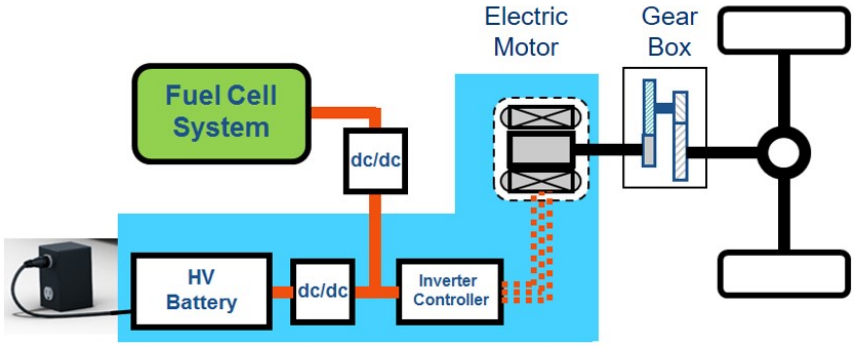

Figure 1.4: Typical fuel cell propulsion system.

An FCS for automobiles comprises a fuel cell stack and several Balance of Plant (BOP) components. As shown in Fig. 1.5 [15], the essential components of BOP required for an FCS are: (i) a compressor/blower to provide air to the cathode; (ii) a high pressure hydrogen tank to feed hydrogen into the anode; (iii) a coolant system in the stack cooling channel; (iv) a humidifier to humidify the hydrogen and the air flow.

Fuel cells can be made up of different types, and PEMFC is the primary candidate for FCVs. A PEMFC consists of an electrolyte sandwiched between two electrodes. The electrolyte has a special property that allows positive ions (protons) to pass

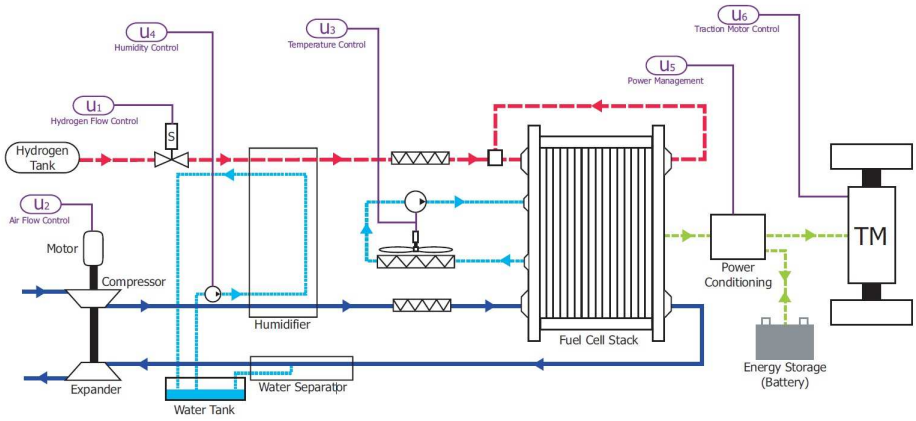

Figure 1.5: Complicated automotive fuel cell propulsion system [15].

through while blocking electrons. As hydrogen molecules pass over an electrode, the anode, they are separated into electrons and hydrogen protons with the help of a catalyst. The most commonly used catalyst employs Pt nanoparticles that are uniformly dispersed on the carbon catalyst carrier. The reaction on the anode side is:

$$H_2 \rightarrow 2e^- + 2H^+. \tag{1.1}$$

The protons (H^+) flow to the cathode side through the electrolyte while the electrons flow through an external circuit, thus generating electricity. On the cathode side, the oxygen reacts with both the hydrogen protons from the electrolyte and the electrons from the external circuit, thus producing water:

$$O_2 + 4e^- + 4H^+ \rightarrow 2H_2O. \tag{1.2}$$

Therefore, the overall reaction of the fuel cell is:

$$2H_2 + O_2 \rightarrow 2H_2O. \tag{1.3}$$

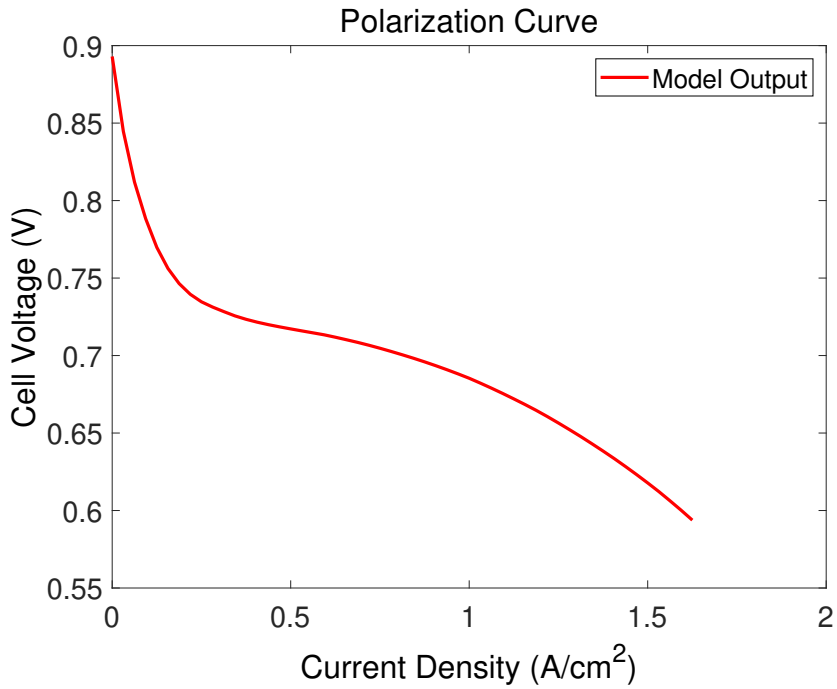

Figure 1.6: A typical fuel cell polarization curve.

The difference in potential of the anode and the cathode creates the voltage of a single cell, which ranges between 0 to 1 volts. As shown in Fig. 1.6, typical relationship under a given condition between the current drawn from the fuel cell and the cell voltage is given in the form of a polarization curve. The specific voltage depends on fuel cell operating conditions and the current drawn from the fuel cell. For example, the Oxygen Excess Ratio (OER), defined as the fuel cell oxygen input flow rate divided by the fuel cell oxygen output flow rate, has strong influence on the voltage produced, as shown in Fig. 1.7. The FCS efficiency is defined by the ratio of FCS output net power and the total consumed hydrogen heating power. The FCS efficiency combined with other subsystem efficiency, such as battery operation efficiency, motor efficiency is the key characteristics to be considered for vehicle level energy management.

The main function of the vehicle level energy management strategy is to coordinate the subsystems and optimize system efficiency while maintaining performance

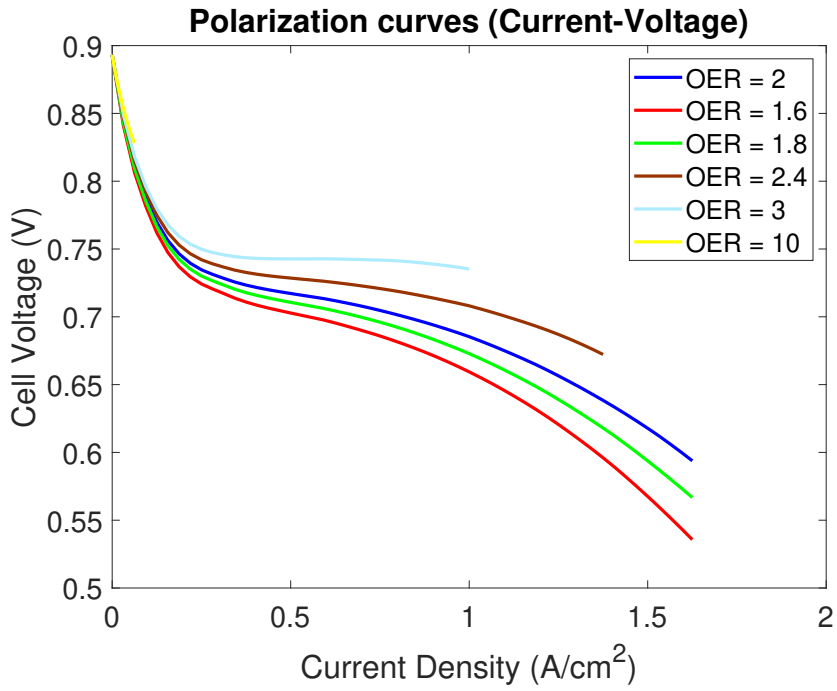

Figure 1.7: Fuel cell polarization curve under different operation OERs.

for safety, drivability and other vehicle attributes, such as charge sustaining performance. For design and performance analysis, fuel cell powertrain system modeling and optimization methodology are of great importance. This thesis will first provide a literature review on the modeling and optimization methodologies for FCVs.

1.3 Literature Review

1.3.1 Fuel Cell Vehicle Powertrain Modeling

Three main types of FCS models are found in open literature. The first is high fidelity models [16, 17, 18, 19, 20, 21, 22, 23]. These models are developed to demonstrate the physical mechanisms in the FCS, and they normally have extremely high computational costs. Weber [22] reviewed modeling of PEMFC transport, where a single fuel cell model can have different dimensions (1-D, 2-D, 3-D) depending on the level of complexity. The 1-D models comprise a detailed sandwich model through the membrane [16, 17]. The 2-D models comprise the 1-D sandwich and also include

the direction which is along the gas flow channel [20]. The 3-D models comprise all three coordinate directions [21]. The second category of fuel cell modeling has medium complexity but retains high fidelity [24, 25, 26, 27, 28, 29]. Siegel et al. [26] proposed and validated a fuel cell model which verifies the evolution of liquid water and nitrogen fronts along the length of the anode channel in a PEMFC operating with a dead-ended anode that is fed by dry hydrogen. McCain et al. [27] analyzed the controllability and observability of the liquid water distribution in the Gas Diffusion Layer (GDL) of a PEMFC using a one-dimensional channel-to-channel unit fuel cell model. Promislow et al. [28] developed a model of a PEMFC which includes slow transient effects of liquid water accumulation and evaporation in Gas Diffusion Electrodes (GDEs) and gas channels. All of the aforementioned models focus on the single fuel cell instead of the entire FCS, while the last category of low complexity models focuses on the FCS [15, 30, 31, 32] for control-oriented applications. For example, Pukrushpan et al. [15] proposed an FCS model with the necessary BOP components, including a compressor, manifolds, an air cooler, and a humidifier. Four interacting submodels, including stack voltage, cell temperature, air pressure, oxygen and hydrogen partial pressures and membrane humidity, are incorporated in the FCS model. The entire FCS has nine dynamic states and four control inputs. Tiss et al. [31] presents a non-linear state-space dynamic non-isothermal PEMFC model. This model represents the fuel cell as an equivalent circuit, which incorporates GDL, membrane and electrodes. The entire model has 18 states.

1.3.2 FCV System Level Optimization

Approaches adopted for HEV/FCV energy management in the past literature generally fall into the following two categories: heuristic control [33, 34] and optimal control [2, 35]. The former has the advantage of a simple design process supported by physical insights, but lacks analytic rigor and systematic approach for guaranteeing

optimal performance. An advantage of the latter is that it relies on an analytical or numerical process to minimize a cost function that reflects performance requirements. Although the topic of energy management for internal combustion engine based HEVs has been well explored and comprehensive results are available [2, 33, 36], there have been less studies exploring FCV energy management [11].

Dynamic Programming (DP), a numerical method for global optimization, has been used to characterize FCV optimal performance [37, 38], also known as the performance ceiling. The DP method relies on prescient knowledge of the entire driving cycle and formulates a cost function that includes fuel consumption, penalty on battery usage, and other relevant performance metrics, such as emissions [36]. This method facilitates the evaluation of the optimal design parameters, such as the number and types of clutches and modes, etc. for HEV [36] and PHEV [39]. Lin [36] and Kim [40] appear to be the first to apply DP method to FCV powertrain configuration analysis and efficiency optimization. Although the use of DP techniques have been reported, most of the studies documented in literature have overlooked the dynamics in their attempt to avoid the curse of dimensionality associated with DP [38, 40]. The quasi-static hypothesis which treats an engine or a FCS as a quasi-static element is typically used in such studies. This assumption, however, is questionable, if not invalid, because the FCS power delivery tests typically show 1 to 10 seconds of settling time and an undershoot [41, 42]. To take advantages of model-based optimization, a better understanding of the FCS dynamics effects on optimal energy management is essential. This will help determine the best energy management scheme for FCVs.

1.3.3 Real-time Energy Management for FCV

As aforementioned, there are two main categories in energy management approaches. Heuristic control approaches can be categorized as either deterministic rule-based methods or fuzzy rule-based methods. Deterministic rule-based meth-

ods use look-up tables to implement deterministic rules and are widely used in current commercialized hybrid vehicles. The advantages of the deterministic rule-based methods are the consistency with performance and implementation simplicity. One drawback, however, is that it is time consuming to calibrate optimal look-up tables. Significant efforts are required to tune the parameters in the chassis dynamometer testing process. On the other hand, the fuzzy rule-based methods have the advantage of using real-time data to determine suboptimal power split performance [43, 44]. Although having certain advantages, the fuzzy rules do not guarantee optimal performance. Most of the aforementioned heuristic control approaches are suitable for online implementation.

The implementation of optimal control methods has to address computational issues. Because of the computational complexity and the lack of full cycle information, deterministic DP is not feasible for real-time implementation [45]. To alleviate the burden of online computation [46, 47], post-processing steps, such as fitting DP results using nonlinear functions [36], or using Recursive Neural Network (RNN) [46] and Reinforcement Learning (RL) [48] to learn and replace the DP approach, have been employed to approximate the results of optimal control. Despite the advantages of these approaches, a disadvantage remains in that the typical deterministic DP-based strategies, even with post-processing methods, are driving cycle dependent. To resolve this problem, Stochastic Dynamic Programming (SDP) and driving pattern detection with multiple driving cycles have been suggested as possible solutions [49]. To represent the stochastic distribution of driver power demand [50], Markov chain models are built on the basis of real-world driving data. These methods provide near-optimal fuel economy, but with the drawback that they fall into an architecture-dependent rule development process. Other model-based control designs, such as the Pontryagin's Minimum Principle (PMP)-based [2, 51], or the Equivalent Consumption Minimization Strategy (ECMS)-based [52, 53] methods have emerged in recent

years to overcome the limitations of DP based methods. The PMP methods realize the minimization of a Hamiltonian equation, and the ECMS methods include an equivalent fuel consumption term in its optimization process based on battery usage.

The PMP-based energy management leads to a Two-Point Boundary Value Problem (TPBVP), which can be solved with shooting methods through offline computations [54]. Previous research has shown that PMP and ECMS are equivalent if a simplified co-state variable model is assumed in PMP and the equivalent consumption weighting factor are selected as a function of the constant co-state value [2, 45, 55]. While offline analysis shows that PMP or ECMS offer near-optimal fuel economy and both have low computation complexity, studies also show that the optimal co-state variable for PMP and the equivalent consumption weighting factor for ECMS are very sensitive to driving conditions [45, 51]. To address this issue, several adaptation methods have been presented [52, 54, 56, 57]. Musardo [52] proposes an on-the-fly algorithm for estimating the equivalence factor according to the driving conditions. The main idea of this approach is to periodically refresh the control parameters based on driving condition predictions from GPS information. Gu [58] presents an adaptation method that focuses on recognizing driving patterns. The past driving conditions within a time window are analyzed periodically, and then matched with one of the representative driving patterns that is associated with a certain standard driving cycle. Onori and Serrao [56, 57] present an adaptation of the equivalence factor based on feedback from the State of Charge (SOC) to compensate for the SOC variations. All of the aforementioned approaches are primarily for HEVs or PHEVs.

The difference between the FCVs and the HEVs is their primary power resource. HEVs and PHEVs use ICE as the primary power resource and it converts the chemical energy to mechanical energy first, and then it either directly delivers the mechanical energy to the driveline, or converts them to electrical energy using a generator. However, fuel cells and batteries are both electrochemical devices and have similar

efficiency maps, which do not allow for much leveraging in terms of energy efficiency optimization. The challenges of dealing with FCS slow dynamics and balancing FCS and batteries' operating conditions lead to substantial differences between conventional HEVs and FCVs, calling for efforts in developing new control strategies.

1.4 Contributions of the Dissertation

As powertrain control strategies have became more complex and sophisticated, energy management controller development and calibration have become more time-consuming and costly. This thesis aims to design a hierarchical control framework for real-time energy management to reduce the controller design and calibration efforts for the automotive industry, using model-based optimization methods. We propose a general control framework called Adaptive Pontryagin's Minimum Principle - Model Predictive Control (APMP-MPC) and evaluate the performance of this algorithm on a high fidelity powertrain model and a testing vehicle. The contributions of this work are three-fold.

The first contribution is the evaluation of the influence of FCS dynamic effects on the overall optimal fuel efficiency and battery usage. To balance the trade-offs between computational efficiency and system performance, we carried out a study, described in Chapter III, in an attempt to answer the following questions: Can the quasi-static hypothesis be used to guide the FCV energy management design without substantial loss of performance? If so, how can the strategies derived from quasi-static optimization be modified to achieve load following in the presence of FC dynamics? To this end, this thesis presents results from the study that evaluates the effects of FCS dynamics on a representative FCV using two levels of DP algorithms: Level 1, where the FCS dynamics are ignored, and Level 2, where the FCS dynamics are incorporated. While Level 1 DP policies are faster to compute, the resulting strategy leads to a load following error when applied to dynamic FCS. Two different strategies

are used to mitigate the load following error. One uses batteries and the other uses FCS. These two strategies are applied to compare the fuel economy with Level 2 DP to demonstrate and quantify the effects of FCS dynamics on the system operating strategy.

The second contribution is the development and evaluation of an optimization-oriented supervisory controller based on PMP to obtain an on-road energy management strategy, which is detailed in Chapter IV. This strategy uses travel time as the only trip information to achieve charge sustaining performance. Using a simple powertrain model to design A-PMP and implementing it on a high fidelity powertrain model, improved performance is demonstrated compared to the proprietary baseline control strategy. Furthermore, the calibration process time is reduced. The proposed algorithm has been validated through both Hardware in the Loop (HIL) and vehicle tests. The application of the algorithm reveals a potential for improvements in fuel economy using the A-PMP versus the default rule-based control method.

The last contribution is the evaluation of a novel hierarchical control structure to mitigate the effects of FCS dynamics. The proposed control algorithm is tested on an FCV powertrain model with simplified FCS dynamics. The effects of load prediction error on the fuel economy performance are also evaluated. Additionally, reducing the effects of prediction error, such as rate load limiter, should also be considered. DP methods are extended to include rate limitation to evaluate the effects of load changing rate on the optimal fuel economy. Moreover, the effects of load changing rate on APMP-MPC methods are also be evaluated. All results are described in Chapter V.

1.5 Outline

This thesis addresses the design of real-time energy management schemes to mitigate the dynamics effects of FCS. The thesis is organized as follows:

Chapter I is an introduction that includes literature review on the FCV energy management.

Chapter II presents control and optimization-oriented models for FCS dynamic effects analysis and real-time energy management algorithm design. Level 1 and Level 2 FCS models are described and the associated powertrain models are detailed.

Chapter III describes the detailed FCV energy management problem formulation. It presents and analyzes the Level 1 DP results, where the fuel cell dynamics are ignored in the DP formulation, and the Level 2 DP results and analysis, where the fuel cell dynamics are included. Finally, the chapter addresses the question raised in Chapter I, namely whether the quasi-static hypothesis can be used to guide the FCV energy management design without substantial loss of performance.

Chapter IV details the design of a novel optimization-oriented supervisory controller, referred to as A-PMP for FCVs. An approach for estimating the optimal value of the co-state variable is developed by studying the standard and synthesized driving cycles. Minimal trip information is needed to implement the proposed algorithm online. The proposed A-PMP is demonstrated on a high fidelity model and shows near-optimal fuel economy with desired charge sustaining performance. The proposed A-PMP algorithm is compared with the DP and PMP-based solutions in the simulation environment. It is also compared with a rule-based method on the high-fidelity powertrain model. Finally, this chapter describes the implementation of A-PMP on a testing FCV and presents the preliminary results of the fuel economy comparison with a baseline algorithm.

Chapter V presents the proposed hierarchical control scheme for handling the FCS dynamics. Model Predictive Control (MPC) is used to solve constrained optimization problems. Prescient MPC results are initially presented to demonstrate the advantage of the proposed APMP-MPC algorithm. Different load predictors for APMP-MPC based energy management are presented and compared. The sensitivity

analysis of the prediction error on fuel economy is performed. Additionally, a rate limiter is incorporated into the energy management design to evaluate the effects of load changing rate on the optimal fuel economy.

Chapter VI draws the conclusions and presents future work of the research on real-time energy management for FCVs.

CHAPTER II

Control and Optimization-oriented Models

Powertrain models are required for solving the energy management problem. This chapter describes the control-oriented and optimization-oriented models that are used in the following chapters to perform FCS dynamic effects analysis and real-time energy management algorithm design.

2.1 FCV Powertrain System Description

Different topologies of FCVs have been described in the available literature, and a detailed review can be found in [59, 60]. The powertrain system configuration adopted in this study is shown in Fig. 2.1. The FCS is the primary energy source in the vehicle that supplies electric energy to the voltage bus. A boost DC/DC converter is included to step up the voltage from the FC. The powertrain also has high voltage batteries, similar to HEVs. A buck-boost converter is employed to provide the bi-directional charging/discharging of the battery. The system level power management block manages power split across different power sources abiding by its rules. Our current work ignores the dynamics and control of the DC/DC converters, due to their fast dynamics compared to FCS.

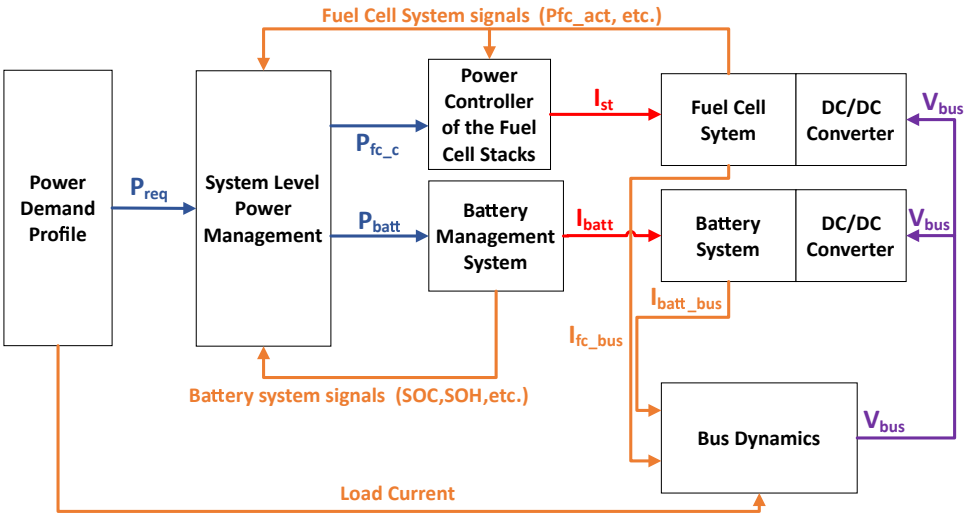

Figure 2.1: Hybrid fuel cell powertrain and its power management systems.

2.2 Fuel Cell System Model

An FCS, updated with recent experimental data, is selected as a representative FCS model for analyzing the dynamic effects of FCS. The FCS is the primary power source that converts chemical energy from hydrogen to electric energy for vehicle operation. The FCS efficiency is defined as

$$\eta_{fcs} = \frac{P_{fc\_o}}{Q_{LHV}^{H_2} W_{H_2}}, \tag{2.1}$$

where P_{fc_o} is the FCS output power, $Q_{LHV}^{H_2}$ is the lower heating value of hydrogen, and W_{H_2} is the hydrogen mass consumed, which can be calculated as

$$W_{H_2} = \frac{I_{st} n_{cell} M_{H_2}}{2F}, \tag{2.2}$$

where I_{st} is the FCS stack current, which can be calculated from P_{fc_o}, n_{cell} is the number of cells in the stack, M_{H_2} is the molar mass of hydrogen, and F is the Faraday constant [38]. An experimental FCS efficiency map is shown in Fig. 2.2. This map is generated under the normal operation condition, where the temperature and humidity

are set to be constant and the OER value is tuned to extract the highest efficiency of the stack.

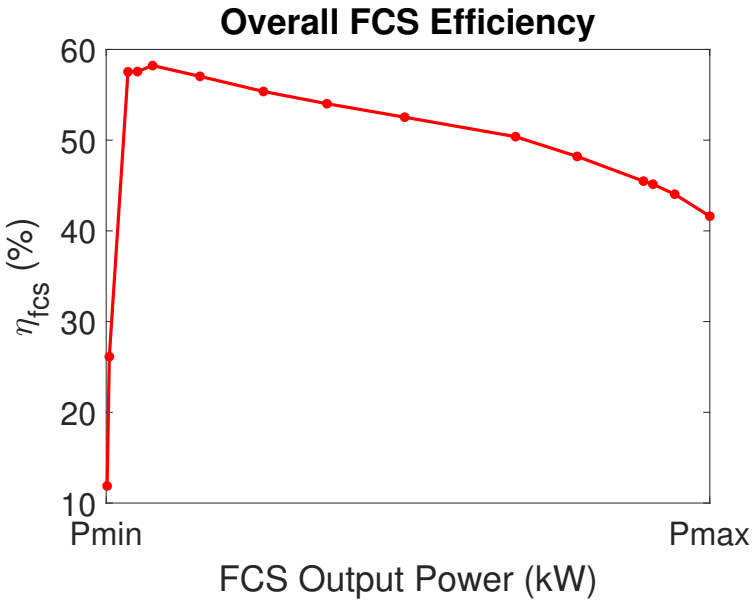

Figure 2.2: Fuel cell system efficiency map.

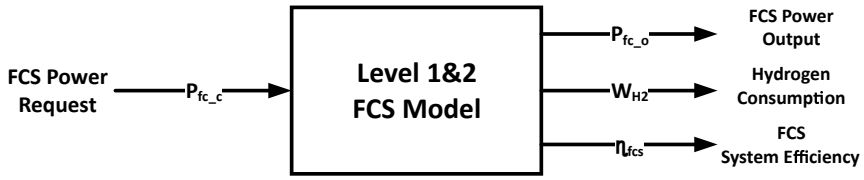

Figure 2.3: FCS model diagram.

It may be reasonable to hypothesize that more complex high fidelity models, which are based on physical principles and do not contain many parameters to fit equations from experimental data, are more suitable for design. However, they incur more computational burden compared to the less complex models. To reduce the computational complexity, a quasi-static model is adopted as Level 1 FCS model in the energy management strategy for FCVs in [40, 51, 61]. For Level 1 FCS model, FCS dynamics are not included in the problem formulation, and a quasi-static approximation is used to represent the fuel cell output power as a function of the net current I_{st}. The fuel consumption of the system is defined by the efficiency and power output

relation given by equations (2.1), (2.2) and Fig. 2.2. As shown in Fig. 2.3, the input of this model is the FCS power request P_{fc_c}, the outputs are the actual output power P_{fc_o}, the hydrogen consumption W_{H_2}, and the FCS efficiency η_{fcs}. Since the model is quasi-static, the power should be balanced:

$$P_{fc\_o}(t) = P_{fc\_c}(t), \tag{2.3}$$

where $P_{fc\_c}(t)$ is the requested power from the FCS at time t, and $P_{fc\_o}(t)$ is the power delivered to the powertrain at time t. To better understand and validate if the static model is sufficient for designing an energy management algorithm, we refer to an FCV model which uses this simple quasi-static model for an FCS as a Level 1 FCV powertrain model. For Level 2 FCV powertrain model, the fuel cell dynamics will be represented as a non-minimum phase first order Linear Time Invariant (LTI) system, which has the state-space representation of:

$$\dot{P}_{fc\_n}(t) = AP_{fc\_n}(t) + BP_{fc\_c}(t), \tag{2.4}$$

$$P_{fc\_o}(t) = CP_{fc\_n}(t) + DP_{fc\_c}(t), \tag{2.5}$$

where the requested power from FCS, P_{fc_c}, is the input, the actual power to the powertrain, P_{fc_o}, is the output, P_{fc_n} is the FCS dynamic state and A,B,C,D are the state, input, output, and feedthrough matrix, respectively. As shown in Fig. 2.4, a standard FCS uses a compressor to deliver air, thus the slow dynamics associated with the compressor will result in a large time constant in power delivery [62]. In addition, since the power used to run the compressor is taken out of the fuel cell, the overall FCS power response can exhibit non-minimum phase behavior. To address this issue, a more realistic FCS model should account for the dynamics of the compressor along with the flow dynamics. Such a model, including compressor motor dynamics and relative flow dynamics, is referred to as a Level 2 FCS model. The associated

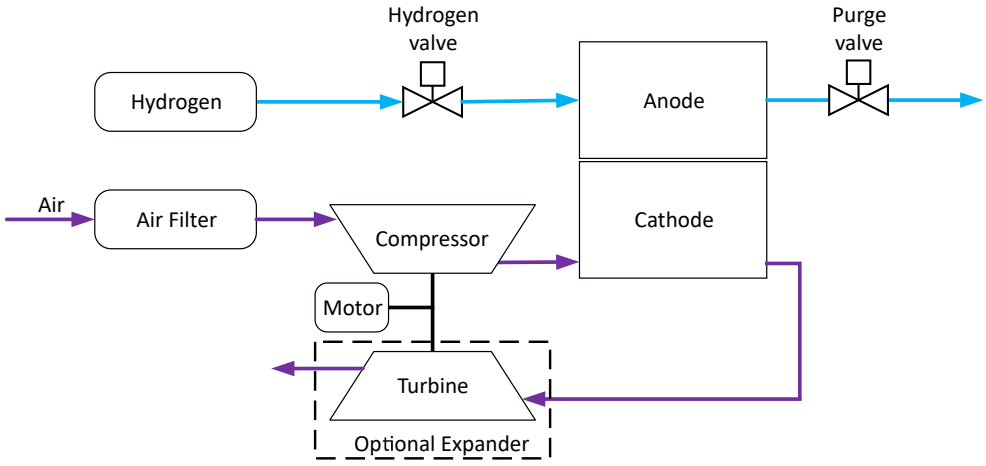

Figure 2.4: Simplified fuel cell system.

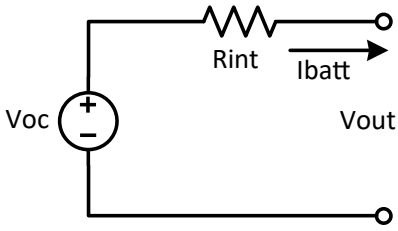

Figure 2.5: One resistance battery model.

powertrain model is called Level 2 powertrain model in this thesis.

2.3 Battery Model

The battery system consists of many cells, with each battery cell modeled as a voltage source in series with a resistance [40]. This one-state battery model is an equivalent circuit model with a voltage source and an internal resistance, which is shown in Fig. 2.5. Power provided by the battery P_{batt} depends on the current I_{batt} drawn from the battery system, and can be calculated as

$$P_{batt} = V_{oc} I_{batt} - I_{batt}^2 R_{int}, \tag{2.6}$$

where V_{oc} is the open circuit voltage of the battery pack and R_{int} is the battery's total internal resistance. Both of the variables are functions of the SOC. The battery

SOC could be calculated using Coulomb counting [63] as:

$$S\dot{O}C = -\frac{I_{batt}}{Q_{batt}}, \tag{2.7}$$

$$= -\frac{V_{oc} - \sqrt{V_{oc}^2 - 4P_{batt}R_{int}}}{2R_{int}Q_{batt}}, \tag{2.8}$$

where Q_{batt} is the battery total capacity, and (2.6) is used in deriving the second equation. In this dissertation, two different battery packages are used. One is based

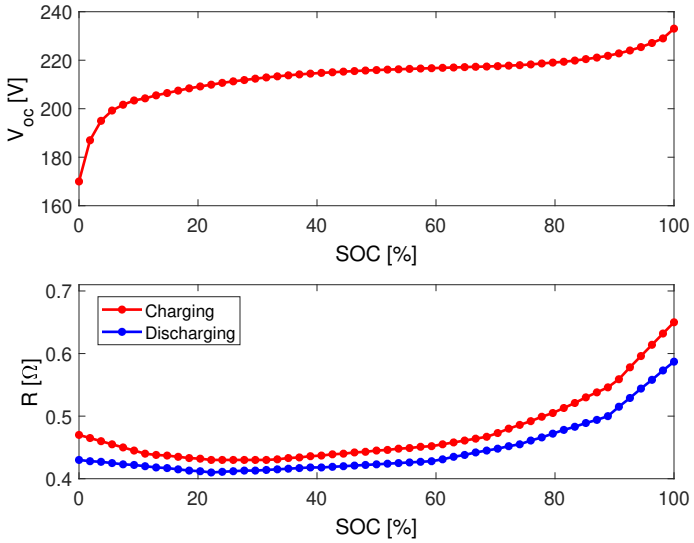

Figure 2.6: Prius battery open circuit voltage and charging/discharging resistance vs. SOC. [64]

on the third generation Prius hybrid vehicle [64], which is used for FCS dynamic effects analysis in Chapter III. The other battery package is adopted from a proprietary high fidelity powertrain model, which is used in Chapter IV.

The Prius battery is a nickel-metal hydride battery with a capacity of 6.5 Ah. Fig. 2.6 illustrates the battery open circuit voltage, as well as the battery charging and discharging resistance as functions of SOC. All of the parameters of the batteries use room temperature and thermal dynamics are ignored in this case.

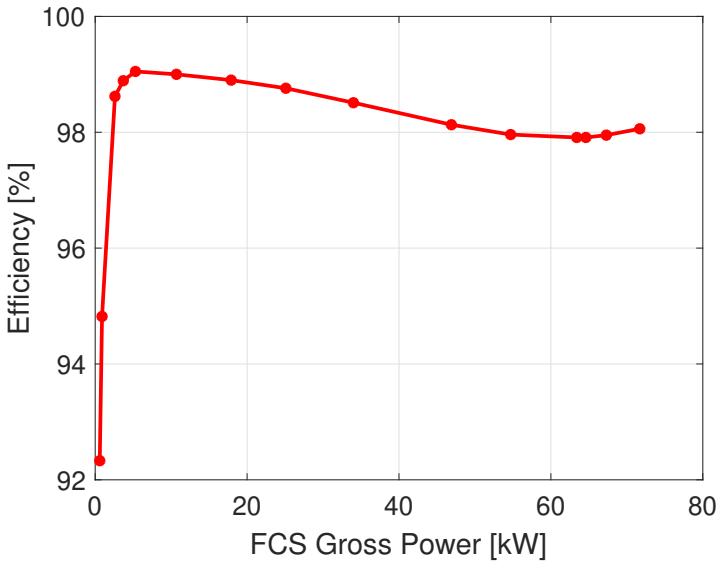

Figure 2.7: FCS DC/DC converter efficiency.

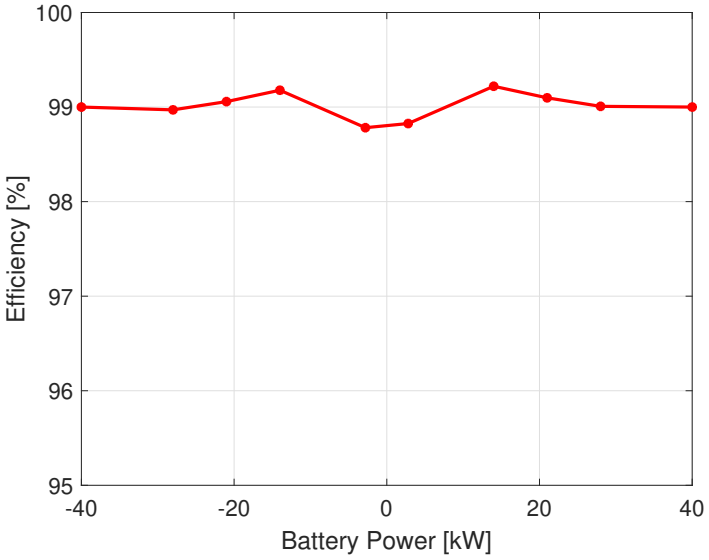

Figure 2.8: Battery DC/DC converter efficiency.

2.4 DC/DC Converter Model

Both of the DC/DC converters are described as static devices due to their fast dynamic response. The efficiency is related to the requested power. The data is updated based on the same proprietary high fidelity powertrain model, which is demonstrated in Fig. 2.7 and Fig. 2.8.

2.5 Load Profile Model

Our case studies are performed using a 2016 Ford Fusion, equipped with FCS, hydrogen storage and a lithium-ion battery pack. Given the vehicle speed profile $v(k)$, the power request, P_{req}, is then calculated as:

$$P_{req}(k) = v(k)\{m\dot{v}(k) + (F_0 + F_1 v(k) + F_2 v(k)^2)\}, \tag{2.9}$$

where the F-terms in (2.19) are used to capture the forces affecting the vehicle motion. Their values are listed in Table 2.1.

Table 2.1: Vehicle model parameters.

Mass (m)	1928 kg
F_0	32.50
F_1	0.1797
F_2	0.02144

In Chapter III, regenerative braking is not addressed. The road grade is also assumed to be zero to simplify the calculations. Four representative cycles—New York City Cycle (NYCC), Highway Fuel Economy Test (HWFET), two Supplemental Federal Test Procedure (Supplemental Federal Test Procedure-1 (SC03) and Supplemental Federal Test Procedure (US06))—whose speed and acceleration characteristics are summarized in Table 2.2, are used to perform quantitative analysis. These four cycles

cover the range from low speed city driving (NYCC) to high speed aggressive highway driving (US06).

Table 2.2: Four representative driving cycle characteristics.

Cycle	NYCC	HWFET	SC03	US06
Average Acc. power (kW)	1.97	10.41	5.27	16.73
Max Acc. power (kW)	32.2	32.4	52.9	100.23
Top speed (mph)	27.7	59.9	54.8	80.3
Average speed (mph)	7.1	48.3	21.6	48.4
Duration (s)	598	765	596	601
Distance (miles)	1.18	10.26	3.6	8.01

However, a realistic load profile should consider all the sub-components' losses, including those occurred in driveline, transmission, and traction motor. Furthermore, the regenerative braking energy cannot be directly calculated from the brake energy, as only a portion of the brake energy can be recuperated and the rest is dissipated. The analysis of the regenerative braking efficiency, as well as the power loss of vehicle dynamics, are beyond the scope of this study. In order to have more realistic load profiles, the driving cycle load profiles used in Chapter IV are obtained from a high fidelity powertrain model. The updated load profiles including realistic regenerative braking energy of the four standard driving cycles are shown in Fig. 2.9.

2.6 Summary

In this chapter, the control- and optimization-oriented models are developed to capture the key dynamics of an FCV vehicle in order to provide an essential tool for the following analysis and real-time energy management algorithm design. The FCS power dynamics model is simplified into a static model (Level 1) and a first order LTI model with non-minimum phase (Level 2). The battery model is a 1 R model with two types of characteristics data. The DC/DC model is a static model with a look

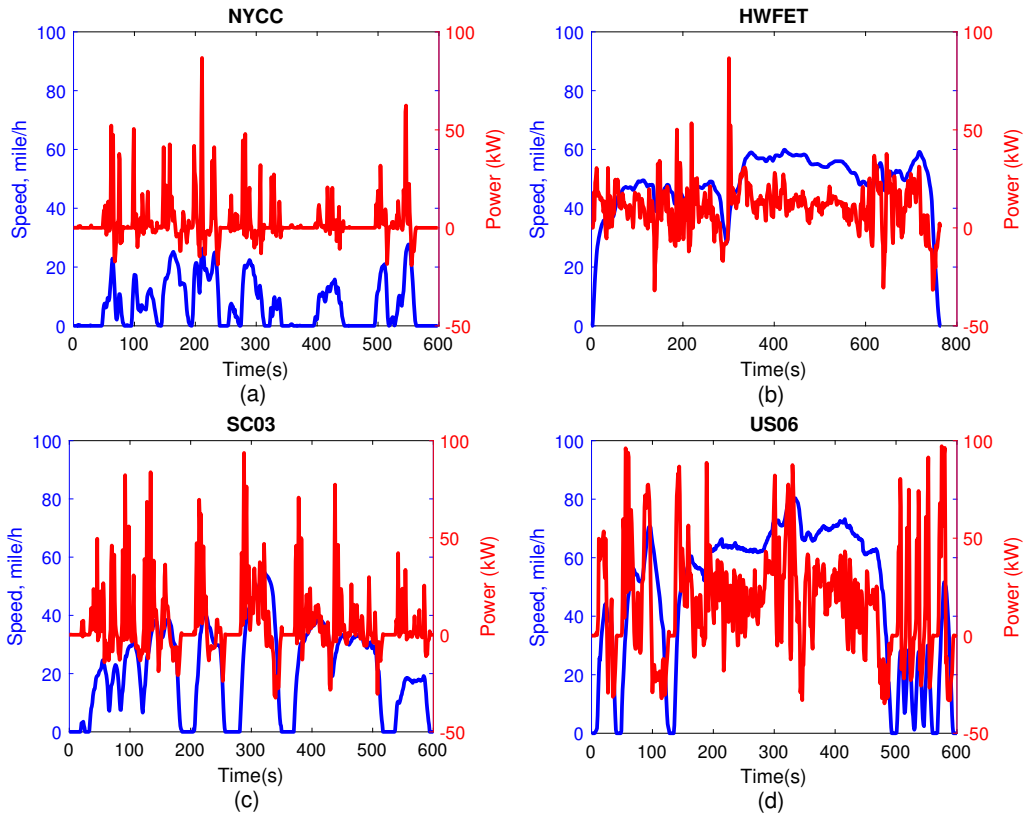

Figure 2.9: Load profile of four standard driving cycles: (a) NYCC, (b) HWFET, (c) SC03, (d) US06.

up table as the efficiency map.

CHAPTER III

Dynamics Effect Analysis of Fuel Cell System on Optimal Energy Management

This chapter investigates the effects of FC dynamics on FCV performance. An evaluation framework based on global optimization method is proposed, and the problem formulation and framework for Level 1 and Level 2 DP are summarized in Fig. 3.1 and Fig. 3.2. Two different FCS models are used as described in Section 2.2: Level 1 FCV powertrain without FCS dynamics, and Level 2 FCV powertrain with 1^{st} order LTI dynamics. The optimal energy management problem formulation is detailed and Level 1 DP and Level 2 DP are used to evaluate and compare the optimal power management strategies on the four given driving cycles with different dynamics assumptions. By directly comparing the outputs of Level 1 and Level 2 DP, differences between the control strategies can be further analyzed and understood.

3.1 Optimal Energy Management Problem

In general, the energy management problem in a hybrid vehicle can be cast as an optimization problem over a finite time horizon [65]. The goal is to find the sequence

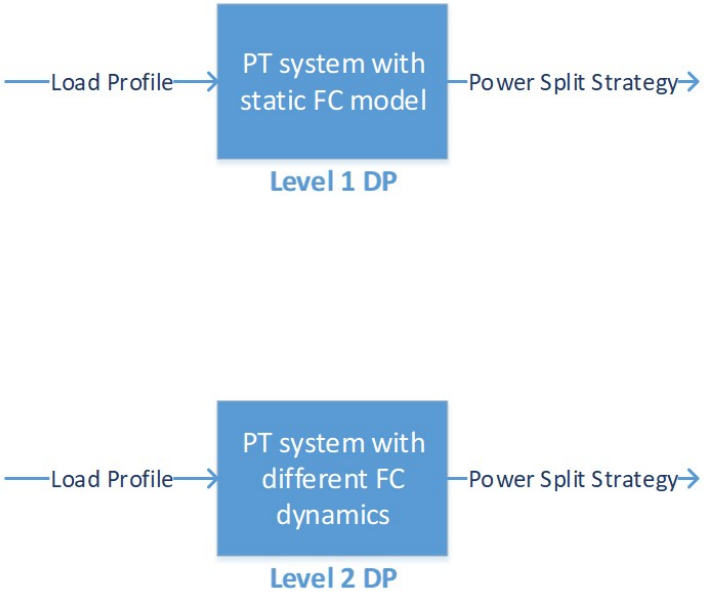

Figure 3.1: Scheme of Level 1 and Level 2 DP.

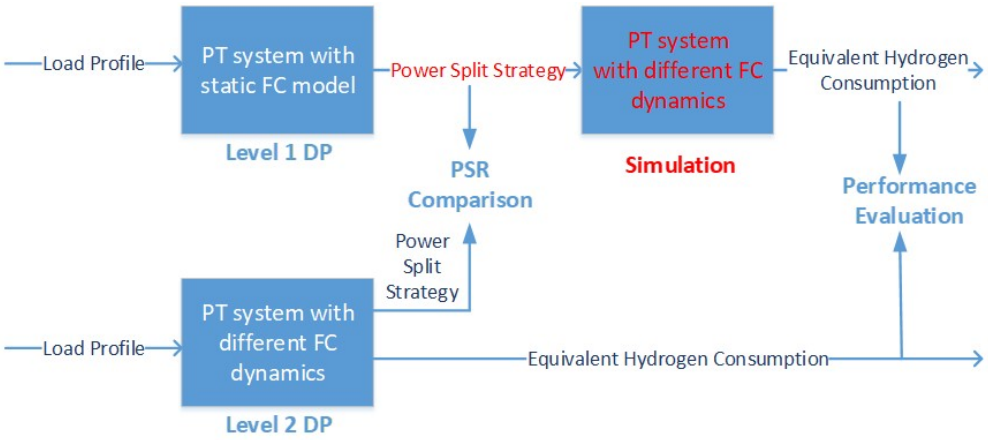

Figure 3.2: Evaluation framework for Level 1 and Level 2 DP.

of controls $u(k)$ that minimizes the cost function $J(x(k_0), u(k), x(k_N))$, defined as:

$$J(x(k_0), u(k), x(k_N)) = \sum_{k=1}^{N-1} W_{H_2}(k) + \alpha \Delta SOC_N{}^2, \tag{3.1}$$

where k represents the index of sampled data, $u(k)$ is the control action, which is the requested power from FCS, $x(k)$ is the system states which differ in Level 1 and Level 2 DP formulations, $[k_0, k_N]$ is the optimization horizon, $W_{H_2}(k)$ is the instantaneous hydrogen consumption, ΔSOC_N is the terminal cost (the difference between the initial state value SOC_0 and terminal state value SOC_N) and α is the terminal cost weighting factor. The optimization will be subject to the following constraints: system dynamics, initial state value, instantaneous state limitations and instantaneous control limitations [2], which are explained in detail in the following subsections.

3.1.1 Level 1 DP

Considering SOC as the only state variable $x(k)$, the following discrete-time nonlinear system

$$SOC(k+1) = SOC(k) - \frac{V_{oc}(k) - \sqrt{V_{oc}^2(k) - 4P_{batt}(k)R_{int}(k)}}{2R_{int}(k)Q_{batt}}\Delta t, \tag{3.2}$$

is discretized from (2.8) where Δt is the sampling time. $P_{fc\_c}(k)$ as the requested power from FCS is the only control variable. Since FCS dynamics are ignored in Level 1 DP, this approach treats the fuel cell as a static map:

$$P_{fc\_o}(k) = P_{fc\_c}(k), \tag{3.3}$$

To ensure the safe and smooth operation of the powertrain, the following inequality constraints are imposed:

$$P_{fc\_cmin} \leq P_{fc\_c}(k) \leq P_{fc\_cmax} \tag{3.4}$$

$$P_{battmin} \leq P_{batt}(k) \leq P_{battmax} \tag{3.5}$$

$$SOC_{min} \leq SOC(k) \leq SOC_{max} \tag{3.6}$$

We also impose one equality constraint for the optimization problem so that the power demands at each sampling time are met:

$$P_{batt}(k) = P_{req}(k) - P_{fc\_o}(k), \tag{3.7}$$

where $P_{req}(k)$ is the requested power. By combining equations (3.2),(3.3),(3.7), the system dynamics associated with the control variable $P_{fc\_c}(k)$ are represented by:

$$SOC(k+1) = SOC(k) - \frac{V_{oc}(k) - \sqrt{V_{oc}^2(k) - 4(P_{req}(k) - P_{fc\_c}(k))R_{int}(k)}}{2R_{int}(k)Q_{batt}}\Delta t. \tag{3.8}$$

3.1.2 Level 2 DP

In Level 2 DP, a new state variable, $P_{fc\_n}(k)$, named FCS dynamic state, is introduced. The system dynamic equation 3.8 is expanded as:

$$SOC(k+1) = SOC(k) - \frac{V_{oc}(k) - \sqrt{V_{oc}^2(k) - 4(P_{req}(k) - P_{fc\_c}(k))R_{int}(k)}}{2R_{int}(k)Q_{batt}}\Delta t, \tag{3.9}$$

$$P_{fc\_n}(k+1) = (1 + A\Delta t)P_{fc\_n}(k) + \Delta t B P_{fc\_c}(k), \tag{3.10}$$

$$P_{fc\_o}(k) = CP_{fc\_n}(k) + DP_{fc\_c}(k), \tag{3.11}$$

where (3.9) is the same as (3.8), and (3.10) and (3.11) are the discrete-time form of (2.4) and (2.5). $P_{fc\_n}(k)$ is the current value of FCS dynamic state, $P_{fc\_o}(k)$ is the current output power of FCS. The values of the parameters are identified through experimental data. The inequality constraints (3.4)-(3.6) and the equality constraint (3.7) are also employed in Level 2 DP optimization.

Our goal is to quantify the performance differences resulting from these two different DP formulations. For computational efficiency, it would be desirable to use Level 1 DP. Thus, our objective also includes establishing the feasibility of using Level 1 DP in lieu of Level 2 DP, and closing the performance gap with a properly designed load compensation strategy.

3.2 Level 1 DP Results and Evaluation

3.2.1 Level 1 DP Results (Baseline Performance)

This section presents the results from the Level 1 DP optimization to provide a baseline for our dynamic effect analysis. The grid size of the control input (P_{fc_c}) and the state variable (SOC) are set to be 0.25 kW and 0.2%, respectively. The initial and final SOC are set to be 0.5. A soft constraint is also included to prevent SOC from over discharging. Terminal cost α is set to 50000 to assure a sufficiently small ΔSOC. Even with a large α, DP may return a non-zero ΔSOC. This deviation of SOC can be converted to equivalent hydrogen consumption when evaluating the fuel efficiency by using:

$$W_{Batt\rightarrow H_2} = \frac{-\Delta SOC \cdot E_{batt}}{\eta_{fcs}\eta_{Batt}\eta_{BDC}\eta_{FCC}Q_{HHV}^{H_2}}, \tag{3.12}$$

where E_{batt} is the battery capacity (kWh), η_{Batt} is the battery charging efficiency, η_{BDC} is the battery DC/DC efficiency, η_{FCC} is the FCS DC/DC efficiency, both of the DC/DC efficiency is assumed to be 1 in the current study.

The Level 1 DP results of all four driving cycles are shown in Table 3.1. H_{2e}(g) is the equivalent hydrogen consumption, which indicates the amount of hydrogen consumed in the corresponding driving cycle. The second value Miles Per Gallon Gasoline Equivalent (MPGe), calculated as:

$$MPG_e = MPkg_{H2} * GGE \tag{3.13}$$

where $MPkg_{H2}$ is the hydrogen consumption defined as mile per kilogram hydrogen, GGE is gasoline gallon equivalent and equals to 1.011 in our case, which means 1.011 kg of hydrogen is equivalent to one gallon of gasoline in terms of energy content.

Table 3.1: Level 1 DP results for different cycles.

Driving Cycle	H_{2e}(g)	MPG_e^1
NYCC	17.37	68.92
HWFET	118.43	87.61
SC03	47.35	76.96
US06	157.69	51.40

[1]Level 1 DP, formulated in (2.8),(2.11)-(2.15) can be solved very efficiently. The computation time is less than 1 minute for each cycle by using an eight core Intel Xeon CPU with 3.40 GHz and 16 GB RAM.

3.2.2 Level 1 DP Evaluation

To analyze the effects of FCS dynamics on energy management performance, we feed Level 1 DP power split results into the powertrain system with different FCS dynamics. The goal of this evaluation is to quantify the impact of FCS dynamics in power delivery. The FCS dynamics are represented by three non-minimum phase first order LTI systems with different settling times. The settling time is defined as the time required for the response to reach and stay within a range of 2% of the final value. The values of the settling times are set to be 1s, 5s and 8s. They are based on the observation of experimental results, which are shown in Fig 3.3. As indicated

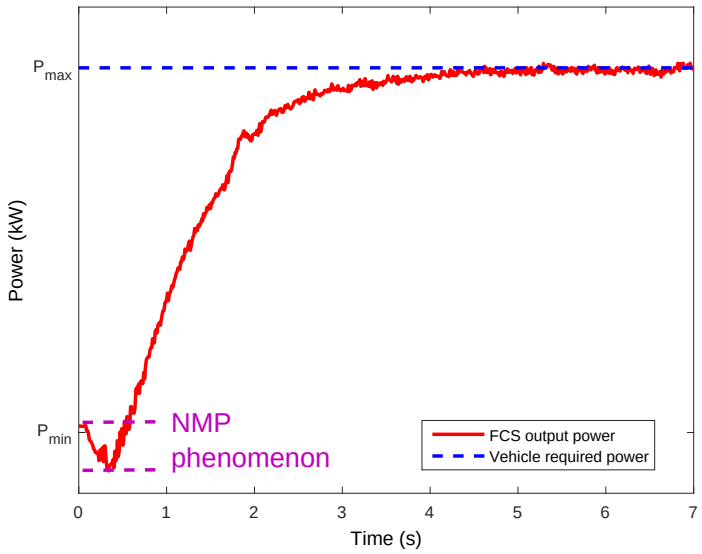

Figure 3.3: Experimental FCS power response.

by Fig. 3.4, ignoring FCS dynamics in DP formulation leads to a power tracking error when the power split strategy is applied to FCS with dynamics. The power tracking error, which can be as large as 10 kW, depending on the driving conditions and FCS dynamics. RMS power tracking error, P_{err}, using Level 1 DP power split strategy for dynamic FCS without battery compensation, are shown in the bottom left plot of Fig. 3.5. An RMS power tracking error as large as 8 kW power is seen on US06 cycle. To meet the drivability requirements, power tracking error has to be mitigated. The performance degradation is quantified by the percentage change of the MPG_e resulted from applying Level 1 DP to FCS with dynamics and with load correction over the baseline MPG_e. The fuel economy decreases with the increase of FCS time constant as expected. Although the sensitivity of fuel economy is not very pronounced for mild driving cycles, it could be significant for more aggressive cycles (0.95% for HWFET; 7.48% for US06). This provides the motivation to include FCS dynamics in designing power split strategy.

3.2.3 Mitigating Power Tracking Error

Power tracking error can be mitigated using battery, which is the conventional method for reducing error to maintain drivability. The performance is evaluated and shown in four subplots of Fig. 3.5. Since battery power is used to compensate for the power tracking error, substantial changes in the SOC will be resulted as a consequence of applying Level 1 DP strategy to dynamic FCS, as shown in Fig. 3.5(b). As much as 16% of the SOC change is seen in the US06 test, thereby violating charge-sustaining requirements. The Fig. 3.5(d) shows the RMS power tracking error, P_{err}, using Level 1 DP power split strategy for dynamics FCS with battery compensation. The power tracking error can be fully compensated using battery on NYCC and HWFET cycle, but not for the SC03 and US06 cycle because the maximum of battery output power is reached, leading to loss of drivability. In summary, ignoring FCS dynamics in DP can lead to several problems, including deteriorated power tracking (drivability), violating charge sustaining, and loss of fuel economy.

3.3 Level 2 DP Results and Comparison

3.3.1 Level 2 DP Results

The DP problem of (3.1), using (3.9)-(3.11) as the underlying system dynamics, is solved for the same four driving cycles and different dynamics. The results on HWFET are shown in Fig. 3.6 for the settling time of FCS power dynamics equals 5 s. To capture the dynamics, the sampling time of Level 2 DP algorithm is set to 0.1s. The grid size of the new FCS dynamic state is set to be 0.25 kW. The differences between the Level 1 evaluation (using the battery as compensation) and Level 2 DP are summarized in Table 3.2, where the performance improvement is defined as the percentage increase of Level 2 DP MPG_e over Level 1 DP MPG_e. For example, if the FCS has slow dynamics with a settling time of 8s, then the fuel economy of Level

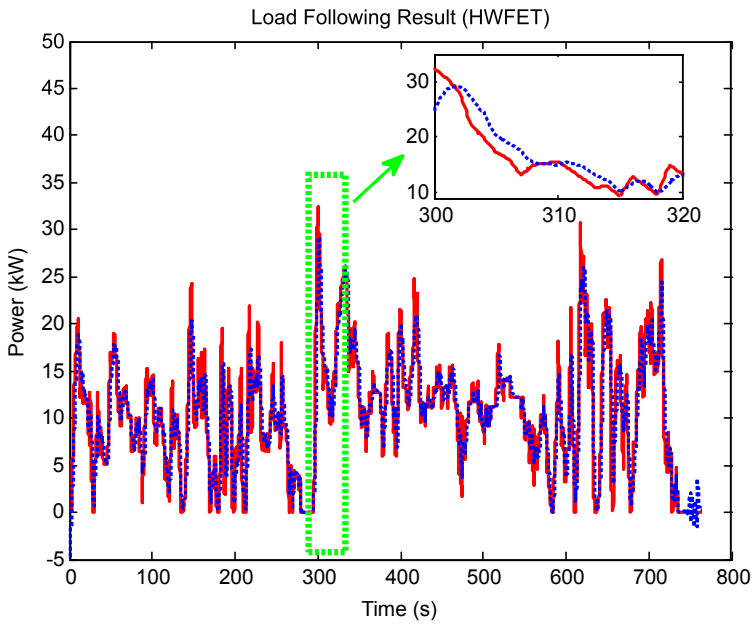

Figure 3.4: Power tracking result for HWFET. Directly implementing Level 1 DP power split strategy to powertrain system with FCS dynamics, the settling time is set to be 5 s.

2 DP for the NYCC driving cycle returns 68.37 MPG_e, while the fuel economy of Level 1 DP returns 64.64 MPG_e, giving a 5.45% improvement. The effects of FCS dynamics are less significant as FCS dynamics become faster, however. For instance, only 0.6% improvement can be identified with FCS having settling time equal to 1 second.

To provide more insights on the performance improvement of Level 2 DP, energy flow chart of Level 1 and Level 2 DP results for HWFET are shown in Fig. 8. Based on the current FCV configuration, the main reason for decreased system overall efficiency is the battery thermal loss. Level 1 DP with battery as the compensation wastes 111 kJ (while Level 2 DP only losses 30 kJ), translating to 0.84% disadvantage in overall powertrain system efficiency, even though the FCS efficiency is slightly higher in Level 1 DP case. The physical reason is that frequent large current charging and discharging is required to compensate for the power tracking error caused by slow

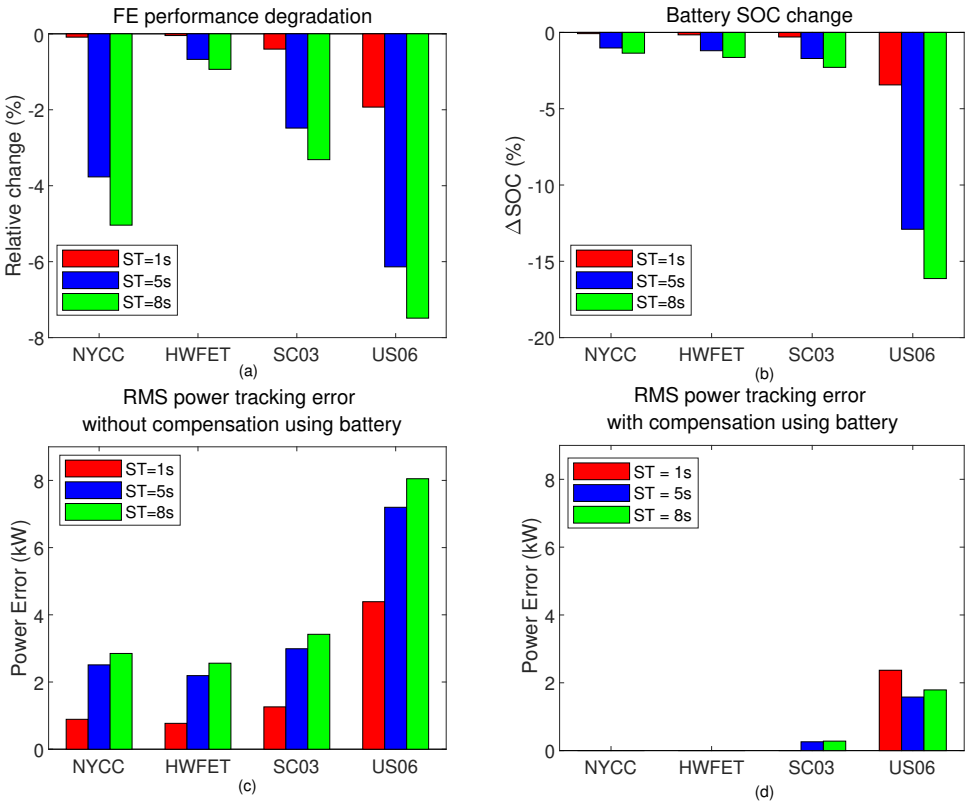

Figure 3.5: Level 1 DP evaluation for four different cycles: (a) Fuel economy comparing with Level 1 DP. (b) Charge sustaining performance. (c) RMS power tracking error without compensation using battery. (d) RMS power tracking with compensation using battery.

Table 3.2: Performance improvement (MPG_e) of Level 2 DP over Level 1 DP using battery for compensating power tracking error.

Driving Cycle \ Settling Time	ST=1s	ST=5s	ST=8s
HWFET	0.1%	0.45%	0.85%
NYCC	-0.2%[1]	4.12%	5.45%
SC03	0.6%	2.62%	3.38%
US06	0.6%	3.6%	3.29%

[1] The performance of Level 2 DP depends on the grid size accuracy. The discretization error may affect Level 2 DP more than Level 1 DP and cause its fuel economy to be worse than Level 1 DP when FCS dynamics are fast and driving cycle condition is not aggressive.

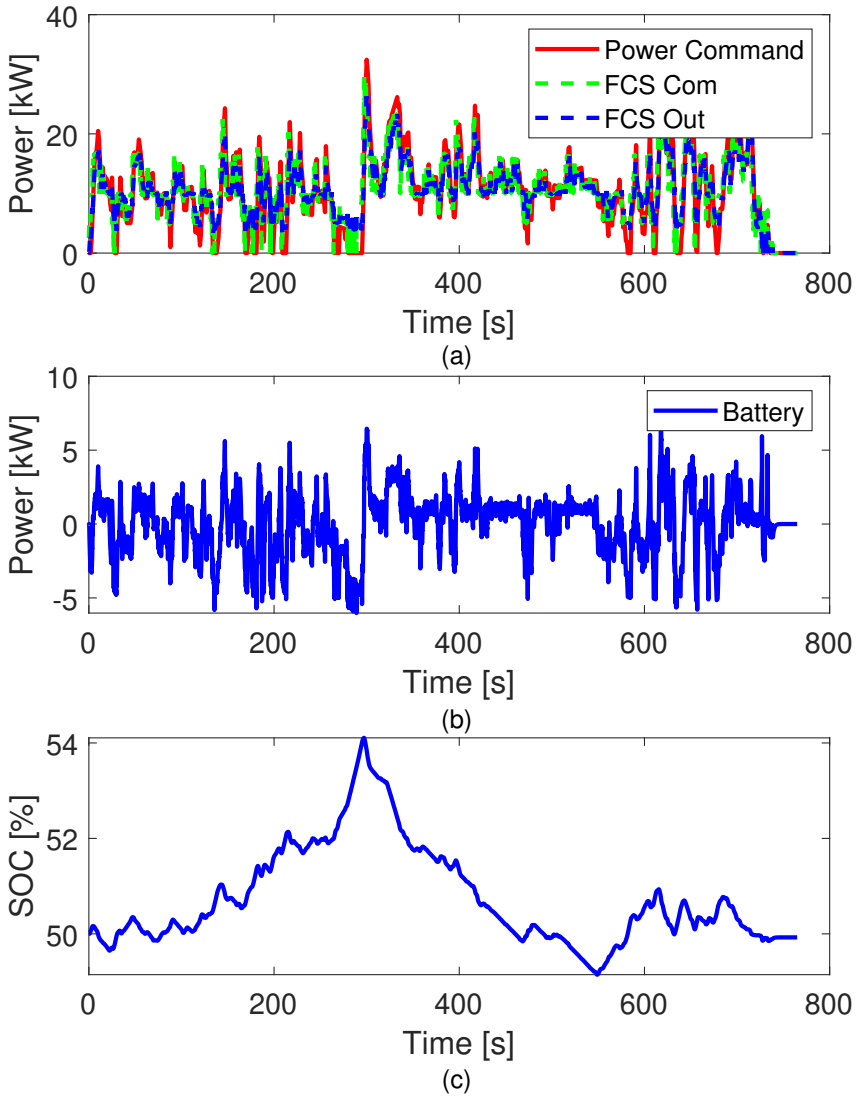

Figure 3.6: Level 2 DP results for HWFET, the ST=5 s: (a) Total power demand and FCS power command and output, (b) battery power output, (c) battery SOC.

fuel cell dynamics when Level 1 DP results are used.

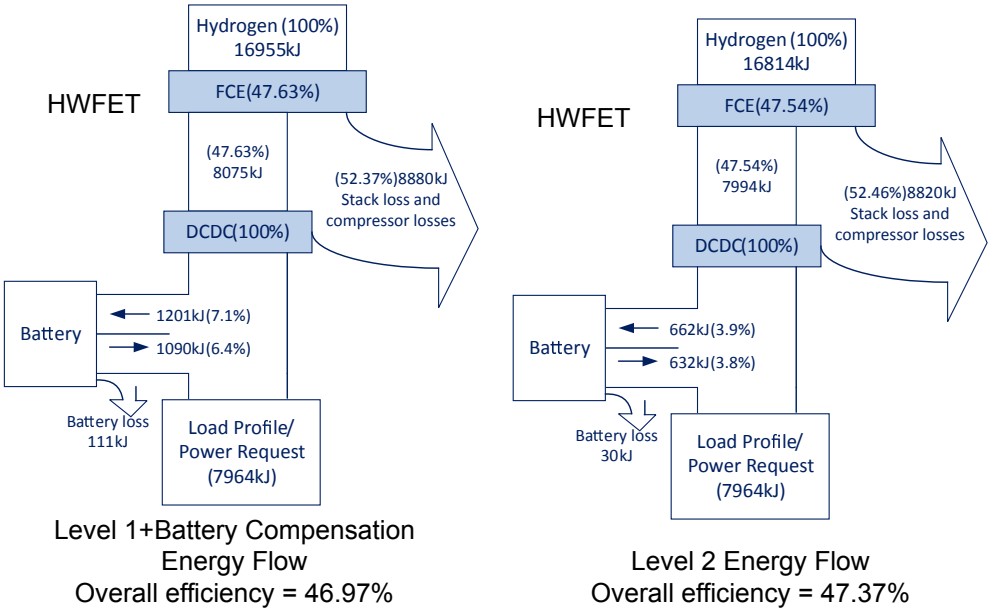

Figure 3.7: Energy flow of Level 1 (left) and Level 2 DP (right) results for HWFET.

It is also noted that, even though the power split strategies (i.e., the commanded power request for fuel cell and battery) resulting from these two level DPs are quite different, the outputs of the FCS are similar (Fig. 3.8). Fig. 3.9 provides the power distribution of Level 1 and Level 2 FCS output power on NYCC and HWFET driving cycles. The comparison motivates us to consider the Level 1 DP results as the desired FC output power, and to design the load compensator to determine the optimal pre-compensator for the FCS to deliver the desired output power.

3.3.2 FCS with a Pre-compensator

To apply Level 1 DP results and minimize the effects of FCS dynamics, we "wrap" the FCS with a pre-compensator so that the combined system will behave "almost" like a static block, as shown in Fig. 3.10. To design a pre-compensator $\tilde{q}$ to achieve this goal for SISO systems represented by the transfer function $\tilde{p}$, one can optimize

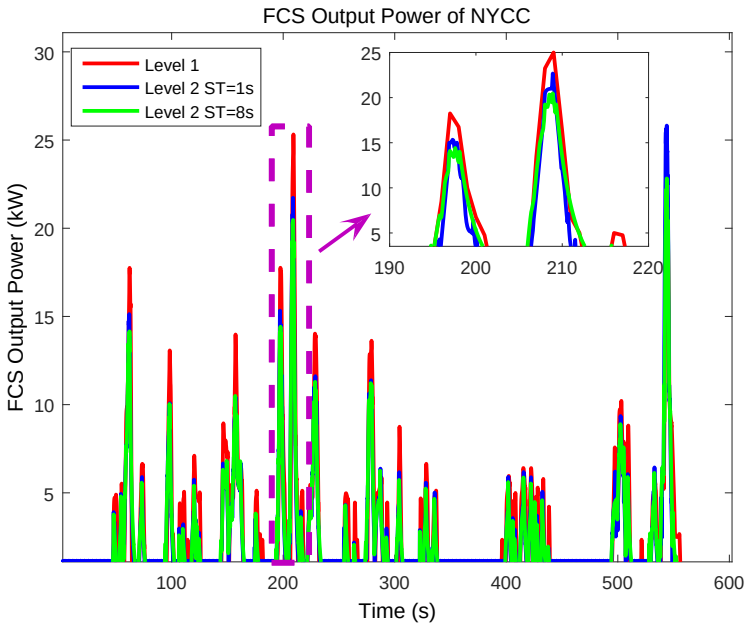

(a)

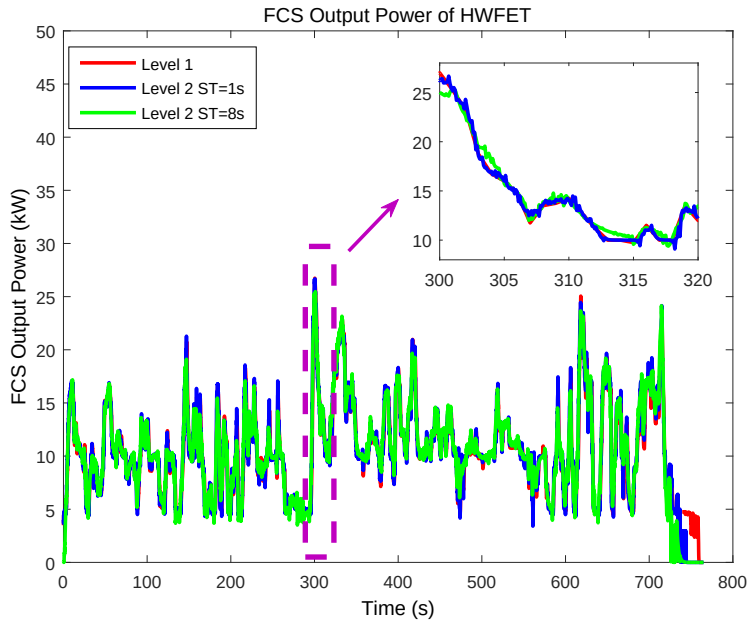

(b)

Figure 3.8: Level 2 DP FCS output power of NYCC and HWFET, (a) NYCC, (b) HWFET.

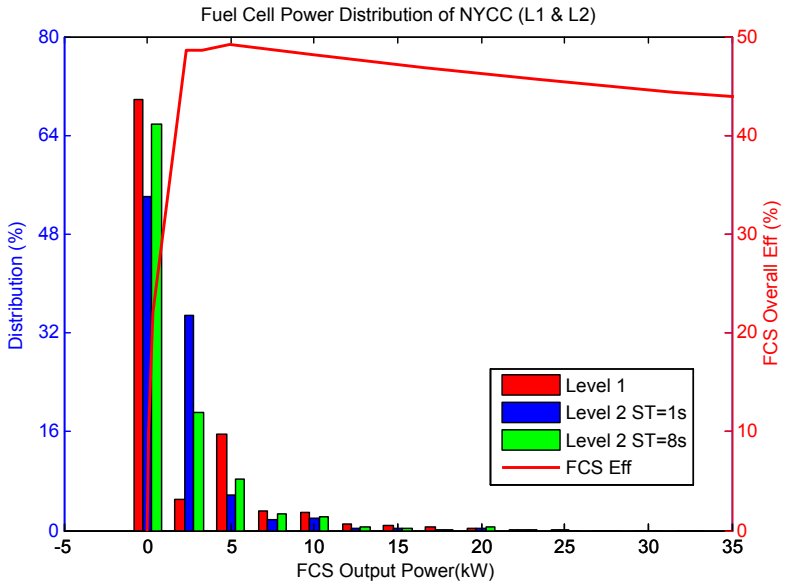

(a)

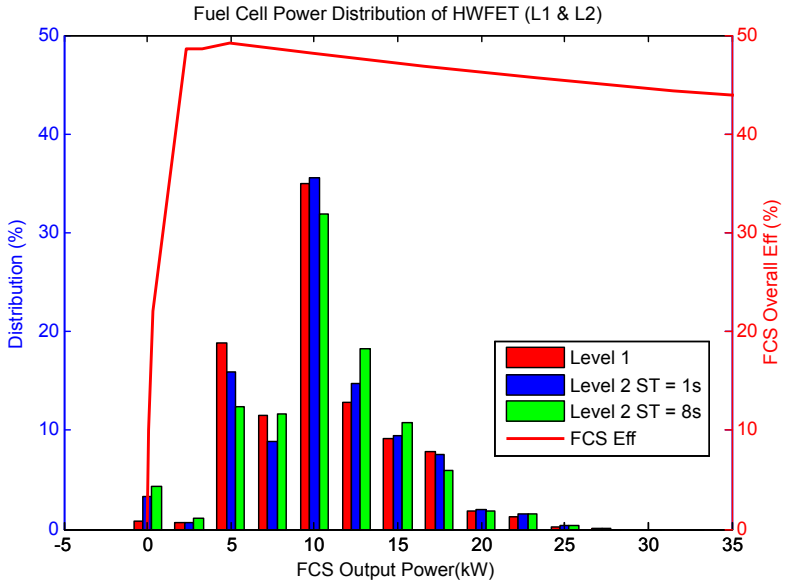

(b)

Figure 3.9: Level 2 DP FCS power distribution of NYCC and HWFET, (a) NYCC, (b) HWFET.

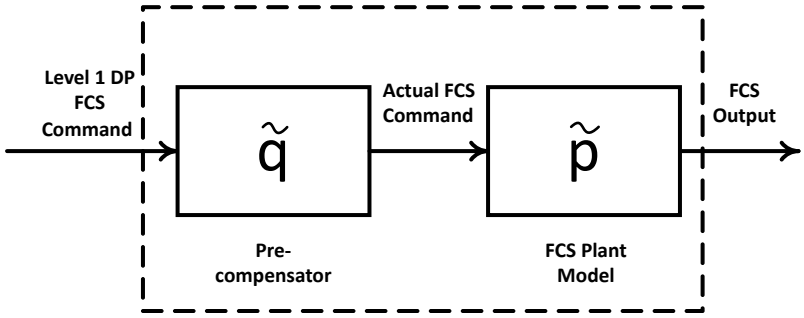

Figure 3.10: Block diagram of FCS with a pre-compensator.

H_2 (Euclidean norm) for a particular input v:

$$\min_{\tilde{q}} \|e\|_2 = \min_{\tilde{q}} \|(1 - \tilde{p}\tilde{q})v\|_2, \tag{3.14}$$

subject to the constraint that $\tilde{q}$ is stable and causal. If $\tilde{p}$ is invertible, namely, $\tilde{p}^{-1}$ is stable and rational, $\tilde{q} = \tilde{p}^{-1}$ is the solution to (3.14). If $\tilde{p}^{-1}$ is strictly rational, then $\tilde{q}$ can be chosen as $\tilde{q} = f\tilde{p}^{-1}$, where f is a low pass filter designed to assure causality. If $\tilde{p}$ is NMP, an "approximate inverse" of $\tilde{p}$ has to be found such that (3.14) is minimized. For NMP systems, the optimal solution depends on the v. To simplfy our case, we treat our input, the power request, as a step signal. Thus, the minimum error norm method [66] could be used to find the inverse of the FC dynamic system. Namely, for a stable NMP system with only one unstable zero, we rewrite:

$$\tilde{p} = p_M \frac{-s + \xi}{s + \xi}, \tag{3.15}$$

where $\xi > 0$ and $-s + \xi$ is the NMP zero of the FC dynamic system and p_M has stable poles and zeros. Then:

$$\tilde{q} = \frac{1}{p_M}. \tag{3.16}$$

For example, if the FC dynamic system has a transfer function of:

$$\tilde{p} = \frac{-0.67s + 1}{2s + 1}, \tag{3.17}$$

then by using the proposed dynamic inversion method, $\tilde{p}$ can be expressed as:

$$\tilde{p} = \frac{0.67s + 1}{2s + 1} \frac{-0.67s + 1}{0.67s + 1}, \tag{3.18}$$

with:

$$p_M = \frac{1}{2s + 1}, \tag{3.19}$$

then, $\tilde{p}$ can be chosen as:

$$\tilde{q} = \frac{2s + 1}{0.67s + 1}. \tag{3.20}$$

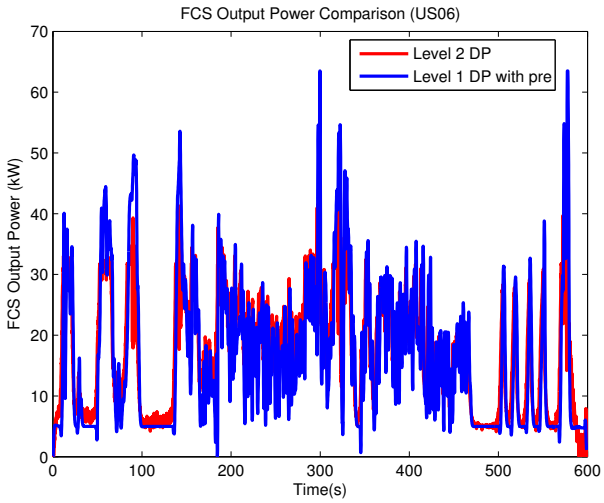

Figure 3.11: Level 1 DP with pre-compensator and Level 2 DP FCS output power comparison (US06).

The performance evaluation of HWFET using the FCS pre-compensator is summarized in Table 3.3. The saturation of the designed pre-compensator is the FCS

Table 3.3: Performance evaluation of HWFET (FCS settling time=8 s).

ST=8s	$H_2e(g)$	MPG_e	Δ SOC	DP Cost
Level 1 with Batt Com	119.58	87.74	-0.06%	119.59
Level1 1 with FCS-Pre/Batt Com	118.86	88.27	-0.09%	118.83
Level 2[1]	118.60	88.49	-0.08%	118.61

[1]The computation time in Level 2 DP, formulated in (8), (11)-(13) and (16)-(18), rises to 12-14 hours by using the same computation machine, which is almost 1000 times more than Level 1 DP. Furthermore, the sensitivity of zero dynamics to fuel economy is very weak, by changing different zero locations, MPG_e is only varying in 0.05% under HWFET and less than 1% under US06.

Table 3.4: Performance evaluation of US06 (FCS settling time=8 s).

$ST = 8s$	$H_2e(g)$	MPG_e	ΔSOC	DP Cost
Level 1 with Batt Com	169.50	47.81	0.03%	169.53
Level1 1 with FCS-Pre/Batt Com	169.07	47.93	-0.03%	169.05
Level 2	163.92	49.44	-0.09%	163.89

Table 3.5: Performance degradation (MPG_e) of Level 1 DP using FCS-pre/Batt for compensating power tracking error over Level 2 DP.

Settling Time / Driving Cycle	ST=1s	ST=5s	ST=8s
HWFET	0.03%	0.13%	0.22%
NYCC	-0.5%	3.71%	5.14%
SC03	0.4%	2.49%	3.29%
US06	0.19%	3.46%	3.14%

power limits, which is the equation (3.4). Level 1 with Batt Com refers to the result using batteries to compensate for the load following error. Level 1 with FCS-Pre/Batt Com refers to the result where the optimal pre-compensator is first used to compensate the FCS dynamics and then the battery is also used as the secondary compensation to achieve power tracking. From Table 3.3, it can be seen that the optimal pre-compensator works fairly well because MPG_e only decreases by 0.22%. However, if we look at all four driving cycles (Table 3.4 and Table 3.5), when an aggressive load (US06 and SC03) and frequent start/stop load (NYCC) are required, the pre-compensator does not perform as well as the Level 2 DP. A comparison of the FCS output power of Level 2 DP and Level 1 DP with pre-compensator for US06 driving cycle is shown in Fig. 3.11. The pre-compensator is designed for scenarios when settling time equals to 8 s.

3.4 Sensitivity Analysis to FCS Dynamics

To better understand the effects of FCS dynamics on optimal energy management performance, extensive analysis is performed with different dynamic models to quantify the performance sensitivity to different parameters in the model.

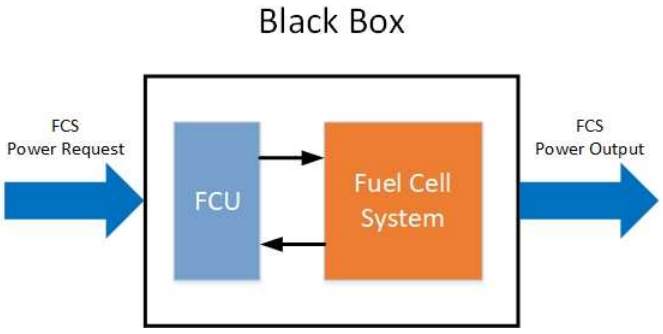

Figure 3.12: Block diagram of an FCS system.

As shown in Fig. 3.12, the actual FCS power response is affected by their own subsystem controller of which the details are generally unavailable. Thus, treating

the overall FCS as a black box, it can be represented by a 1^{st} order LTI transfer function. Assuming an FCS with its own subsystem controller can be simplified as a 1^{st} order LTI system with non-minimum phase phenomenon, the state-space realization is shown in (2.4) and (2.5), and the associated transfer function of the FCS can be described as:

$$G(s) = \frac{Y(s)}{X(s)} = \frac{P_{FCS\_out}}{P_{FCS\_in}} = k\frac{-\tau_1 s + 1}{\tau_2 s + 1}, \tag{3.21}$$

where k is the DC gain of the transfer function and k is assumed to be 1. τ_1 is the time constant of zero dynamics and $1/\tau_1$ is the zero location. τ_2 is the time constant of the characteristic equations and $1/\tau_2$ is the pole location. The time constant value τ_1 represents the speed of the power response.

3.4.1 Evaluation of the Effects of Model Parameter Variation on Optimal Energy Management

All model based control methods face the challenges of model parameter variation. To address this issue, the robustness of the algorithms needs to be tested so that the sensitivity of the proposed algorithm can be understood. Towards this objective, a US06 cycle is selected as the representative driving cycle to implement three Level 2 DP strategies using different FCS dynamics with ST=1 s, 5 s, and 8 s. Each of these three strategies is applied to three different models. Thus, nine results are generated and shown in Fig. 3.13 and Fig. 3.14, where "Strategy Generation Model" refers to the FCS model that is included in the DP strategy and "Strategy Implementation Model" refers to the FCS model that is used for performance evaluation. In terms of the fuel economy and charge sustaining performance, the strategy generated with slower dynamics is more robust than those with fast FCS dynamics.

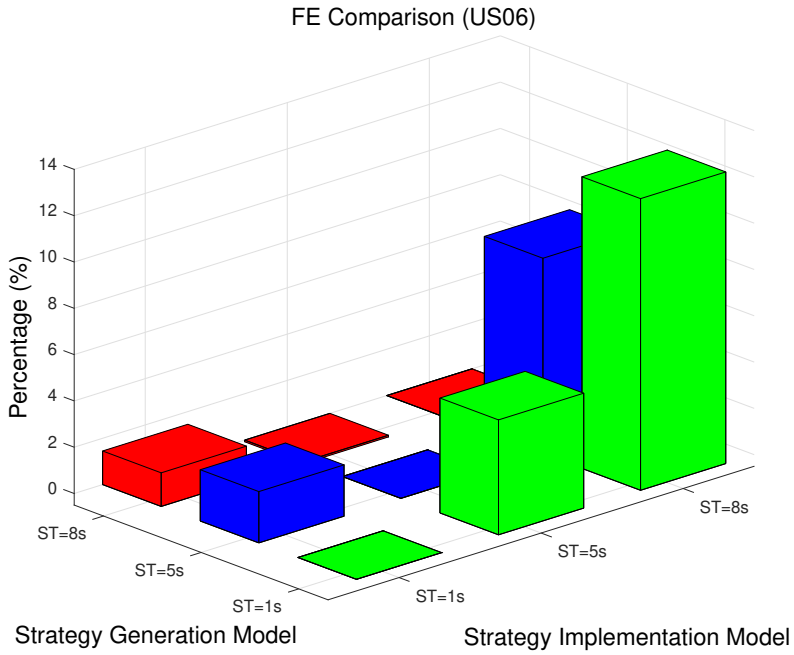

Figure 3.13: Robustness of fuel economy on different FCS dynamics.

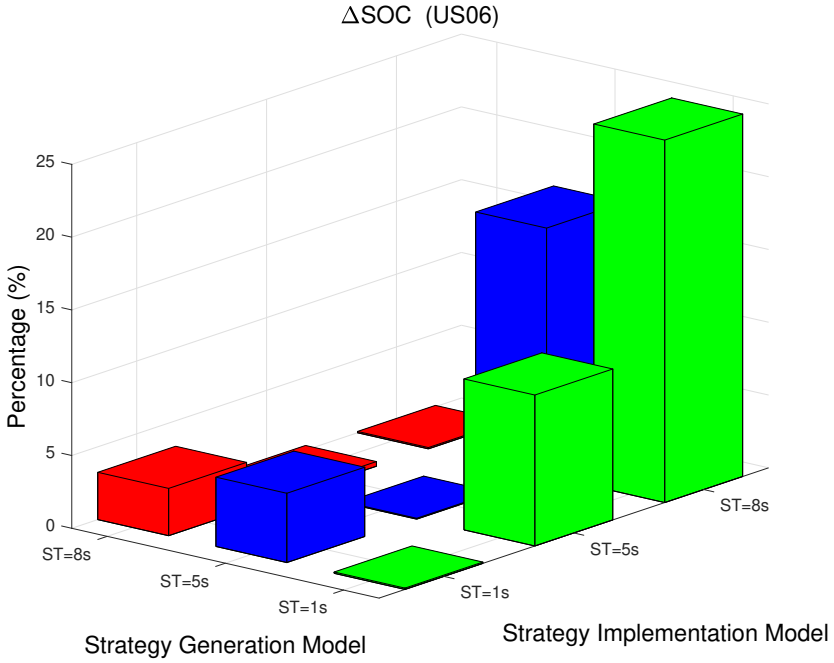

Figure 3.14: Robustness of charge sustaining performance on different FCS dynamics.

3.4.2 Evaluation of the Effects of Zero-Dynamics on Optimal Energy Management

3.4.2.1 Definition of Energy Deficiency

For a system represented by (3.21), the unit step response can be derived as:

$$y(t) = 1 - e^{-\frac{1}{\tau_2}t} - \frac{\tau_1}{\tau_2}e^{-\frac{1}{\tau_1}t}, \tag{3.22}$$

where $y(t)$ is the FCS power output. The initial condition:

$$y(0) = -\frac{\tau_1}{\tau_2}, \tag{3.23}$$

and the final value is 1 kW. Fig. 3.15 shows three different step responses for different τ_1, τ_2. The energy deficiency during the transient is defined as the integration of the power tracking error along the entire transient process until the FCS output power reaches the steady state value, namely,

$$Err(t) = \int_0^t (1 - y(\tau))\, d\tau. \tag{3.24}$$

By substituting (2.28) into (2.30), the energy deficiency can be calculated explicitly as:

$$Err = -(\tau_2 e^{-\frac{t}{\tau_2}} - \tau_2) - (\tau_1 e^{-\frac{t}{\tau_2}} - \tau_1), \tag{3.25}$$

where t is time. As t goes to infinity, the cumulative energy deficiency is:

$$Err = \tau_1 + \tau_2. \tag{3.26}$$

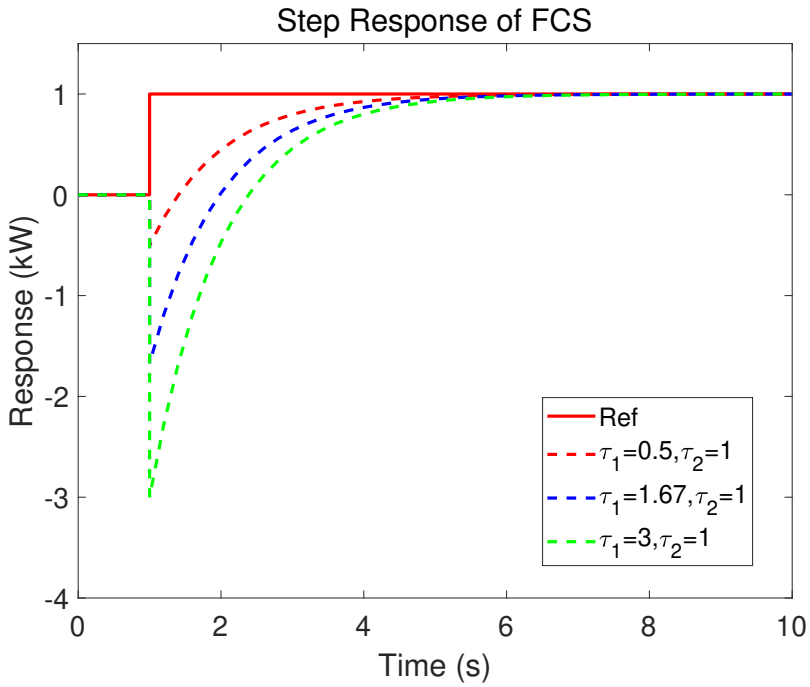

Figure 3.15: Step responses of different energy deficiency levels: model 1 (energy deficiency is 1.5 kJ, τ_1=0.5, τ_2=1), model 2 (energy deficiency is 2.67 kJ, τ_1=1.67, τ_2=1), model 3 (energy deficiency is 4 kJ, τ_1=3, τ_2=1)

Thus, two evaluations can be made to further address the effects of zero-dynamics on optimal energy management. In the first evaluation, the zero location is varied while maintaining the same transient energy deficiency, and the poles are adjusted accordingly. In the second evaluation, the total transient energy deficiency is varied while maintaining the same pole, and the zeros are adjusted accordingly. The different dynamic characteristics evaluated are shown in Table 3.6 and Table 3.7.

In all the evaluations, the Level 1 DP strategy is fed into the Level 2 powertrain, and the fuel economy is compared with the Level 2 DP results. The comparison shows that the fuel economy is very sensitive to the zero locations. When the zero dynamics are aggressive, the battery has to heavily compensate for the dynamic effects, which leads to severe battery charge sustaining issues. Furthermore, when the FCS dynamics are included in the Level 2 DP, the fuel economy performance is not as sensitive as the Level 1 DP evaluation results. In this context, higher fuel economy degradation

Table 3.6: Transfer functions used in zero dynamic effects evaluation (different zero locations with the same energy deficiency).

Zero Location	Zero Dynamics Time Constant	Transfer Function	A_k	B_k	C_k	D_k
0.45	2.22	$\frac{-2.22s+1}{0.45s+1}$	0.800	0.090	13.190	-4.933
0.60	1.67	$\frac{-1.67s+1}{s+1}$	0.905	0.095	2.670	-1.670
0.80	1.25	$\frac{-1.25s+1}{1.42s+1}$	0.932	0.097	1.324	-0.880
1.00	1.00	$\frac{-s+1}{1.67s+1}$	0.942	0.097	0.957	-0.599
1.50	0.67	$\frac{-0.67s+1}{2s+1}$	0.951	0.098	0.668	-0.335
2.00	0.50	$\frac{-0.5s+1}{2.17s+1}$	0.955	0.098	0.567	-0.230

Table 3.7: Transfer functions used in zero dynamic effects evaluation (different energy deficiency with the same pole location).

Zero Location	Zero Dynamics Time Constant	Transfer Function	A_k	B_k	C_k	D_k
2.00	1.00	$\frac{-0.5s+1}{s+1}$	0.905	0.095	1.500	-0.500
0.60	1.00	$\frac{-1.67s+1}{s+1}$	0.905	0.095	2.670	-1.670
0.33	1.00	$\frac{-3s+1}{s+1}$	0.905	0.095	4.000	-3.000

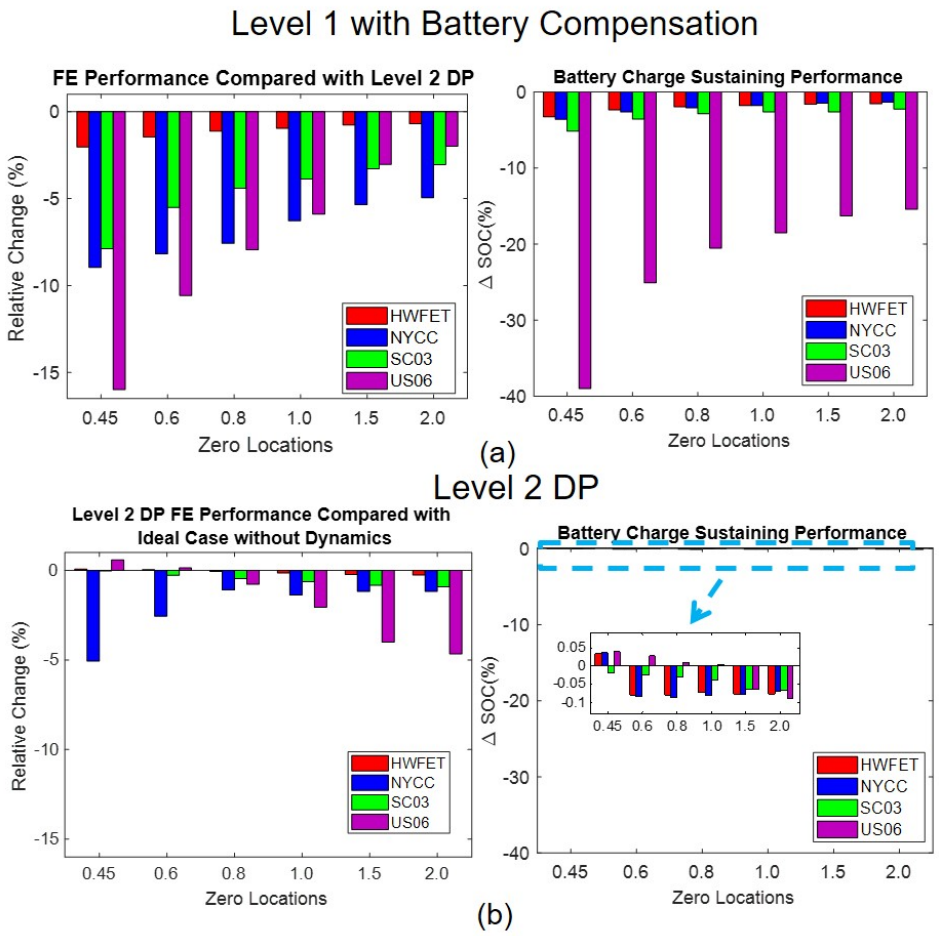

Figure 3.16: Sensitivity analysis of zero locations on fuel economy and charge sustaining performance, (a) Level 1 DP with battery compensation, (b) Level 2 DP.

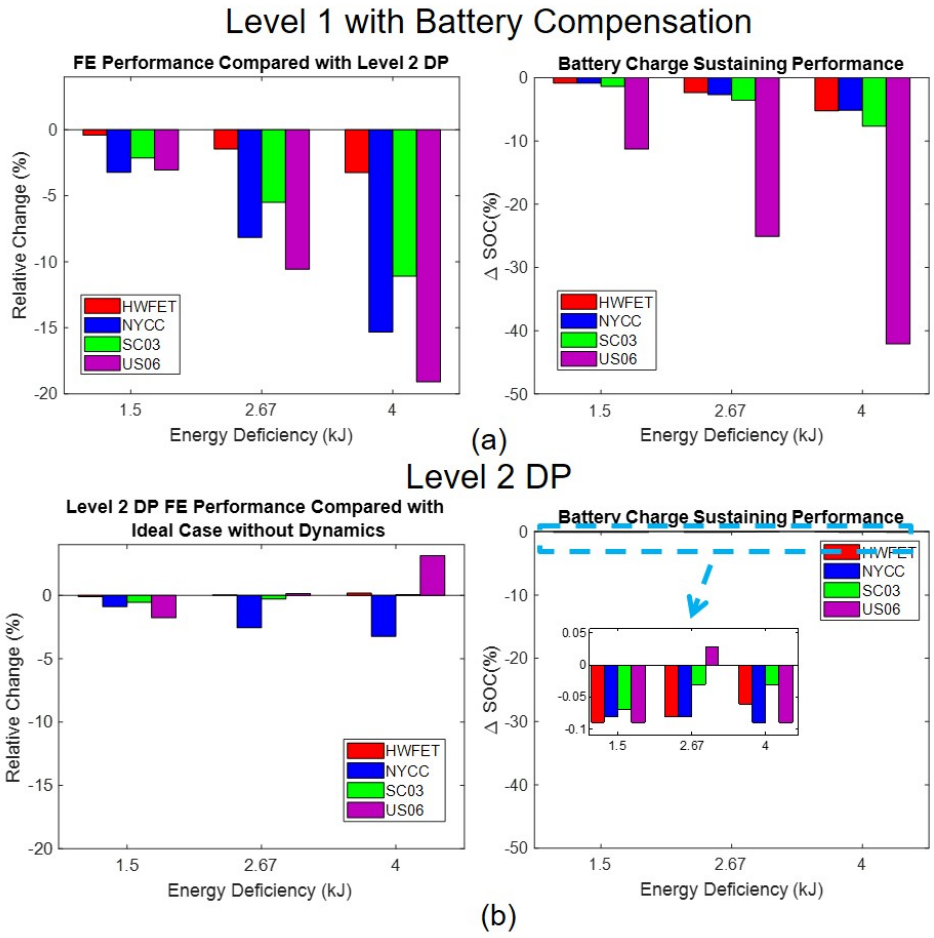

Figure 3.17: Sensitivity analysis of energy deficiency Level on fuel economy and charge sustaining performance, (a) Level 1 DP with battery compensation, (b) Level 2 DP.

is attributable to aggressive driving cycles, such as US06. For a city cycle like NYCC, the fuel economy performance is also sensitive because many stop-n-gos are included in the driving cycle.

When the evaluation is performed by varying the total energy deficiency value, the results are shown in Fig. 3.17. The similar performance are observed. When the FCS dynamics are included in the Level 2 DP, the fuel economy performance is not as sensitive as the Level 1 DP evaluation results. When the FCS dynamics are not included in the Level 1 DP, the battery has to heavily compensate for the dynamic effects, which leads to severe battery charge sustaining issues and attenuate the fuel economy performance. In conclusion, when the tolerance of the loss of fuel economy is less than 3%, the FCS dynamics can be ignored at the vehicle level energy management design if: (1) the energy deficiency due to the nonminimum phase is less than 2.5 kJ for a 1 kW power request, (2) the FCS dynamics settling time is less than 3 s.

3.5 Conclusion

In this chapter, we propose a comprehensive and systematic framework for analyzing the dynamic effects of FCS on optimal energy management applications. A Ford Fusion equipped with FCS, hydrogen storage, and Li-ion battery pack is considered as the representative powertrain system. Two levels of DP approach are adopted to derive optimal power split strategies, where FCS dynamics are ignored at Level 1 but incorporated at Level 2 DP problem formulation. While the analysis confirms that the fuel cell dynamics can be ignored if they are fast enough (i.e., with settling time less than 1 second), it also reveals that substantial loss of performance can occur if the slow dynamics (i.e., with settling time equal to 8 seconds) are not included in DP. Incorporating FCS dynamics into the DP formulation can help reduce battery loss. To retain the computational advantage of Level 1 DP, we also exploit pre-

compensation of FCS, so that the quasi-static assumption used in Level 1 DP can be better satisfied, thereby justifying the DP approach that ignores the dynamics. Given the NMP characteristics of FCS, perfect compensation is not possible, which motivates us to develop the real-time optimal power management strategies to be discussed in subsequent chapters.

CHAPTER IV

An Optimization-oriented Supervisory Controller Design for Hybrid Fuel Cell Electrified Vehicles

Computation complexity makes the DP approach unsuited for online implementation. To address this issue, the design of a novel optimization-oriented supervisory controller for FCV, referred to as A-PMP, is proposed in this Chapter. An approach for estimating the optimal value of the co-state variable is developed by studying the standard and synthesized driving cycles. Minimal trip information is needed to implement the proposed algorithm online. The proposed A-PMP is demonstrated on a high fidelity model to show near-optimal fuel economy with desired charge sustaining performance. Furthermore, this chapter also details the validation of the proposed A-PMP method in the HIL lab and the test results on a testing FCV.

4.1 Problem Formulation

In general, the real-time power and energy management problem in a hybrid vehicle can be cast into an optimization problem over a finite time horizon [65]. Our goal is to find the sequence of controls $u(k)$ that leads to the minimization of the cost

function $J(x(k_0), u(k), x(k_N))$, defined as:

$$J(x(k_0), u(k), x(k_N)) = \sum_{k=k_0}^{N-1+k_0} W_{H_2}(k), \tag{4.1}$$

where k represents the discretized time index, $u(k)$ (the requested power from FCS $P_{fc\_c}(k)$) is the control action, $x(k)$ (the SOC) is the system state, $[k_0, k_N]$ is the optimization horizon, $W_{H_2}(k)$ is the instantaneous hydrogen consumption. The optimization problem (4.1) is to be solved subject to the system dynamics and constraints [2] while following a load profile. The detailed system dynamics and constraints information can be found in Chapter III.

4.2 Pontryagin's Minimum Principle

The Pontryagin's Minimum Principle(PMP) is used to find the best possible control for taking a dynamical system from one state to another, especially under the state or input constraints [67]. The principle states that the control Hamiltonian must take an extreme value over controls in the set of all permissible controls. The PMP is a generalization of the Euler-Lagrange equation in the Calculus of Variation, which provides a set of necessary conditions for global optimality of a constrained optimization problem [45]. By translating energy management problem into an optimal control problem, one can exploit PMP to derive sub-optimal solutions in lieu of computational simplicity [68]. Considering the energy management problem in (4.1) and all the constraints, a Hamiltonian equation H is defined as:

$$H(SOC(k), u(k), k, \lambda(k)) = \lambda(k) f(SOC(k), u(k)) + W_{H_2}(k)\Delta t, \tag{4.2}$$

where $\lambda(k)$ is the co-state variable associated with the optimization problem. $W_{H_2}(k)$ is the FCS hydrogen consumption at time k. $f(SOC(k), u(k))$ is the system dynamics

defined in Chapter III. The objective now is to find an optimal control sequence $u(k)$ that minimizes the Hamiltonian equation at each sampled time:

$$u^*(k) = \underset{u(k)}{\operatorname{argmin}} H(SOC(k), u(k), k, \lambda(k)), \tag{4.3}$$

and also satisfies all constraints. At the same time, the co-state variables should satisfy the adjoint equation:

$$\lambda(k+1) = -\frac{\partial H(SOC(k), u(k), k, \lambda(k)}{\partial SOC(k)}\Delta t + \lambda(k). \tag{4.4}$$

4.2.1 PMP Implementation

To implement the PMP algorithm as an online energy management strategy, an initial value of λ is needed so that λ can be calculated according to (4.4) and updated with time. Note that PMP provides sufficient conditions for a global optimal solution if the fuel consumption rate is a convex function of battery power and $\dot{SOC}$ is a concave function of battery power and the SOC [69]. These conditions are not satisfied for the battery configuration under consideration. Thus, even with the optimal λ_0, PMP may not give the global optimal solution. Moreover, the partial derivative of the Hamiltonian equation with respect to the state $SOC(k)$ is required to implement (4.4). Using (2.7) and (4.2), (4.4) can be expressed as:

$$\lambda(k+1) = -\frac{1}{Q_{batt}}\left(\frac{\partial I_{batt}(k)}{\partial V_{oc}(k)}\frac{\partial V_{oc}(k)}{\partial SOC(k)} + \frac{\partial I_{batt}(k)}{\partial R_{int}(k)}\frac{\partial R_{int}(k)}{\partial SOC(k)}\right)\Delta t + \lambda(k). \tag{4.5}$$

To have a closed-form expression for $\frac{\partial V_{oc}(k)}{\partial SOC(k)}$ and $\frac{\partial R_{int}(k)}{\partial SOC(k)}$, one can use data-fitting methods to extract the analytical expressions and use them in (3.5) [51]. We observe that the variation of $\lambda(k)$ with respect to time is negligible [2]. Fig. 4.1 show that the co-state variable only varies 0.5% from the initial value on the US06 driving cycle. By implementing a constant $\lambda(k)$ in US06 cycle, the SOC trajectory of the PMP results

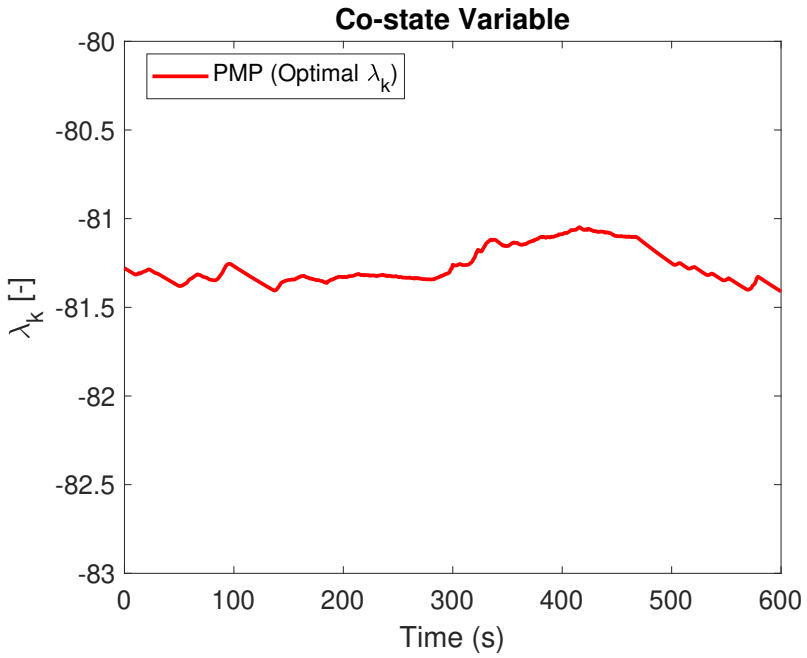

Figure 4.1: Optimal trajectory of the co-state variable.

are almost the same as the global optimal DP results, as shown in Fig. 4.2.

To evaluate if the dynamics of $\lambda(k)$ can be omitted with $\lambda(k)$ being kept as constant, performance sensitivities on four representative cycles are generated and shown in Table 4.1. These four cycles cover a wide vehicle speed range from low speed city driving (NYCC) to high speed aggressive highway driving (US06). The PMP-based TPBVP energy management problem is solved using the shooting-method with the design model discussed in Section 2.1, but with a constant λ. DP is also used to provide a benchmark. MPG_e, defined as miles per gallon gasoline equivalent, is a measure of the average distance traveled per unit of energy consumed. ΔSOC reflects the charge-sustaining performance, and is defined as $SOC(k_N) - SOC(k_0)$. λ_0 is the co-state value. The small deviation of SOC can be converted to equivalent hydrogen consumption [14]. The difference between the DP and PMP results is less than 0.55%. It proves that PMP algorithm even with constant λ can be used to develop a near-optimal energy management strategy. Thus, constant co-state λ are used in this study for PMP algorithm. To further evaluate the PMP-based algorithm, a simple

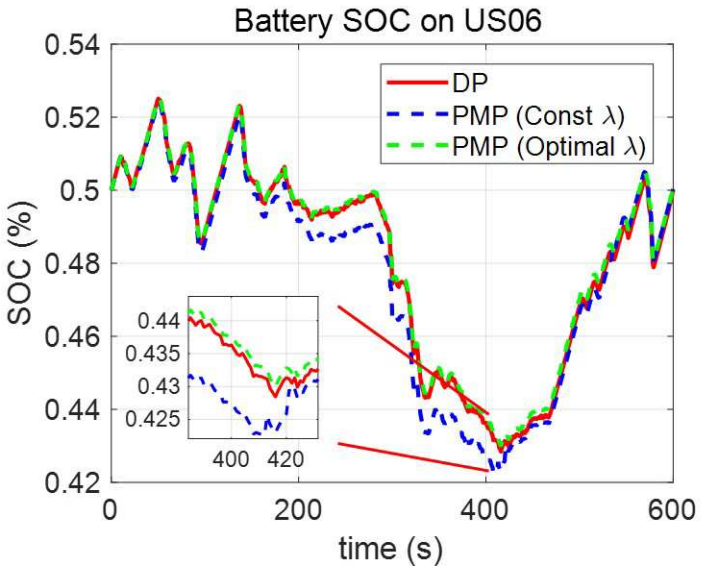

Figure 4.2: SOC trajectories to different PMP implementation strategies.

load following controller, which means that the FCS follows the power demand as much as possible, is defined as a rule-based controller. This controller can be used as a baseline to show the advantages of using PMP-based algorithm.

Table 4.1: Comparison of performances between DP and PMP-based algorithm.

Cycle Name	DP		PMP			MPG_e Diff
	MPG_e	ΔSOC	MPG_e	ΔSOC	λ_0	PMP over DP
HWFET	87.59	0.008%	87.49	-0.22%	-76.85	-0.11%
NYCC	68.94	0.01%	68.58	-0.06%	-74.39	-0.52%
SC03	76.98	-0.071%	76.95	-0.02%	-74.92	-0.04%
US06	50.69	0.003%	50.55	0.03%	-80.83	-0.28%

4.2.2 Co-state Estimation

While the PMP-based methods using constant co-state λ provide near-optimal solutions compared with DP, its performance depends on a good estimation of the co-state value. Simulation results have shown that the optimal value of λ_0 is strongly dependent on the driving cycles. Kim [70] claims that the co-state λ_0 can be estimated from an approximation model with two representative parameters, the effective SOC

Table 4.2: Comparison of performances between rule-based and PMP-based algorithm.

Cycle Name	Rule-based		PMP			MPG_e Diff
	MPG_e	ΔSOC	MPG_e	ΔSOC	λ_0	PMP over Rule-based
HWFET	87.15	0%	87.49	-0.22%	-76.85	+0.39%
NYCC	67.49	0%	68.58	-0.06%	-74.39	+1.62%
SC03	75.93	0%	76.95	-0.02%	-74.92	+1.34%
US06	49.40	-3%	50.55	0.03%	-80.83	+2.33%

drop rate $\dot{SOC}_{eff}$ and the effective mean power P_{mean}. In this section, three test scenarios are analyzed to understand the relationship between the co-state value and the power distribution. The framework is shown in Fig. 4.3 and the details are described in the following subsection.

4.2.3 Designed Test Scenarios

Table 4.3: Co-state value of different driving cycles.

Cycle	HWFET	UDDS	SC03	Artemis Urban	JC08	US06
λ_0	-78.75	-73.45	-73.70	-73.52	-73.45	-80.10

Six standard driving cycles are used and the corresponding PMP-based problems are solved for each cycle. Fig. 4.4 shows the Cumulative Distribution Function (CDF) of 6 representative driving cycles. UDDS and SC03 have similar load distribution, while others, such as US06, have different CDFs. Table 4.3 shows that the co-state values are very close for those driving cycles with similar power CDF (e.g. UDDS and SC03) even though their power profiles are different (see Fig. 4.5). Based on this observation, we hypothesize that load distribution provides the most important information to estimate the co-state value. To validate the hypothesis on the relationship between power distribution and λ_0, three other scenarios are evaluated:

1. The UDDS driving cycle is segmented into small windows where the total

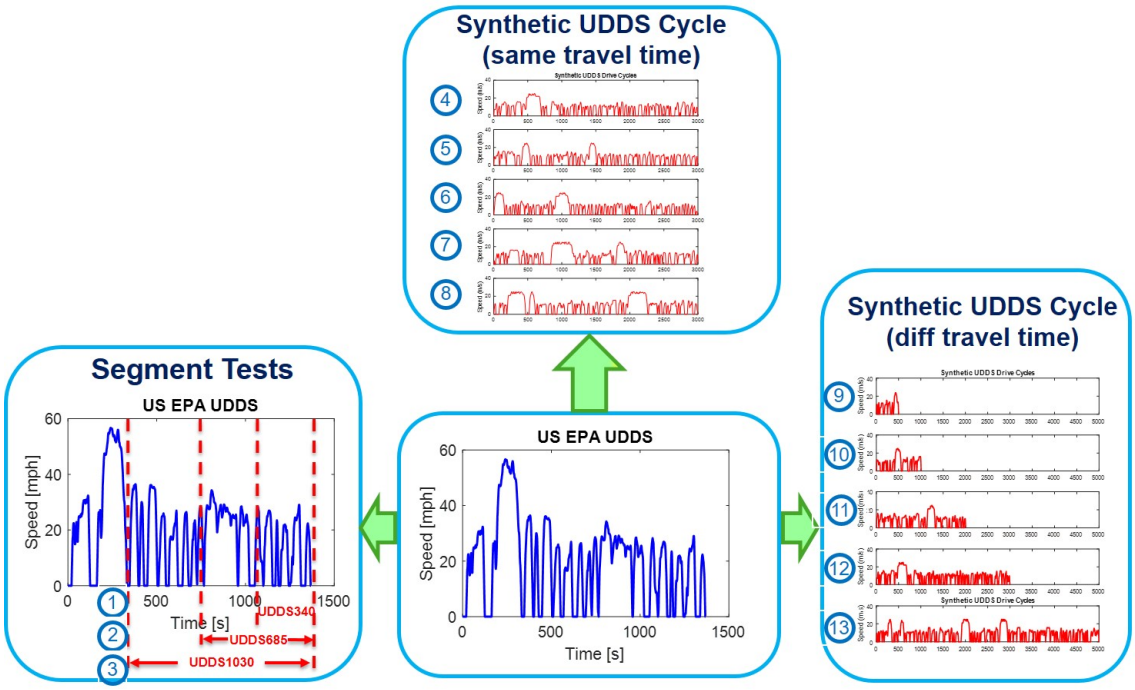

Figure 4.3: Three test scenarios used to estimate the constant co-state value.

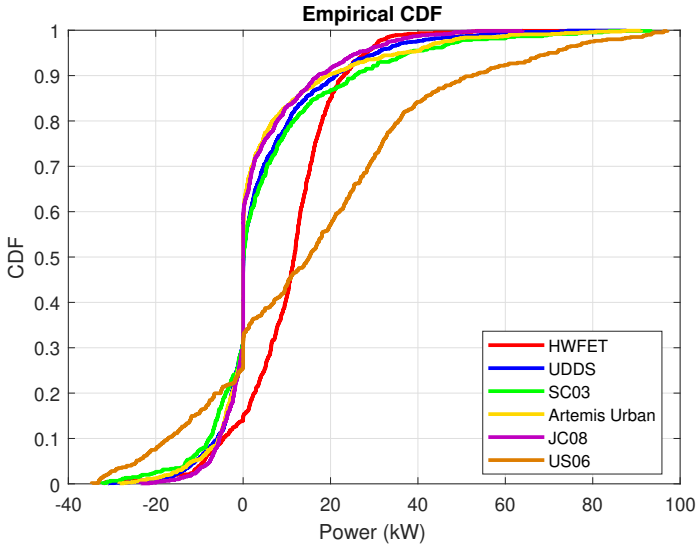

Figure 4.4: Empirical cumulative distribution function.

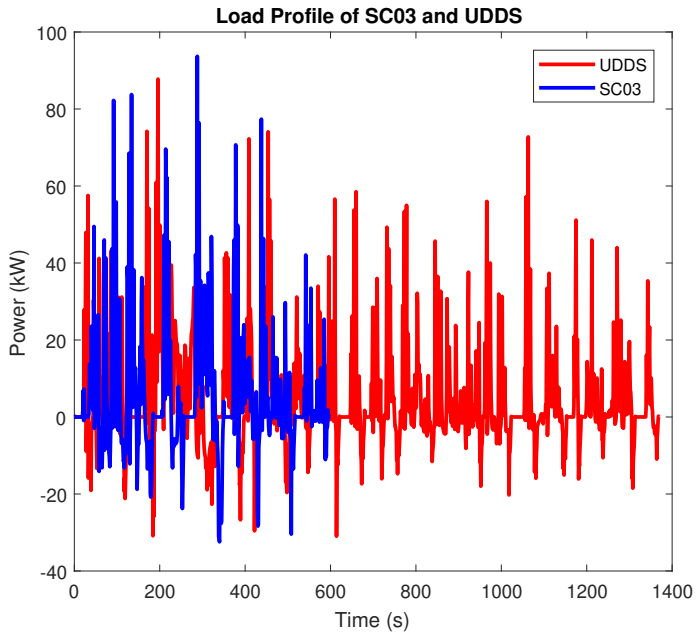

Figure 4.5: Load profile of SC03 and UDDS.

travel time is used to define the segmented UDDS cycle (UDDS340, UDDS685, UDDS1030). The times of the segmented cycles are picked to ensure the initial and final speed are zero.

2. The speed and acceleration profiles of UDDS are used to generate the probability transition matrix for a Markov chain model to create 5 synthetic load profiles with the same trip time (3000s) and the same power distribution, but distinctively different time traces.

3. The same Markov chain model is used to generate five different load profiles with different trip time (500s, 1000s, 2000s, 3000s, 5000s) and the same power distribution.

The PMP-based algorithm is then used on all thirteen cycles. The optimal λ_0 values are shown in Table 4.4, Table 4.5, and Table 4.6, respectively. All thirteen synthetic cycles return similar optimal λ_0 as a result. Therefore, if the load distribution of two driving cycles are similar, the corresponding optimal λ_0 are close.

Furthermore, it also proves that the total travel time is relatively unimportant compared with load distribution.

Table 4.4: Co-state value of different segmented UDDS driving cycles.

Cycle	UDDS1	UDDS2	UDDS3
λ_0	-74.52	-74.27	-74.41

Table 4.5: Co-state value of different synthetic UDDS driving cycles (same travel time).

Cycle	UDDS4	UDDS5	UDDS6	UDDS7	UDDS8
λ_0	-74.56	-74.16	-74.61	-74.62	-74.74

Table 4.6: Co-state value of different synthetic UDDS driving cycles (different travel time).

Cycle	UDDS9	UDDS10	UDDS11	UDDS12	UDDS13
λ_0	-74.70	-74.74	-73.80	-74.56	-74.64

4.3 Adaptive-PMP Based Supervisory Controller

The previous section shows that the optimal co-state value is closely related to the patterns of a driving cycle. Average power is adopted here as a key parameter to represent load distribution. Fig. 4.6 plots the optimal λ_0 against the average power for the 19 standard cycles. A data fitting method is used to fit the data with a 3^{rd} order polynomial:

$$\lambda = p_1 P_{avg}^3 + p_2 P_{avg}^2 + p_3 P_{avg} + p_4, \tag{4.6}$$

where P_{avg} is the average power over the entire driving cycle, p_1 to p_4 are the coefficients of the polynomial equation. Fig. 4.6 shows satisfactory fitting results.

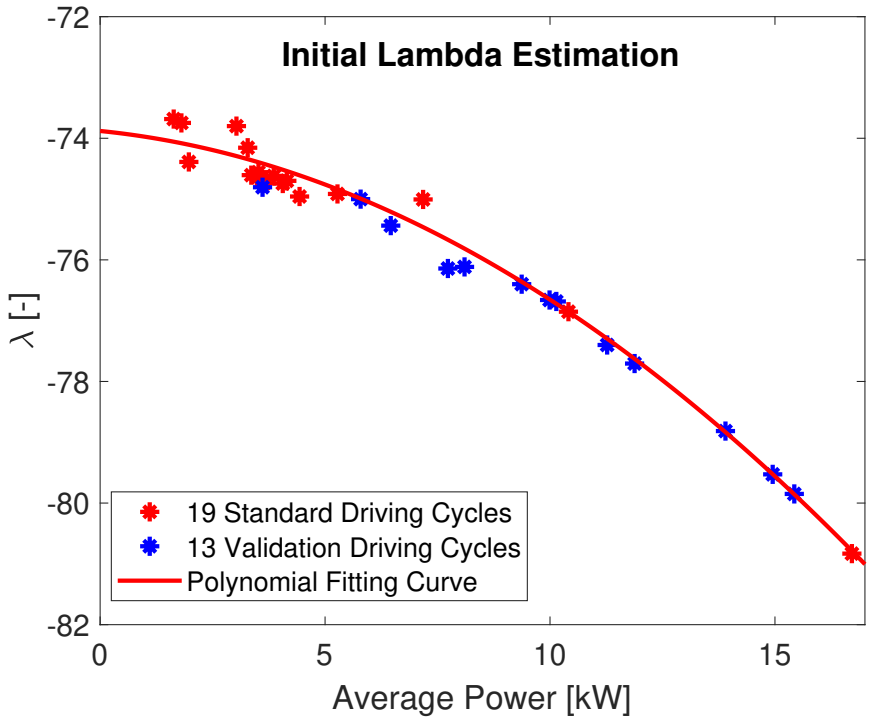

Figure 4.6: Fitting $\lambda 0$ using polynomial equation.

The R-square and RMSE values are shown in Table 4.7.

Table 4.7: Fitting results of initial co-state estimation.

	R-square	RMSE
Fitting Data (19 Driving Cycles)	0.92	0.27
Validation Data (13 Driving Cycles)	0.94	0.20

With the insights learned from the analysis above, two special features are proposed to update the co-state value online. First, a recursive average power is updated online as:

$$P_{avg}(k) = \frac{P_{req}(k) + (k-1)P_{avg}(k-1)}{k}. \tag{4.7}$$

The recursive average power and the total average power of HWFET driving cycle

are shown in Fig.4.7.

Second, to ensure that the charge sustaining performance is met, an additive penalty function, given by:

$$\gamma(SOC, k) = 100(SOC(k) - SOC(0))e^{-(\frac{T_{total}-T_k}{\mu})}, \tag{4.8}$$

is incorporated in the cost function, where T_{total} is the total travel time, T_k is the current travel time, and μ, which is set to be 100 for the case study, is a parameter introduced to scale the effects of the additive penalty function. This penalty function is added as the second part of co-state value to be interpreted as a weighting factor to the battery SOC dynamics to ensure the SOC trajectory goes back to the initial value at the end of driving cycle. It will not affect the hydrogen consumption in the cost function which is the second part of the Hamiltonian equation. Thus, the updated Hamiltonian is:

$$H(SOC(k), u(k), k, \lambda(k)) = \\ (\lambda(k) + \gamma(SOC, k))f(SOC(k), u(k)) + W_{H_2}(k)\Delta t, \tag{4.9}$$

where $\lambda(k)$ is calculated online without any prediction of the driving information, $\gamma(SOC, k)$ serves as an SOC governor to ensure a charge sustaining performance.

4.4 A-PMP Algorithm Discussion and Evaluation

Table 4.8: Comparison of performances on IM240, EUDC, and IHWY driving cycles.

Cycle Name	DP		A-PMP		Rule-based		MPG_e Diff	MPG_e Diff
	MPG_e	ΔSOC	MPG_e	ΔSOC	MPG_e	ΔSOC	A-PMP over DP	A-PMP over Rule-based
IM240	68.59	-0.08%	68.48	-0.71%	67.85	0%	-0.16%	+0.93%
EUDC	75.47	-0.08%	75.46	-2.17%	74.68	0%	-0.01%	+1.04%
IHWY	91.21	-0.06%	90.96	0.27%	90.48	0%	-0.27%	+0.53%

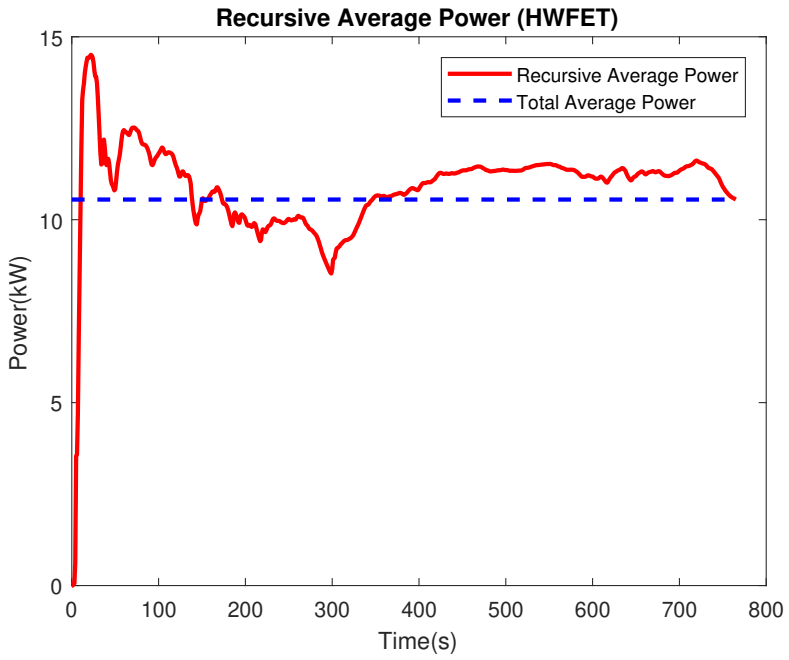

Figure 4.7: Recursive average power.

Table 4.9: Comparison of performances on UDDS+MNHA and UDDS5000 driving cycles.

Cycle Name	DP		A-PMP		Rule-based		MPG_e Diff	MPG_e Diff
	MPG_e	ΔSOC	MPG_e	ΔSOC	MPG_e	ΔSOC	A-PMP over DP	A-PMP over Rule-based
UDDS+MNHA	82.22	-0.05%	81.50	1.60%	81.11	0%	-0.88%	+0.93%
UDDS5000	85.92	-0.06%	84.62	-0.66%	83.33	0%	-1.62%	+1.43%

The proposed A-PMP algorithm with the parameter chosen as: $\mu = 100$ is first implemented on the Level 1 powertrain to evaluate the performance. Three randomly picked driving cycles, Inspection and Maintenance Driving Cycle (IM240), Extra-Urban Driving Cycle (EUDC) and India Highway Driving Cycle (IHWY) are used. The results are shown in Table 4.8, the MPGe performance degradation is less than 0.3% compared with optimal performance (obtained by DP) in standard cycles and the ΔSOC is less than 2.2%. To evaluate the robustness of the A-PMP, UDDS driving cycle is combined with the Manhattan Bus Cycle (MNHA), which provides some unknown load variation in between of the driving cycles. A new generated synthetic driving cycles, UDDS 5000, is also used to evaluate the robustness of the proposed A-PMP. As seen in Table. 4.9, MPGe performance degradation is less than 1.7% compared with optimal performance for a 1.4 hrs drive.

More sensitivity analysis are performed to evaluate the effectiveness of the proposed A-PMP algorithm. Fig. 4.8 shows the fuel economy and charge sustaining performance evaluation with/without the additional penalty function. As can be seen, the charge sustaining performance is improved over the selected four representative driving cycles without loss of fuel economy. Fig. 4.9 provides the effects of the estimation error on the total travel time for US06 driving cycle. The performance indicates up to 20% estimation error can be accepted if the fuel economy degradation is less than 0.5%. The sensitivity analysis of weighting factor on fuel economy for US06 is shown in Fig. 4.10. The fuel economy is compared with the one with zero penalty ($\mu = 0$). It shows that the fuel economy can be improved by using larger weighting factor.

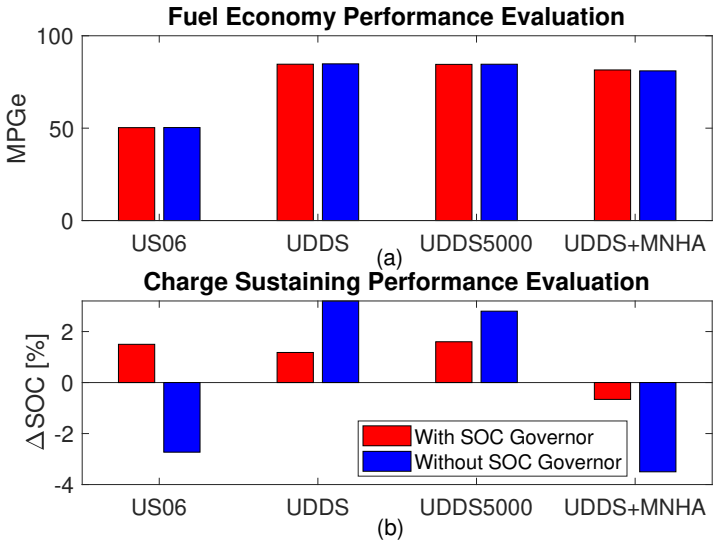

Figure 4.8: Effects of SOC governor on A-PMP algorithm: (a) fuel economy (MPGe) performance comparison, (b) charge sustaining performance (ΔSOC) comparison.

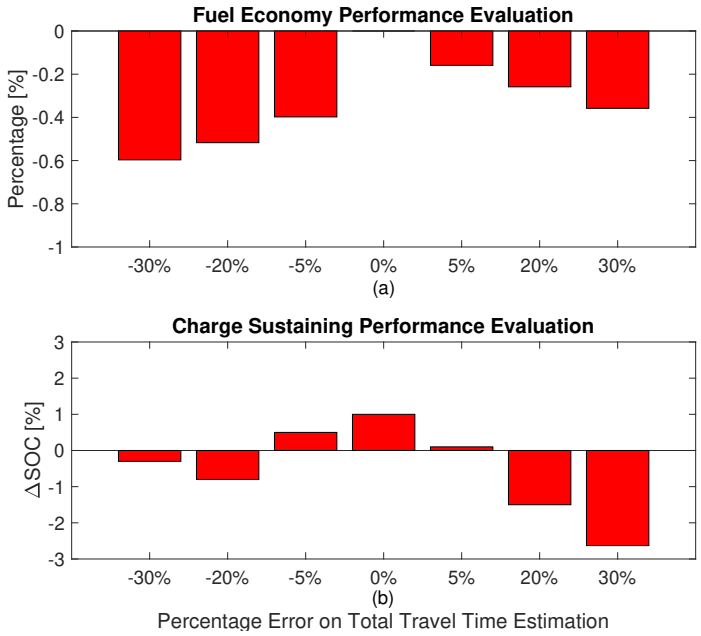

Figure 4.9: Effects of total travel time estimation error on A-PMP algorithm for US06 driving cycle, where T_{total} equals 600 s for perfect time estimation: (a) fuel economy (MPGe) performance comparing with perfect time estimation, (b) charge sustaining performance (Δ SOC) comparing with perfect time estimation.

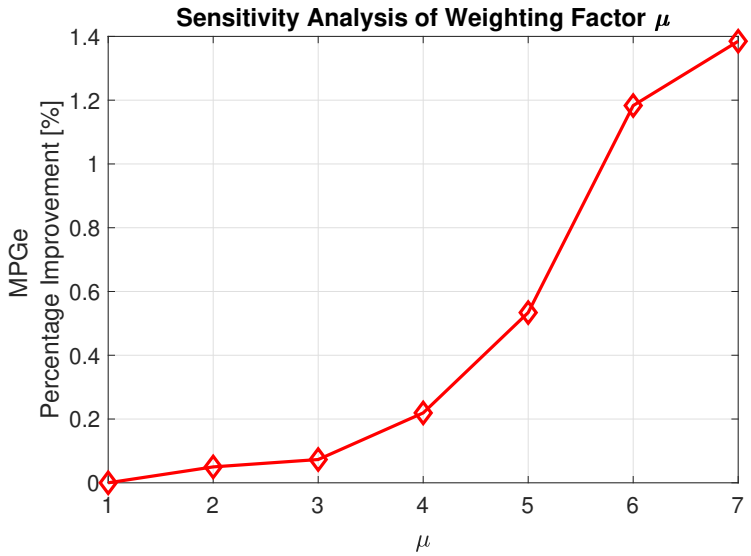

Figure 4.10: Sensitivity analysis of weighting factor on MPGe for US06 driving cycle (comparing with $\mu = 0$).

4.5 Validation of the A-PMP on a Proprietary High Fidelity FCV Powertrain Model

In this section, the proposed A-PMP algorithm is implemented on a proprietary high fidelity powertrain model. The proprietary high fidelity model consists of several subsystems: a driver model, an FCS, a battery system and auxiliary systems such as low voltage electronic devices, transmission, driveline, chassis, brakes and steering. It also includes the vehicle system control (VSC) with the proprietary energy management module. The current energy management uses a baseline strategy based on power demand and the actual battery SOC. This method works well on the dynamometers, but its calibration follows a trial and error method and is time consuming. Referring to the discussions in previous sections, the proposed A-PMP accomplishes the following objectives:

1. Achieving near-optimal fuel economy on every driving conditions.

2. Requiring minimal *a priori* knowledge about the driving cycle.

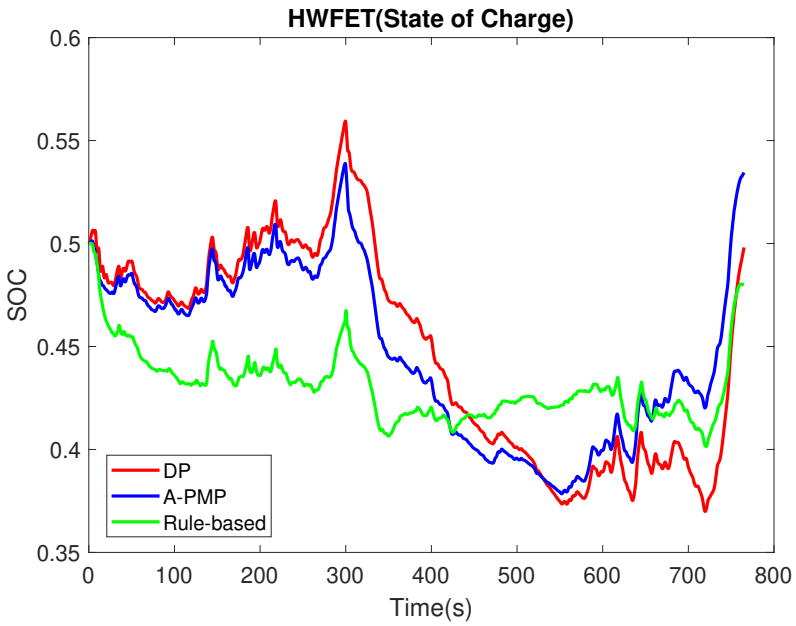

Figure 4.11: SOC trajectory for HWFET.

3. Maintaining charge-sustaining performance.

4. Assuring real-time implementable.

Results of A-PMP algorithm with SOC governor on three standard cycles (HWFET, UDDS and Federal Test Procedure 75 (FTP-75)) are summarized here. Table 4.8 compares the performance of three strategies on a proprietary high fidelity power-train model: the global optimal strategy obtained through DP, a rule-based control strategy used as a baseline, and the proposed A-PMP strategy. As stated previously, the PMP with an optimal estimation of the co-state variable provides a sub-optimal solution. The performance degradation compared with DP is within 0.55%, and the performance improvement compared with the baseline strategy is as high as 1.4%. Note that the proposed A-PMP only uses the total travel time as *a priori* information.

Fig. 4.11 and Fig. 4.12 shows the SOC trajectories of three algorithms. The SOC trajectories of A-PMP and DP on HWFET are nearly identical. The battery system is charged in the first half of the driving cycles and then discharged afterwards.

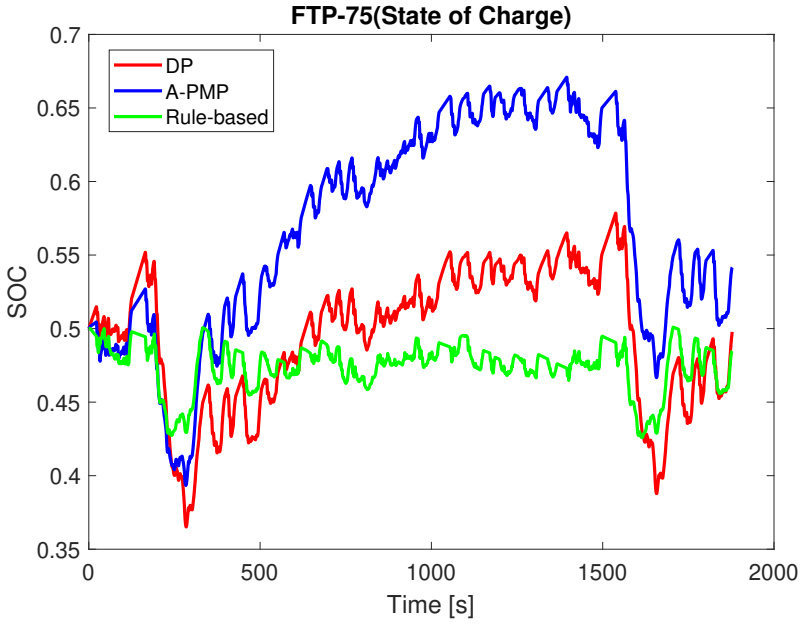

Figure 4.12: SOC trajectory for FTP-75.

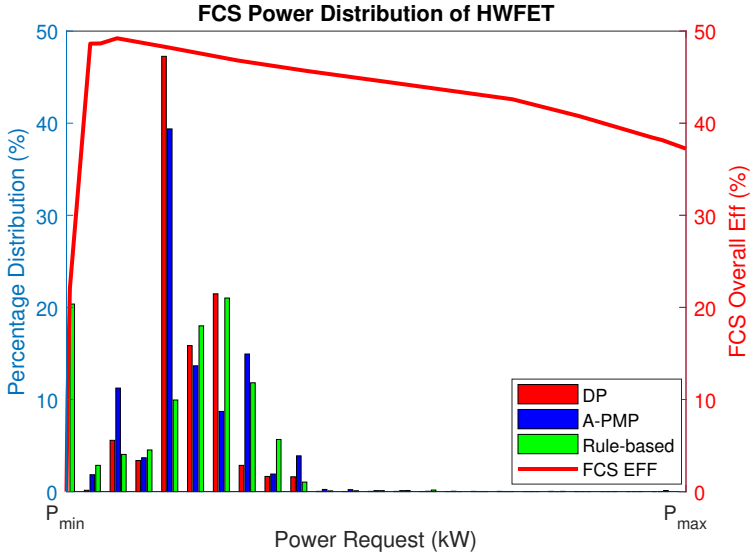

Figure 4.13: FCS net power distribution and the FCS efficiency of HWFET.

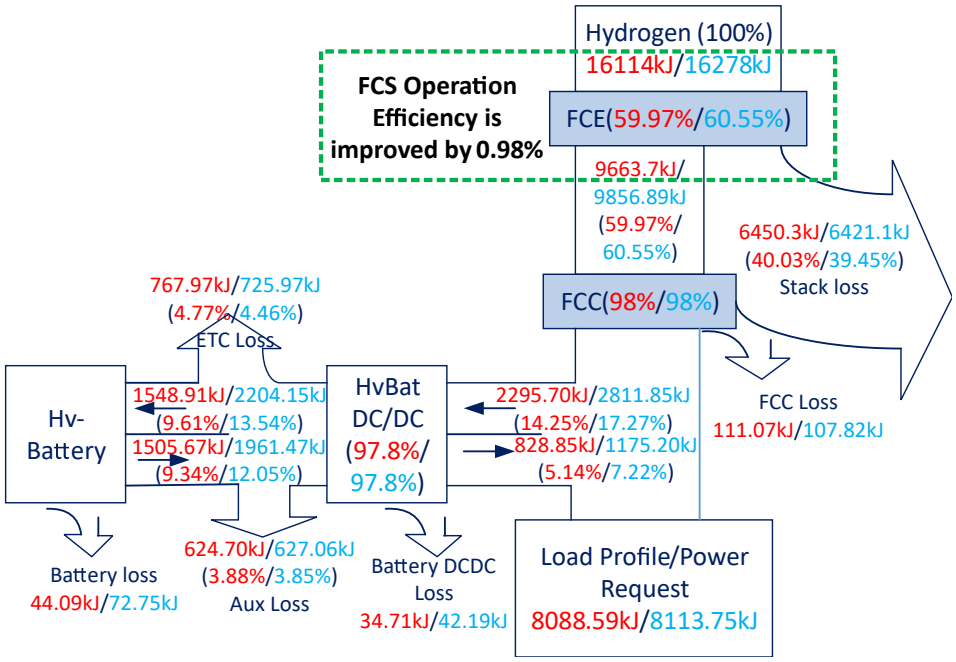

Figure 4.14: Energy flow of baseline strategy (red color) and A-PMP strategy (blue color) on HWFET cycle.

The baseline algorithm, however, has drastically different charging/discharging profile as it uses the battery very conservatively. On the other hand, there are noticeable differences in SOC trajectories between DP and A-PMP on the FTP-75, especially around 400 sec. This is due to the drastic change in driving conditions where the load profile changed quickly.

Table 4.10: Comparison of performances.

Cycle Name	Baseline	DP		A-PMP	
	MPG_e	MPG_e	Improv.	MPG_e	Improv.
HWFET	76.20	77.08	1.15(%)	77.04	1.10(%)
UDDS	65.80	71.11	8.07(%)	67.20	2.13(%)
FTP-75	64.90	69.51	7.10(%)	69.45	7.01(%)

To understand why A-PMP improves the fuel economy, the FCS net power distributions of these three strategies on HWFET cycle are plotted in Fig. 4.13. Furthermore, the energy flow chart of the baseline strategy and the A-PMP strategy are

compared in Fig. 4.14. From Fig. 4.13, the distribution of A-PMP is very similar to DP, where both strategies operate FCS near the optimal efficiency point. However, the baseline strategy does not account for FCS efficiency in the tuning process. Results in Fig. 4.14 show that the total traction power requested by the motor are almost the same ($8088.59kJ$ vs. $8113.75kJ$) in both strategies, which makes the efficiency and energy flows comparable. The A-PMP algorithm improves FCS efficiency from 59.97% to 60.55%. However, given the characteristic of the FCS, where the FCS efficiency curve is very flat over 80% of its operation range, the leverage is small. Additionally, a cost of improving the FCS efficiency is to operate the battery more aggressively. This can be observed from the battery loss, which increased from $44.09kJ$ to $72.75kJ$, and the total energy flow into the HvBat DC/DC, which increased from $2295.70kJ$ to $2811.85kJ$, and finally the total energy flow out of the HvBat DC/DC, which increased from $828.85kJ$ to $1175.20kJ$. Therefore, we can conclude that the energy management improves the FCS efficiency with a model-based optimization method.

4.6 Validation of the A-PMP Algorithm on HIL Lab and Testing Vehicle

4.6.1 Testing FCV

An FCV workhorse based on a Fusion Energi Plug-in Hybrid is selected as the testing vehicle to validate the proposed A-PMP algorithm. The system configuration is shown in Fig. 1.4. The FCS is the primary energy source. The power split between the FCS and the battery is attained by the power converters, as depicted in Fig. 1.4. A boost DC/DC converter is included to step up the voltage of the FCS. The testing vehicle has a Li-ion battery pack as the secondary power resource. A buck-boost converter is employed because of the bidirectional charging/discharging features of

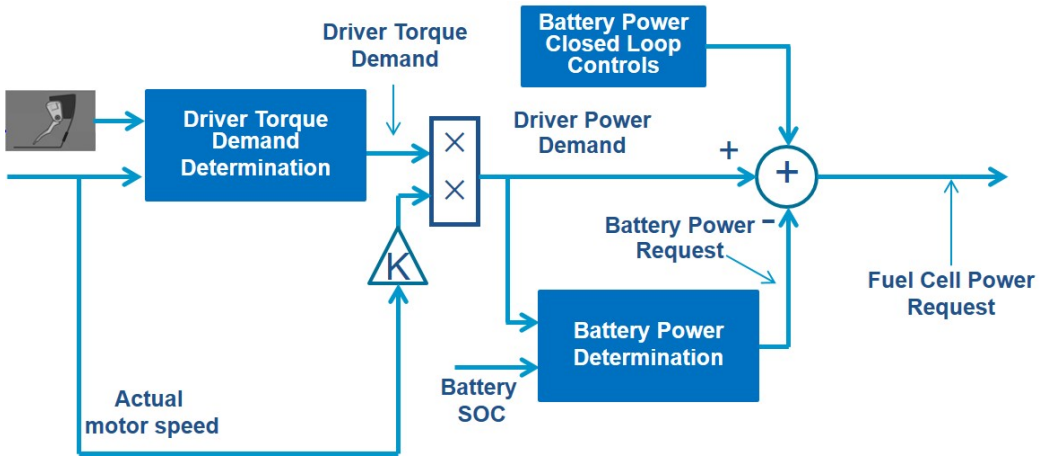

Figure 4.15: Testing FCV energy management scheme.

the battery. The chosen topology with 2 DC/DC converters for boosting the FCS stack voltage and the battery voltage provides the most flexibility for splitting power and isolating the source/load interactions. The testing FCV powertrain consists of a 125kW peak traction system, a 60kW Li-ion battery pack and a 65kW fuel cell engine.

A default energy management scheme is shown in Fig. 4.15. It relies on the rule-based control strategy and includes multiple temperature and operation dependent energy management look-up tables to decide the optimal battery power request. The rule-based energy management also includes the FCS start-stop mode and the ECU pull-up pull-down strategy which is detailed in Fig. 4.17. The inputs of those look-up tables are estimated drive power demand and the normalized battery SOC. The output is the optimal battery power. The FCS power request is then calculated by subtracting the driver power demand by battery power request. To compare the proposed A-PMP algorithm with a default rule-based control, the look-up tables are replaced by A-PMP algorithm, which is shown in Fig. 4.16.

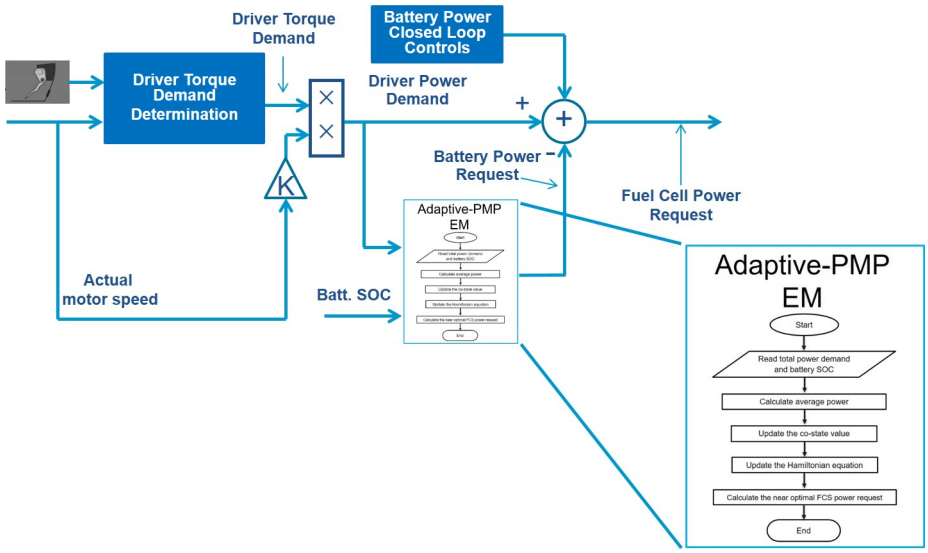

Figure 4.16: Real-time energy management using A-PMP on the testing vehicle.

4.6.2 HIL Test Results

HIL, is a technique that is used in the development and testing of complex real-time embedded systems. HIL simulation provides an effective platform to evaluate the control performance for the plant under control without involving real hardware. The proposed A-PMP is implemented in a Micro Auto Box (MABx), which is a compact, stand-alone prototyping unit with real-time hardware, I/O, and signal conditioning. This MABx also serves at the interface between all of the subsystem controllers and the vehicle control modules. The detailed setup of the HIL test is shown in Fig. 4.18. The signal interface was done using Controller Area Network (CAN) communication. The functionality of the proposed A-PMP algorithm was tested in the HIL lab. This test validated the communication established between the vehicle ECU and the MABx. The total power request signal and the high voltage battery SOC signal was sent from ECU to MABx. The A-PMP used those signals as input to calculate and provide the battery power request back to ECU to replace the default rule-based control command.

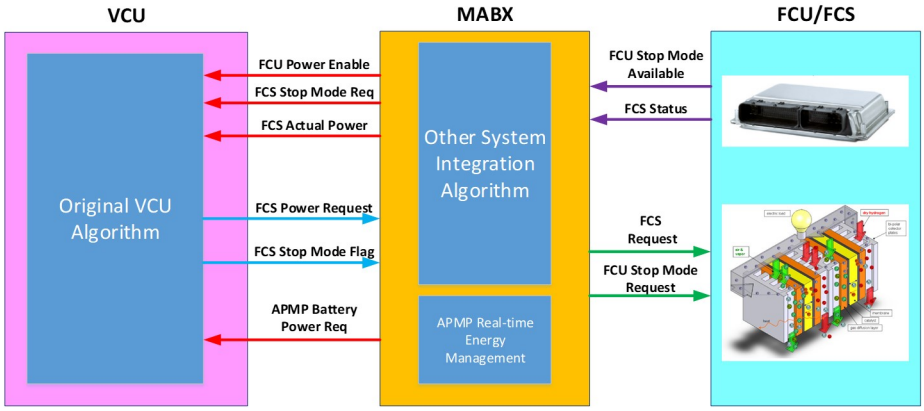

Figure 4.17: Testing FCV energy management main structure.

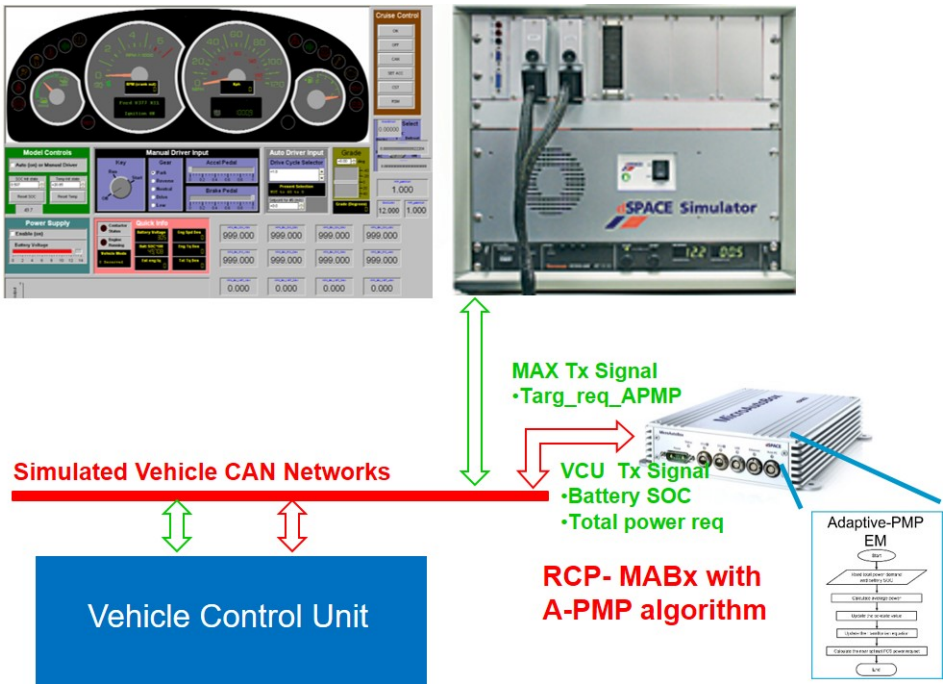

Figure 4.18: HIL test setup.

4.6.3 Vehicle Test Results

Vehicle tests are performed to validate that the proposed A-PMP algorithm can be implemented in real-time and the performance is compared with the default rule-based controller. UDDS driving cycle is a typical cycle which is used by the OEMs calibration team to generate the rule-based energy management controller. Thus, it is selected to validate the algorithm. Federal Test Procedure 4 (FTP-4) (each includes 2 UDDS with 10mins as the rest time in the middle for data saving and configuration) test, which is shown in Fig. 4.19, is chosen to validate the A-PMP algorithm on a Dyno Lab. The speed profile of the experiment tests are shown in Fig. 4.19(b). The speed difference between the two testing algorithm is very small, which makes the performance comparable. The FCS power demand and output are shown in Fig. 4.20 and 4.21. The hydrogen measurement device is not available on the vehicle, thus hydrogen consumption is calculated using the theoretical equation (2.2) in Chapter II, which is restated here:

$$W_{H_2} = \frac{I_{st} n_{cell} M_{H_2}}{2F}, \tag{4.10}$$

where I_{st} is the FCS stack current, n_{cell} is the number of cells in the stack, M_{H_2} is the molar mass of hydrogen, and F is the Faraday constant [38]. The equivalent hydrogen consumption is also calculated using the conversion equation (2.20) in Chapter II:

$$W_{Batt \to H_2} = \frac{-\Delta SOC \cdot E_{batt}}{\eta_{fcs} \eta_{Batt} \eta_{BDC} \eta_{FCC} Q_{HHV}^{H_2}}, \tag{4.11}$$

where E_{batt} is the battery capacity (kWh), η_{Batt} is the battery charging efficiency, η_{BDC} is the battery DC/DC efficiency, η_{FCC} is the FCS DC/DC efficiency, both of the DC/DC efficiency is calculated from the experiment data. The battery charging rate is assumed to be $2C$, which is used to converted the ΔSOC to equivalent hydro-

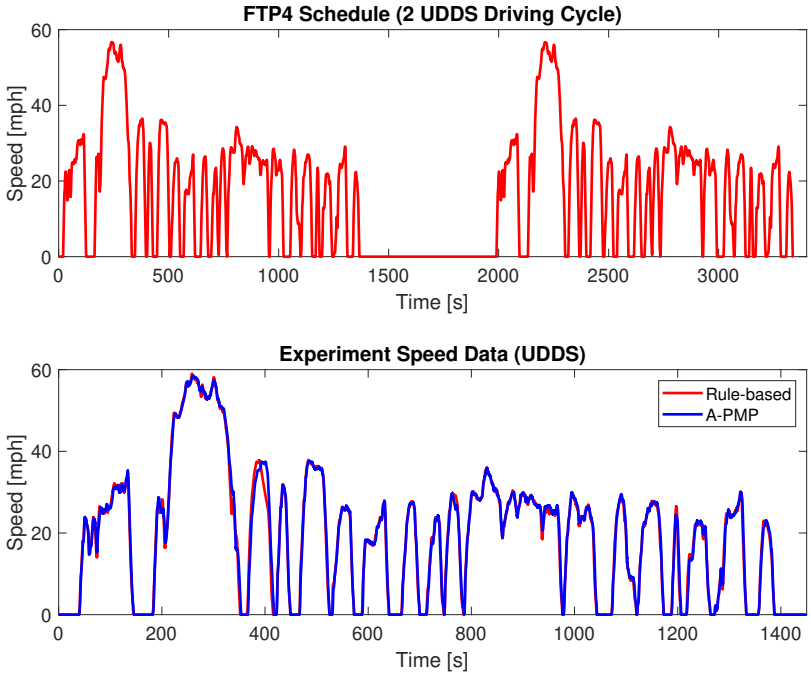

Figure 4.19: Speed profile of the vehicle tests: (a) FTP-4 driving cycle scheduled, (b) experiment data from the vehicle tests.

gen consumption. The system efficiency is calculated using the total electric energy divided by the total equivalent hydrogen energy consumption. The vehicle test results are shown in Table 4.11. Comparing the A-PMP method with the default rule-based method, the proposed A-PMP shows 7.2% reduction on equivalent hydrogen consumption, 6.8% improvement on electric system efficiency and 5.9% improvement on overall system efficiency.

The energy losses are compared for both strategies, and the energy flow chart is shown in Fig. 4.22. The FCS systems losses are compared in Table. 4.12, and the power distribution data are shown in Fig. 4.23 and 4.24. It could be easily observed that the A-PMP algorithm operates the FCS at a higher efficiency. All the other energy losses are shown in Table. 4.13.

However, charge sustaining performance failed during the vehicle tests. There are two reasons that cause this issue: FCS power command was not followed, thus the

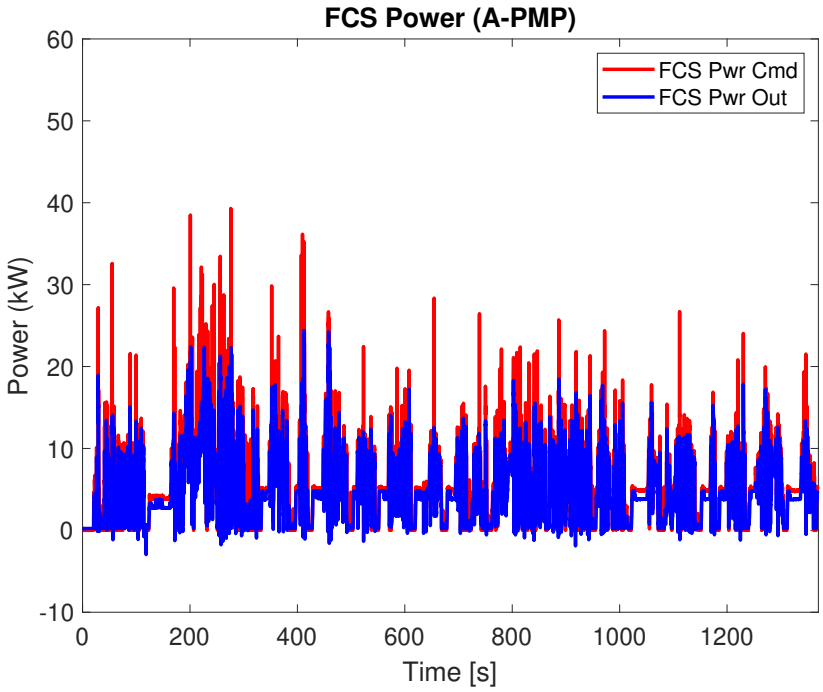

Figure 4.20: FCS power time trace data of A-PMP.

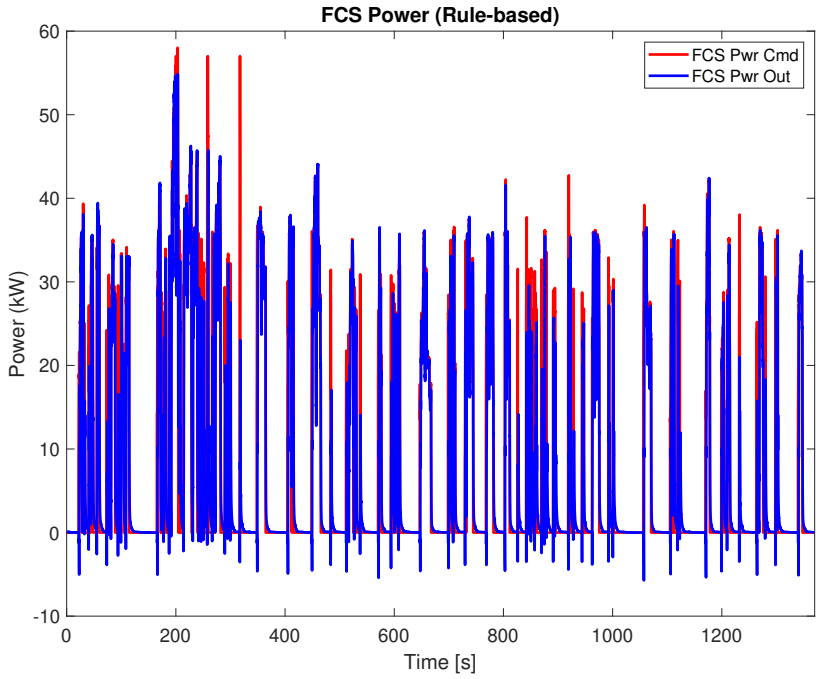

Figure 4.21: FCS power time trace data of a rule-based control.

Table 4.11: Performance evaluation on dyno tests.

	Ini SOC [%]	End SOC [%]	ΔSOC [%]	H_2 [g] (Calculated)	FCS EFF [%]	H_2E [g]	Total Elec Energy [kJ]	Elec SYS EFF [%]	Total Motor Energy [kJ]	Total Eff [%]
Rule-based	39.7	40.9	1.2	159.6	51.1	158.1	9500	50.1	5126	27.0
A-PMP	49.4	37.7	-11.7	99.9	55.5	146.7	9400	53.5	5036	28.6

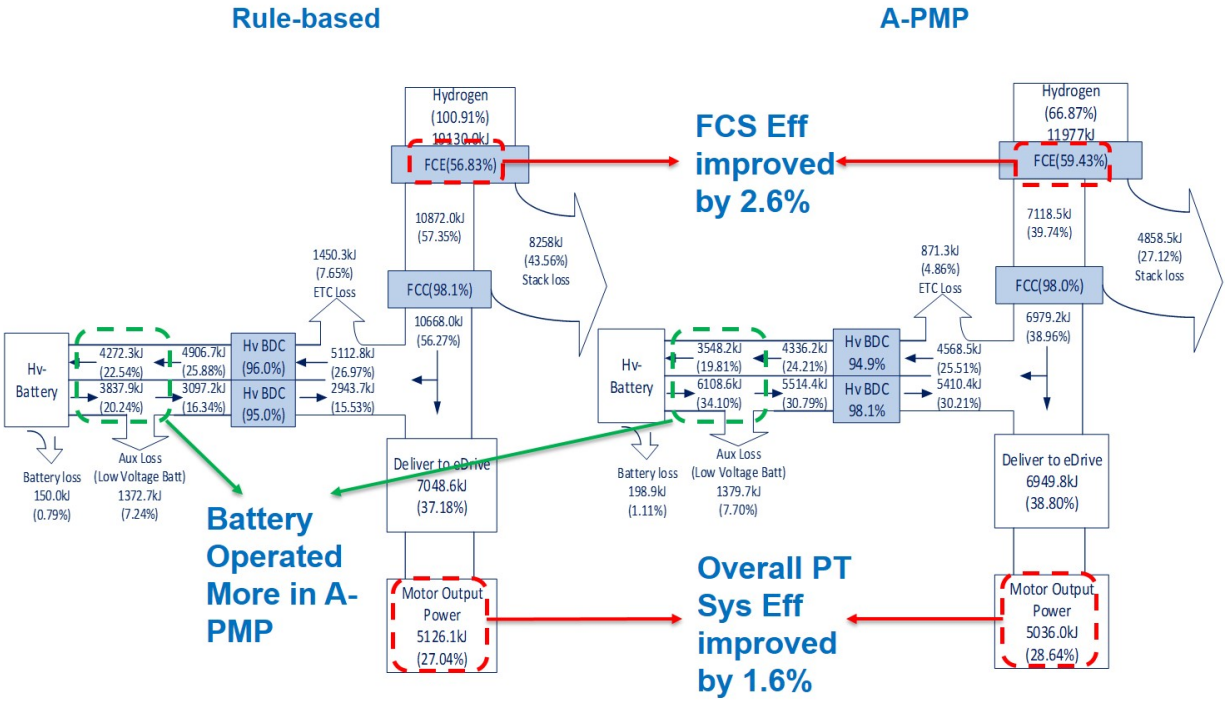

Figure 4.22: Comparison of energy flow chart of A-PMP and rule-based method.

Table 4.12: FCS energy efficiency comparison.

	Hydrogen Consumed Energy	FCS Eff (without ETC)	FCS Eff (with ETC)
Rule-based	19130.9kJ	56.83%	51.10%
A-PMP	11977kJ	59.43%	55.55%

Table 4.13: Energy consumption comparison.

	HV Battery Charging Energy	HV Battery Discharging Energy	Battery Energy Loss	Aux Loss	Energy Delivered to eDrive	Motor Output Energy
Rule-based	4272.3kJ	3837.9kJ	150kJ	1372.7kJ	7048.6kJ	5126.1kJ
A-PMP	3548.2kJ	6108.6kJ	198kJ	1379.7kJ	6949.8kJ	5036.0kJ

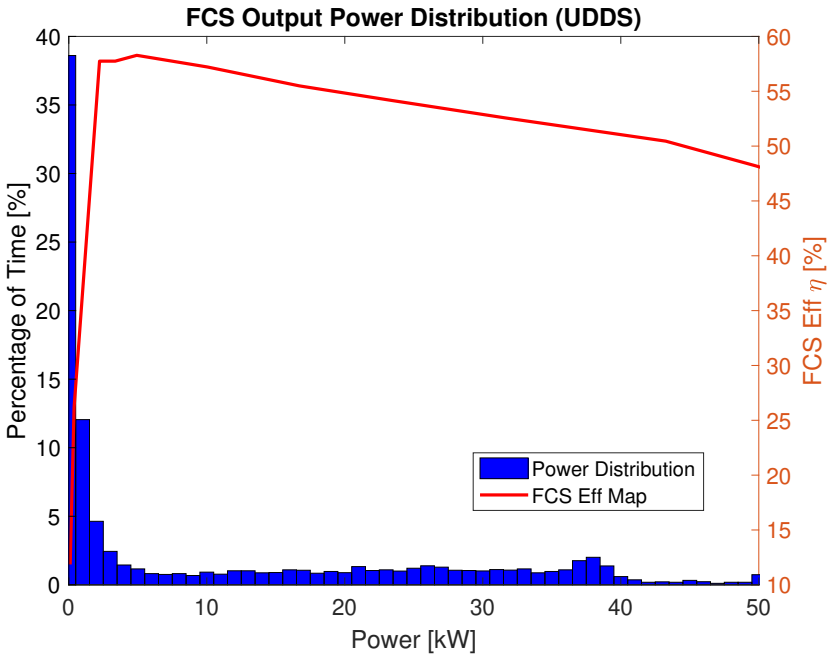

Figure 4.23: FCS output power distribution (Rule-based).

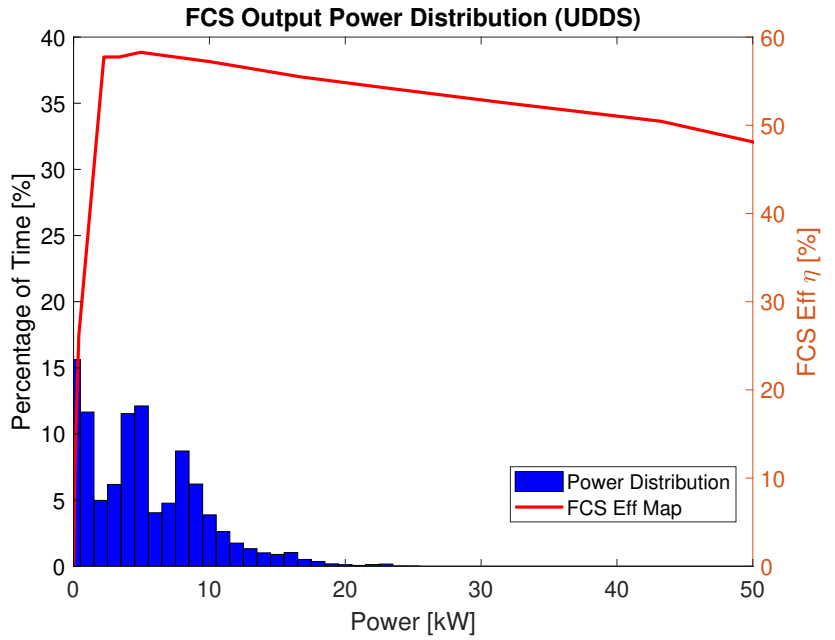

Figure 4.24: FCS output power distribution (A-PMP).

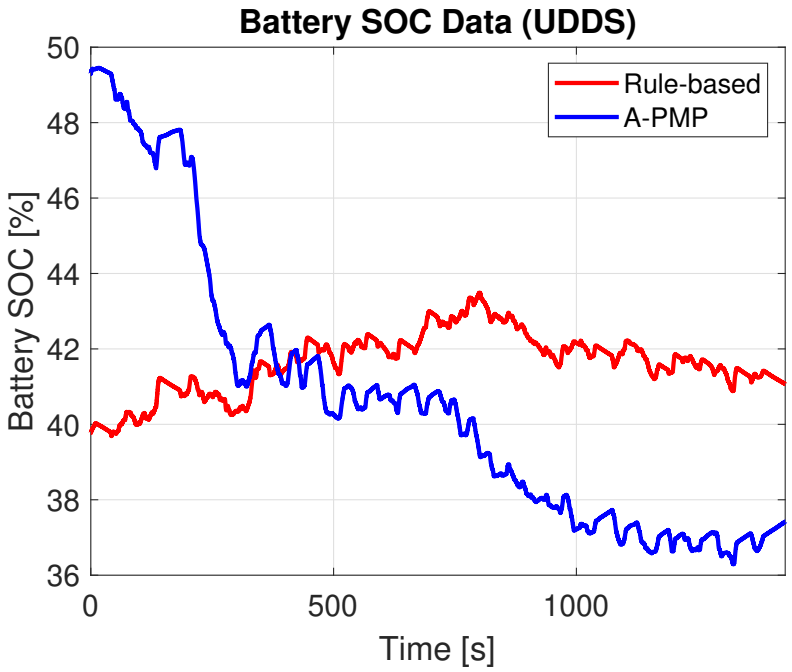

Figure 4.25: Comparison of battery SOC on rule-based control and A-PMP control on UDDS.

battery had to compensate the tracking error and battery SOC dropped faster; the penalty weighting factor of SOC governor was not large enough to compensate the effects of FCS dynamics. It should be noted that the Level 1 powertrain model does not consider FCS dynamics. Thus, ignoring FCS dynamics in energy management may lead to violation of charge sustaining.

In conclusion, the proposed A-PMP was successfully implemented on a FCV testing vehicle. The vehicle tests showed a potential improvement of using model-based real-time optimization on energy management. Future vehicle tests will focus on improving the charge sustaining performance by tuning of the parameters, while demonstrating appreciable fuel economy benefits.

4.7 Conclusion

In this chapter, we proposed an optimization-oriented supervisory controller based on PMP to obtain an on-road energy management strategy. This strategy uses travel

time as the only trip information to achieve charge sustaining performance. An FCV workhorse based on a Fusion Energi Plug-in Hybrid equipped with FCS, hydrogen storage, and Li-ion battery pack is considered as the representative powertrain system to validate the algorithm. Using a simple powertrain model to design A-PMP and implementing it on a proprietary high fidelity powertrain model without calibration, we have demonstrated improved performance compared to the proprietary baseline control strategy. Numerical simulation shows improvements ranging from 1.1% to 7.0% with regen braking on representative driving cycles. The proposed A-PMP algorithm has been validated through both the HIL test and vehicle test. The HIL test validates that the proposed algorithm is functionally implementable in real time. From the vehicle test results on UDDS, the A-PMP shows a potential improvement of 5.9% on overall system efficiency.

CHAPTER V

Hierarchical Controller Design for Real-Time Energy Management

As discussed in Chapter III and Chapter IV, one of the greatest challenges in achieving real-time energy management of FCVs is to mitigate the effects of FCS dynamics. The A-PMP algorithm proposed in Chapter IV does not consider the FCS transient dynamics. To address the aforementioned challenges imposed by the nature of the FCV real-time energy management problem, we propose a hierarchical optimal control strategy, which solves optimization problems associated with both long term optimal power split ratio and short term FCS transient power dynamics to achieve better fuel economy. The chapter is organized as follows: Section 5.1 details the problem formulation and the suggested control architecture; Section 5.2 evaluates the prescient APMP-MPC fuel economy performance on selected driving cycles; Section 5.3 performs the sensitivity analysis to load prediction error, and also analyzes the effect of load governor on reducing the sensitivity to the load prediction error; Section 5.4 provides the conclusion.

5.1 Problem Formulation and Proposed Control Architecture

Not considering FCS dynamics in energy management algorithm design may create problems, such as deteriorated power tracking (drivability), violations in charge sustaining, and a loss of fuel economy. Thus, the performance gap is identified to understand the motivation of introducing APMP-MPC control scheme. We apply the A-PMP algorithm to the Level 2 FCV powertrain model, where the FCS is modeled as a 1^{st} order LTI system and settling time equals to 5 s. The transfer function is:

$$P_{fc\_o} = \frac{-0.33s + 0.67}{s + 0.67}. \tag{5.1}$$

Fuel economy and charge sustaining performance (i.e. dSOC) are used as the main performance evaluation metrics in this section. From the simulation on the selected 12 driving cycles, the A-PMP can maintain a very good charge sustaining performance (Fig. 5.2). However, the fuel economy improvement is limited due to the effects of FCS transient power dynamics (Fig. 5.1). Potential improvements as large as 8% are identified on the US06 cycle.

Using a classical dynamic inversion based pre-compensator to mitigate the effects of FCS transient power is a possible solution. Four driving cycles, NYCC, US06, UDDS, and a California Unified Cycle (LA92) are selected to evaluate the performance of pre-compesator. The algorithm is similar to the pre-compensator proposed in Chapter II, however, the DP FCS power command is replaced by the A-PMP power command. The schematic of APMP with a Pre-compensator (APMP-Pre) controller is shown in Fig. 5.3. As shown in Fig. 5.4, given the non-minimum phase characteristics and the constraints on power command, the performance of the APMP-Pre algorithm is not very effective, even comparing with the A-PMP only algorithm. The reason is due to the high frequency of violations on FCS power command, which is

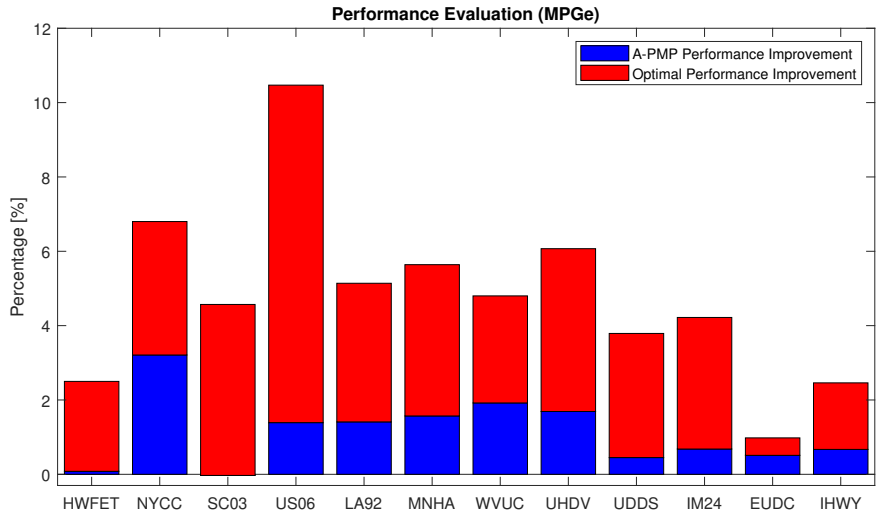

Figure 5.1: MPG_e performance evaluation on selected driving cycles. Blue color shows the performance improvement of A-PMP over the baseline load following algorithm. The combination of blue and red color shows the performance improvement of Level 2 DP over the baseline algorithm.

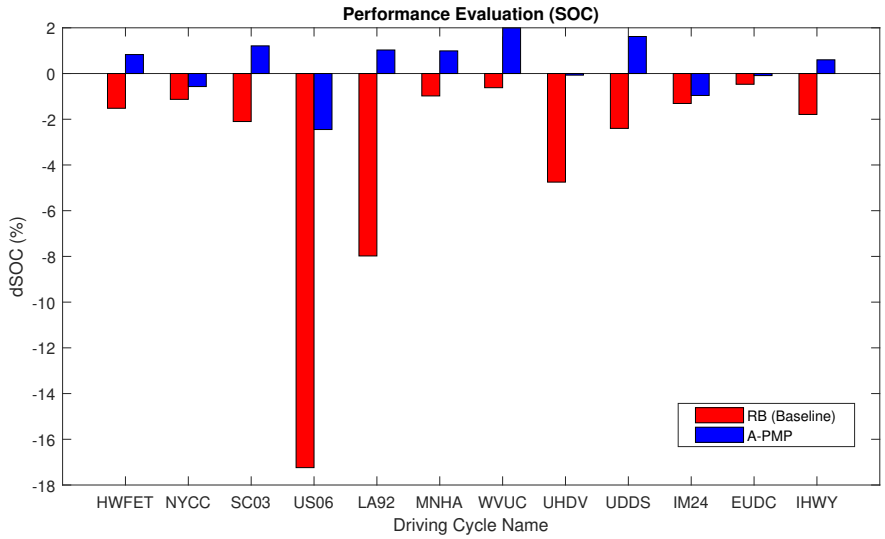

Figure 5.2: Charge sustaining performance evaluation on selected driving cycles. Blue color shows the dSOC of A-PMP. The red color shows the dSOC of the baseline algorithm.

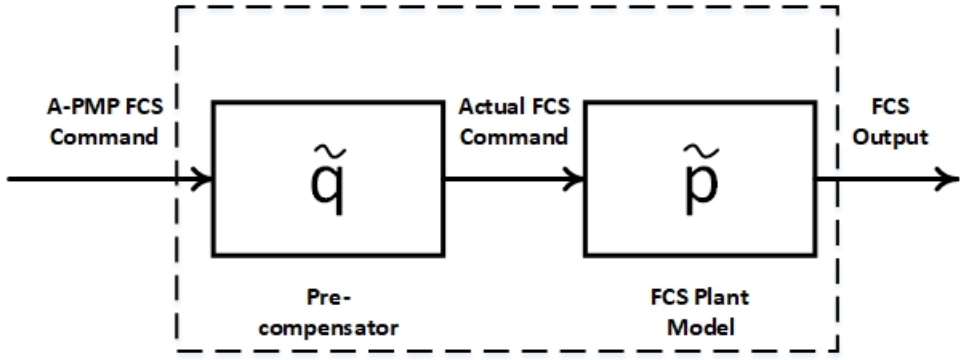

Figure 5.3: Schematic of APMP-Pre controller.

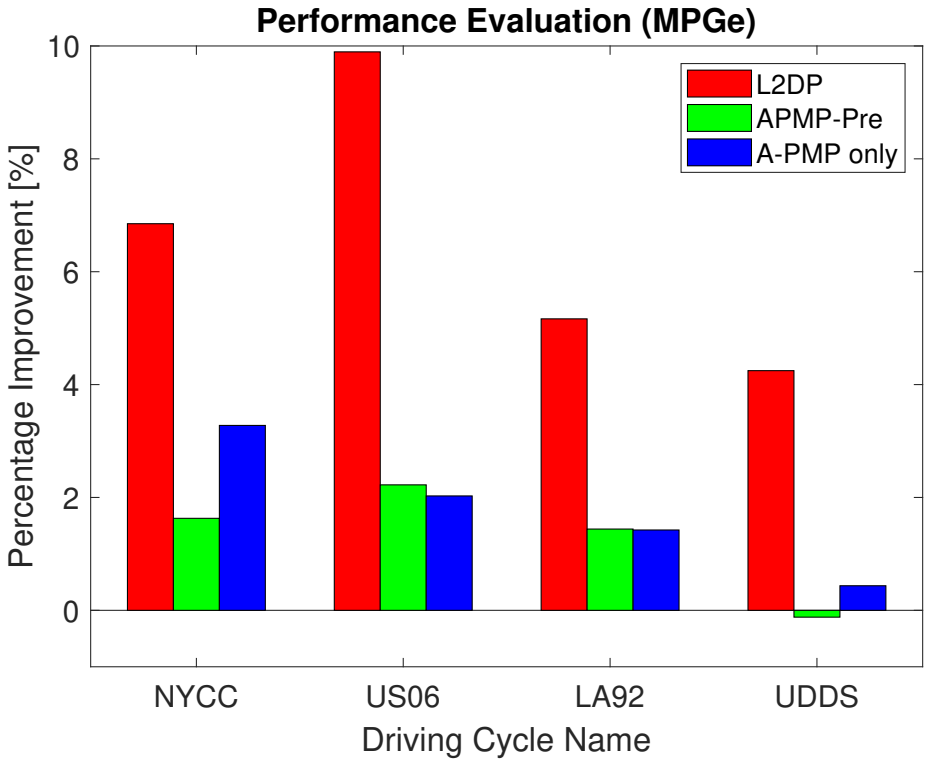

Figure 5.4: Fuel economy performance evaluation on four selected driving cycles.

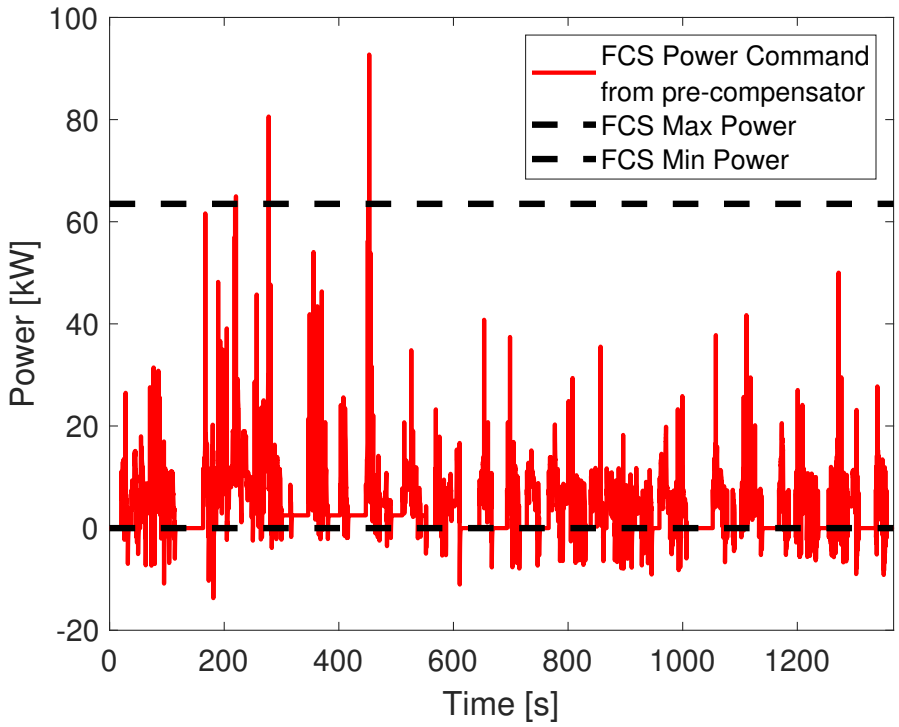

Figure 5.5: Violation of FCS power constraints on pre-compensator command for UDDS.

demonstrated in Fig. 5.5. This deviated the optimal FCS power trajectory and cause performance degradation. A better control structure to handle the FCS dynamics under constraints is necessary.

The ultimate real-time energy management should include the following functionalities:

- Satisfy the on-demand nature of the problem, which means the power request profile from the driver is not known a priori and the sub-optimal solutions need to be calculated in real-time.
- Achieve the charge sustaining performance over global time horizon.
- Handle presence of disturbance, such as sudden change of auxiliary power.
- Mitigate the effect of FCS power dynamics, which is modeled as an NMP system.

These characteristics make the control algorithm development quite challenging. Research on real-time energy management considering transient system response is very active and is motivated by the lack of tools to balance the time scale of the transient system behavior and the long prediction horizon. A multi-scale MPC framework has been proposed to address this problem [71]. The high level MPC operating at a slower rate acts as a long-term fuel and battery SOC optimization controller, while the low level MPC works at a higher sampling rate and calculates the control inputs so that a smooth supply of the driver torque demand is achieved. However, to satisfy charge sustaining performance over the global time horizon via MPC, either approximating the cost-to-go function, or regulating the terminal SOC reference in each control horizon has to be employed [72]. The first method is too complicated to generalize and it requires information of the driving cycles, the second method is very conservative. From another point of view, PMP based methods have been identified as potential candidates to handle FCS dynamics, however, to include the

FCS dynamics into PMP problem formulation means to introduce another co-state variable. Introducing additional co-state variables will make it more challenging to solve the optimal co-state values offline, not to mention online implementation.

The hierarchical control schematic is then shown in Fig. 5.6, which includes three key components of the proposed APMP-MPC controller. The three components are load prediction, high level A-PMP algorithm, and low level MPC controller, whose functions will be discussed in detail in the following subsections.

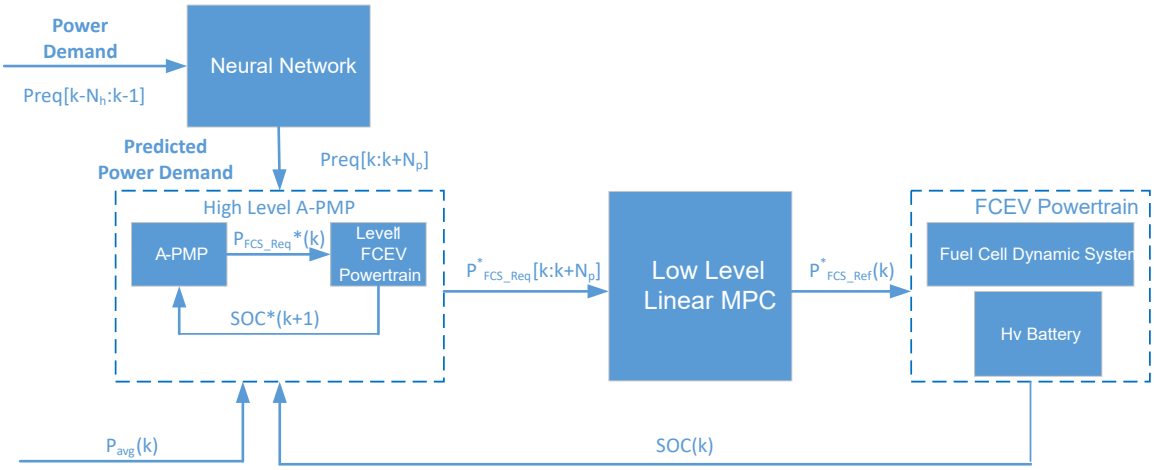

Figure 5.6: Schematic of proposed hierarchical controller.

5.1.1 Load Prediction

One of the essential elements in implementing MPC is the future driving information. Current solutions to load prediction fall into two main categories: one is GPS/ITS based prediction [73], the other is statistics and cluster analysis based method [74]. A detailed review on driving condition prediction can be found in [75]. To implement a close-to-perfect load prediction is beyond the scope of our study, thus, only simple prediction methods are used to evaluate the performance of the proposed APMP-MPC. In this proposal, we first used presient MPC, and this type of MPC assumes all short term future load information are known. In other words, the predicted power demand sequence is assumed to be perfect. The proposed hierarchical

controller will be referred to as a Prescient APMP-MPC. This type of MPC cannot be applied in real time because of the unrealistic assumption of known load profile, but it provides an assessment of the best achievable performance.

5.1.2 High Level A-PMP Algorithm

The high level A-PMP algorithm uses the predicted power demand sequence P_{req}[k:k+N_p] as the input to predict FCS power demand sequence $P^*_{FCS\_Req}$[k:k+N_p] for the low level MPC controller. In this chapter, we use $x[k_1 : k_2](k_2 > k_1)$ to denote the sequence of $x(k_1), x(k_1 + 1), ..., x(k_2)$. Thus, at each time k, the A-PMP needs to solve the Hamiltonian equation N_p times, where N_p is the prediction horizon:

$$u^*[k : k + N_p] = \underset{u[k:k+N_p]}{\operatorname{argmin}} H(SOC[k : k + N_p], u[k : k + N_p], [k : k + N_p], \lambda[k : k + N_p]), \tag{5.2}$$

which is updated using (4.5). The Hamiltonian which needs to be minimized at each time k is given by (4.11). The detailed high level algorithm is summarized below:
Algorithm 5.1:

1. Step 1: At travel time k, generate the predicted power demand sequence: P_{req}[k:k+N_p].

2. Step 2: Define a new variable, t_h, with the initial value of 0, which is the time stamp along the prediction horizon N_p. Request the following input information from ECU: $P_{avg}(k)$, $SOC(k)$, $P_{req}(k)$.

3. Step 3: Use $P_{avg}(k + t_h)$, $P_{req}(k + t_h)$ and $SOC(k + t_h)$ as inputs to determine the FCS power request $P^*_{FCS\_Req}(k + t_h)$ by solving (3.5), with the updated Hamiltonian equation (3.11).

4. Step 4: If $t_h < N_p$, the following actions are performed:

(a) Feed the FCS power request $P^*_{FCS\_Req}(k+t_h)$ to the Level 1 FCV powertrain system model and compute the $SOC^*(k+t_h+1)$, and update the average power using:

$$P_{avg}(k+t_h+1) = \frac{P_{req}(k+t_h+1)\Delta t + (k+t_h)\Delta t P_{avg}(k+t_h)}{(k+t_h+1)\Delta t}. \quad (5.3)$$

(b) Update $\lambda(k+t_h+1)$ and $\gamma(SOC, k+t_h+1)$ using $P_{avg}(k+t_h+1)$ and $SOC(k+t_h+1)$.

(c) Set $t_h = t_h + 1$.

(d) Repeat steps 3, 4(a), 4(b), 4(c) until $t_h = N_p$.

5. Step 5: When $t_h > N_p$, assemble the predicted FCS power demand sequence $P^*_{FCS\_Req}$[k:k+N_p] and send to low level MPC controller.

Remark 5.1.1 It needs to be re-emphasized that the A-PMP algorithm is utilized for primarily two reasons:

- Directly using MPC could potentially pose an issue with approximating the long term cost-to-go function. This approximation is used to convert the terminal constraints to the constraints under each prediction horizon. This approximation approach is either a case-by-case estimation based on the driving condition, or too conservative that it is unable to produce optimal solution [72, 74]. The A-PMP method, proposed in Chapter IV, demonstrates capability to overcome this issue.

- Another advantage of using A-PMP is to solve energy management problem of not requiring the driving cycle information a priori.

5.1.3 Low Level MPC Controller Design

The low level MPC controller aims at tracking the FCS power request sequence generated by the high level A-PMP. To ensure that output command is tracked, we define an augmented system with the extended state $z_k = [x_k^T \ u_{k-1}^T \ r_k^T]^T$, where z_k is the augmented state, x_k is the FCS dynamic state, u_{k-1} is the FCS power command at the time instant k-1, which is used to update the power command u_k, and r_k is the specified tracking command. For the augmented system, the tracking error can be defined as the output explicitly. In our study, we modified the conventional tracking Linear Quadratic-Model Predictive Controller (LQ-MPC) problem to suit our case. The objective of the conventional tracking LQ-MPC is to follow a specified command (set-point) r. Specifically, if $r \equiv$ const, the control design objective is to achieve convergence of the output to the command:

$$y_k \to r \ as \ k \to \infty. \tag{5.4}$$

Equation (5.4) is known as the offset free tracking property. It is used even when command r is slowly varying. However, the power command varies quickly, which violates the constant set-point tracking assumption. To avoid violation of assumption, we set r_k as zero, which is used as a constant tracking command. The FCS power request $P^*_{FCS\_Req}(k)$ is defined as w_k which is treated as a disturbance in the output dynamics. Thus, the augmented system dynamics are:

$$x_{k+1} = Ax_k + Bu_k \tag{5.5}$$

$$u_k = u_{k-1} + \Delta u_k \tag{5.6}$$

$$r_{k+1} = r_k \tag{5.7}$$

where Δu_k is the difference between u_k and u_{k-1}. The output, which is the tracking error, equals to:

$$e_k = \begin{bmatrix} C_k & D_k & -1 \end{bmatrix} z_k + D_k \Delta u_k - w_k, \tag{5.8}$$

where w_k is a power disturbance, which equals the FCS power reference. The cost function that captures the tracking performance is given by:

$$J = \sum_{i=k}^{k+N_p} e_i^T Q_e e_i + \Delta u_i^T R \Delta u_i, \tag{5.9}$$

where e_k is the FCS power tracking error at time k, Q_e is the error state cost, and R is the control input cost. Then the tracking problem can be formulated as an LQ-MPC problem with a prediction horizon N_p, given as:

$$\Delta u[k : k + N_p]^\star = \underset{\Delta u[k:k+N_p]}{\operatorname{argmin}} \; J, \tag{5.10}$$

This optimization is subject to three constraints:

1. System dynamics:

$$z_{k+1} = \begin{bmatrix} A_k & B_k & 0 \\ 0 & I & 0 \\ 0 & 0 & I \end{bmatrix} z_k + \begin{bmatrix} B_k \\ I \\ 0 \end{bmatrix} \Delta u_k, \tag{5.11}$$

$$e_k = \begin{bmatrix} C_k & D_k & -I \end{bmatrix} z_k + D_k \Delta u_k - I w_k. \tag{5.12}$$

2. Power limits:

$$z_k(2) + \Delta u_k \leq u_{max} \tag{5.13}$$

$$-z_k(2) - \Delta u_k \leq u_{min} \tag{5.14}$$

$$-(e_k + w_k) \leq 0 \tag{5.15}$$

$$e_k + w_k \leq y_{max} \tag{5.16}$$

where $e_k + w_k$ is the actual FCS power output $P_{fc\_o}(k)$, and $z_k(2)$ is u_{k-1}.

3. FCS power slew rate:

$$|\Delta u_k| \leq S \tag{5.17}$$

where S is the maximum slew rate of the FCS power.

We can now summarize the proposed control algorithm.

Algorithm 5.2: Given the predicted power request $P_{req}[k : k+N]$, the APMP-MPC is proposed to solve the optimization problem:

1. Step 1 to Step 5 are the same as the Algorithm 5.1.

2. Step 6: Solve the MPC tracking problem using CVXgen, retrieve the optimal control command Δu_k, update the FCS power request command as:

$$u(k) = u(k-1) + \Delta u_k. \tag{5.18}$$

3. Step 7: Update the current travel time $k = k + 1$, until it reaches $k_0 + N - 1$.

The flow chart in Fig. 5.7 illustrates the main steps of APMP-MPC algorithm.

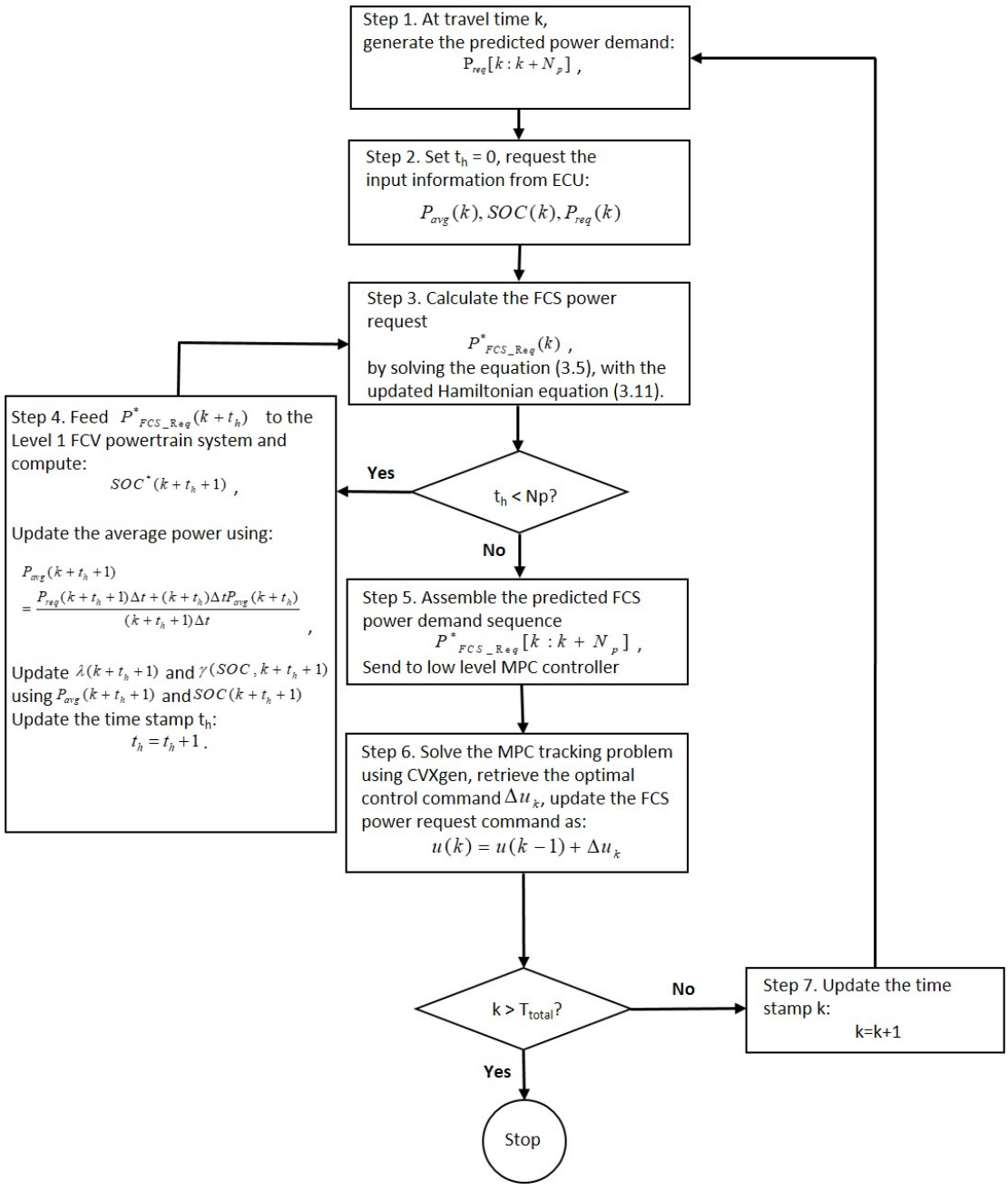

Figure 5.7: Flowchart of APMP-MPC algorithm.

5.2 Performance Evaluation of Prescient APMP-MPC

The US06 cycle is used at the beginning of the evaluation to prove the effectiveness of the proposed APMP-MPC controller. Fig. 5.8 compares the performance of five strategies on the Level 2 powertrain model: (1) the global optimal strategy obtained through Level 2 DP, (2) the A-PMP strategy, (3) the proposed APMP-MPC strategy, the prediction horizon is 5s, which is the settling time of the FCS power dynamics, (4) the PMP+MPC strategy that uses the offline calculated optimal lambda for the high level A-PMP algorithm, and (5) the baseline strategy which uses a simple FCS load following controller. The first four algorithms are compared with the baseline controller and the percentage improvements are shown in Fig. 5.8. As stated previously, the A-PMP controller has as large as 8% of MPGe degradation compared to the Level 2 DP controller. This degradation can be mitigated by using APMP-MPC, and the resulting improvement of MPGe is 5.95%. Fig. 5.9 shows the SOC trajectories of four algorithms. The SOC trajectories of APMP-MPC and DP on US06 are nearly identical. The baseline algorithm, however, has very different charging/discharging performance as the battery only works passively to compensate for the power deficiency generated by the FCS transient dynamics. MPC tracking performance is also shown in Fig. 5.10, and a large error in the estimation of co-state value is found when the load changes rapidly.

Followed by the US06 cycle, four additional representative cycles, NYCC, UDDS, US06 and LA92, are selected to evaluate the performance of the proposed controller. These driving cycles cover both the city cycles and the high load aggressive cycles. Fig. 5.11 shows MPGe improvements of APMP-MPC over APMP are ranging between 0.23% to 5.95%, depending on the driving cycle. The city cycles, NYCC and UDDS may not have a promising fuel economy improvement because they comprise of frequent start-stops. This feature makes the MPC controller work around the low power request and activate the constraints more frequently, which deviates the op-

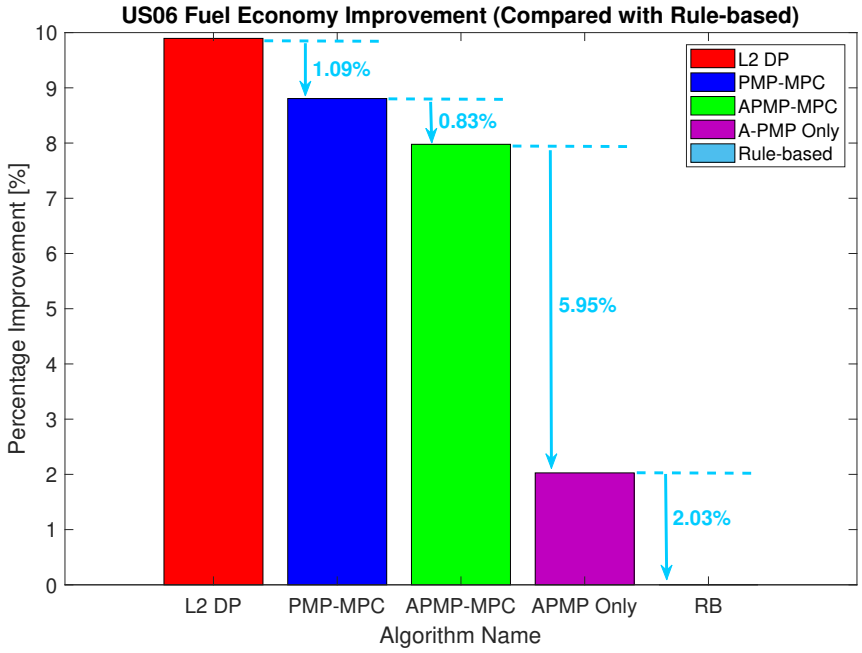

Figure 5.8: US06 fuel economy improvement.

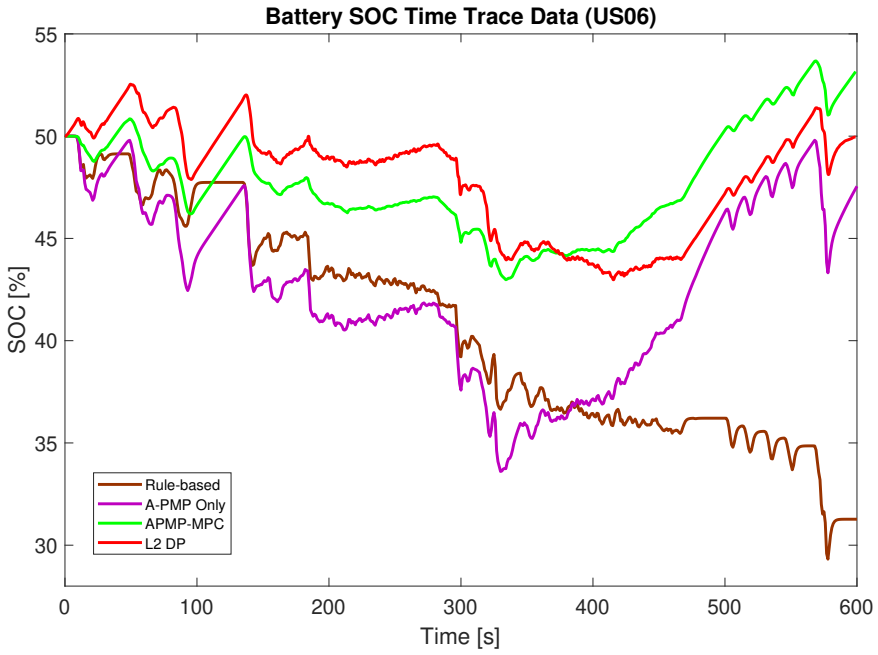

Figure 5.9: Battery SOC trajectory comparison on US06.

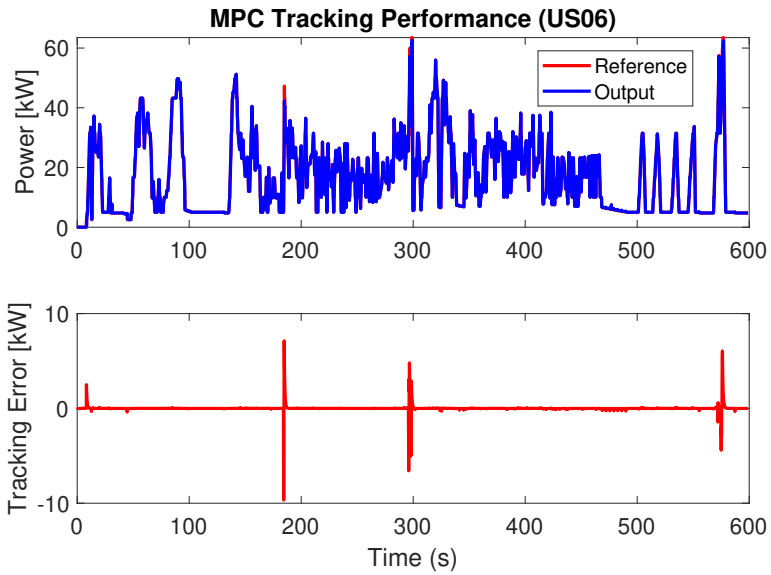

Figure 5.10: MPC tracking performance evaluation.

timal trajectory higher. On the other hand, there are noticeable differences in SOC trajectories between Level 2 DP and APMP-MPC on the UDDS and LA92 cycles (Fig. 5.12 and Fig. 5.13). Difference between the former is due to the drastic change in driving conditions, where the load profile changes quickly. Difference in the latter is due to inaccuracy of initial estimation for the co-state value on LA92.

Simulation time is dependent on hardware used. In our case, the algorithm is simulated using an eight core Intel Xeon CPU with 3.40 GHz and 16 GB RAM. The simulation time and the travel time information is shown in Table 5.1. The simulation time is one third of the real time, which implies a good opportunity to apply APMP-MPC in real-time. Moreover, the MPC solver adopted here, CVXGEN, is claimed as the fastest linear MPC solver in the world that provides the interface c-code and simplifies implementation in vehicles. Comparing with the computation time of APMP-Pre, which is shown in Table 5.2, the computation complexity is higher since the pre-compensator is a simple feed-forward controller and it can be computed quickly.

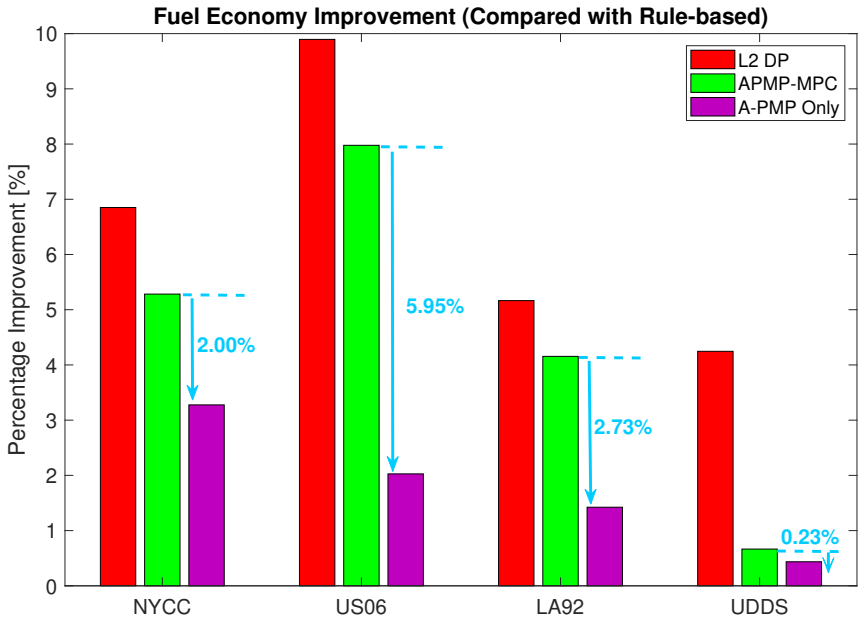

Figure 5.11: Fuel economy improvement on selected driving cycles.

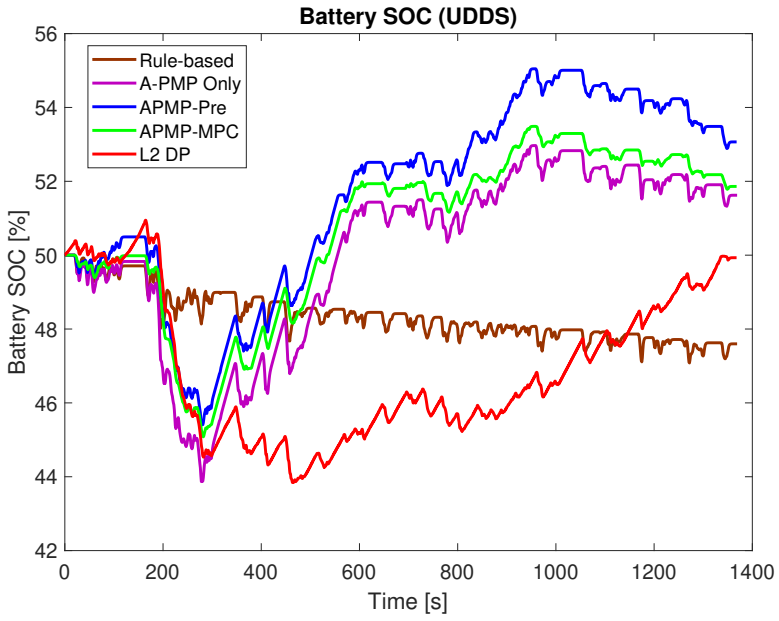

Figure 5.12: Battery SOC trajectory comparison on UDDS.

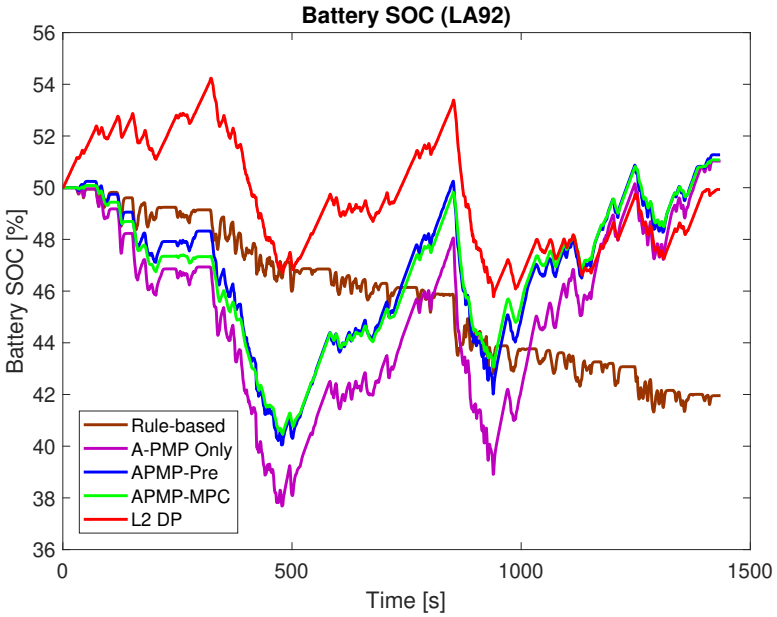

Figure 5.13: Battery SOC trajectory comparison on LA92.

Table 5.1: Computation time of the proposed APMP-MPC algorithm.

Driving Cycle	Travel Time (s)	Simulation Time (s)
NYCC	598	202
US06	600	207
LA92	1435	498
UDDS	1368	469

The simulation results are generated using an eight core Intel Xeon CPU with 3.40 GHz and 16 GB RAM.

Table 5.2: Computation time of the APMP-Pre algorithm.

Driving Cycle	Travel Time (s)	Simulation Time (s)
NYCC	598	28.8
US06	600	29.6
LA92	1435	60.9
UDDS	1368	58.9

The simulation results are generated using an eight core Intel Xeon CPU with 3.40 GHz and 16 GB RAM.

5.3 Effects of Load Prediction Error on the APMP-MPC Performance

As demonstrated in Section 5.2, the benefits of the Prescient APMP-MPC algorithm are based on the assumption of perfect load prediction. The Prescient APMP-MPC cannot be applied in real time because of the unrealistic assumption, but can be used to evaluate and compare with other APMP-MPC-based power management strategies. To achieve this goal, this section discusses the effects of load prediction error on the fuel economy performance. Different load prediction methods, referred to as Frozen Time (FT) APMP-MPC, Exponential Varying (Exp) APMP-MPC, Preview APMP-MPC are proposed and their performance are evaluated. Additionally, a rate load limiter that can reduce the effects of prediction error is imposed and sensitivity analysis is conducted.

5.3.1 Horizon Load Predictors

Horizon load predictors can be divided into two main categories. The first one is model-based, and the other is GPS and Intelligent Transportation System (ITS) based [75]. It needs to be emphasized here that most of the up-to-date load predictors are velocity predictors [74]. The load profiles are then calculated using the power demand generation equations. In the model-based methods, a good understanding of the combined system of drivers and vehicle dynamics is required to extract a parametric model to predict the load requirements. This means that a better prediction on driver behavior also needs to be considered during the load predictions. In our study, the prediction horizon needs to be up to 5 s. In reality, the relationship between predicted future velocities and total fuel consumption is very complicated. Without any load condition preview, it is almost impossible to extract a perfect prediction longer than 5 s. Simpler model-based predictors can also be found in literature [49,

72, 76, 77, 78]. Di Cairano et al. introduces the FT MPC [76] where the same amount of power demand as that of the current step over the entire prediction horizon. Its performance heavily depends on the load fluctuation rate. Bohan et al. [78] and Sun et al. [72] present the exponential varying based load predictor, where the unknown driver demand torque is assumed to be exponentially decreasing and the velocity is also varying exponentially. This prediction method relies on the exponential-varying assumption of the future driving information, which impedes its extensive application if the assumption is violated. Another highly adopted prediction method is solving dynamic decision-making problems by using Markov chain. This stochastic method is used by [49, 76, 77] to design stochastic MPC. The driver behavior is modeled as a Markov chain based on standard cycles.

The second category, which includes data driven methods, can be further divided into two classes. The first one uses using artificial intelligence methods, such as neural network [79], fuzzy logic pattern recognition [80] or support vector machine [81]. The prediction accuracy of these approaches highly depends on the chosen standard driving cycles. One may end up with under-fitting or over-fitting the data and getting unrealistic results. The challenges of aforementioned prediction problem can be alleviated by involving more advanced techniques in ITS [73, 82, 83, 84]. Fig. 5.14 demonstrates a recent idea proposed by Sun et al. [73]: through using onboard GPS, those vehicular telemetry technologies have enabled vehicles to access information of the traffic and road conditions. These information can be extracted from vehicle-to-vehicle or vehicle-to-infrastructure communications using onboard sensors. These advanced technologies motivate us to consider load preview information while evaluating load prediction errors. In our study, due to the limitations of the ITS data and the lack of driver data to implement artificial intelligence methods, three horizon load predictors are selected and investigated to understand the effects of load prediction error on APMP-MPC algorithm:

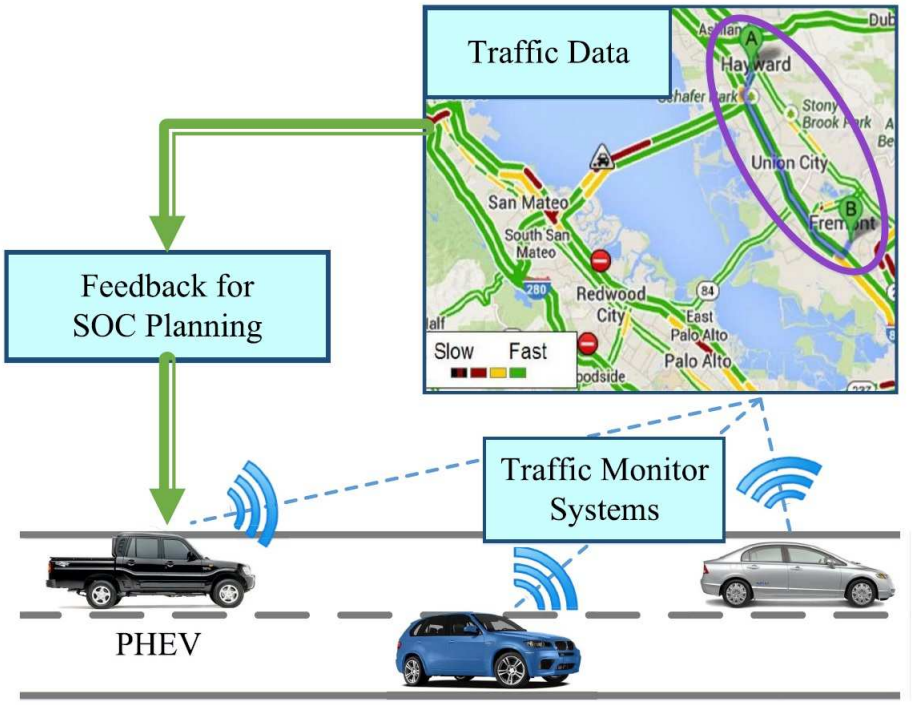

Figure 5.14: Traffic flow provided by Google maps [5].

- Frozen-time load predictors [74]:

$$P_{req}(k+i) = P_{req}(k), i = 1, ..., N_p. \tag{5.19}$$

This predictor assumes the power demand to be constant in the entire prediction horizon. It is simple and can be used as a baseline to evaluate fuel economy performance, but it does not incorporate any preview information and can not predict well for fast load changes.

- Exponentially varying load predictors:

$$P_{req}(k+i) = P_{req}(k) * (1+\epsilon)^i, for\ i = 1, 2, ..., N_p, \tag{5.20}$$

where i is the time step and ϵ is the parameter. Instead of using both the exponentially varying torque and velocity equations as shown in [74], our study

directly predicts the load since both the FCS and battery are electric power resources.

- Load predictors with preview information:

$$P_{req\_pred}(k+i) = P_{req}(k+i) + \beta * i * P_{req}(k+i), for\ i = 1, 2, ..., N_p, \quad (5.21)$$

where β is the weighting factor of the prediction error. The first part, $Preq(k+i)$, represents the perfect load at time $k+i$ which is available from the advanced ITS technology. The second part, $\beta * i * Preq(k+i)$ represents a percentage relative error which can be treated as a signal disturbance, and it is a time varying load prediction error. The maximum percentage variation over the entire prediction horizon is $100 * \beta * N$. The reasons of using this method are:

  - With the preview information, the vehicle load profile trajectory over a short horizon (less than $10s$) is available.
  - The estimation errors increase as the prediction time horizon becomes longer.

  Thus, a time-varying prediction error which is dependent on the preview information of the load is proposed.

5.3.2 Simulation Results and Comparison

In this section, a more comprehensive comparative analysis of the aforementioned load prediction methods is presented. The objective is to understand the effects of load prediction error on the APMP-MPC fuel economy performance. For real-time energy management, the A-PMP algorithm developed in Chapter IV can be directly implemented. Based on our analysis in the previous Chapters, the performance of A-PMP is acceptable if the FCS dynamics is fast. If the FCS dynamics is slow, one

drawback, however, is that the A-PMP can only extract a sub-optimal solution since FCS dynamics is not included in the algorithm design process. A possible option to address the slow FCS dynamics is to implement the APMP-MPC algorithm. Though the improvement of using prescient APMP-MPC is as high as 5.95%, it cannot be used in real-time. Thus, we will implement the FT APMP-MPC, Exp APMP-MPC and the Preview APMP-MPC on the selected driving cycles and compare their performance with the prescient APMP-MPC to quantify the effects of the load prediction error.

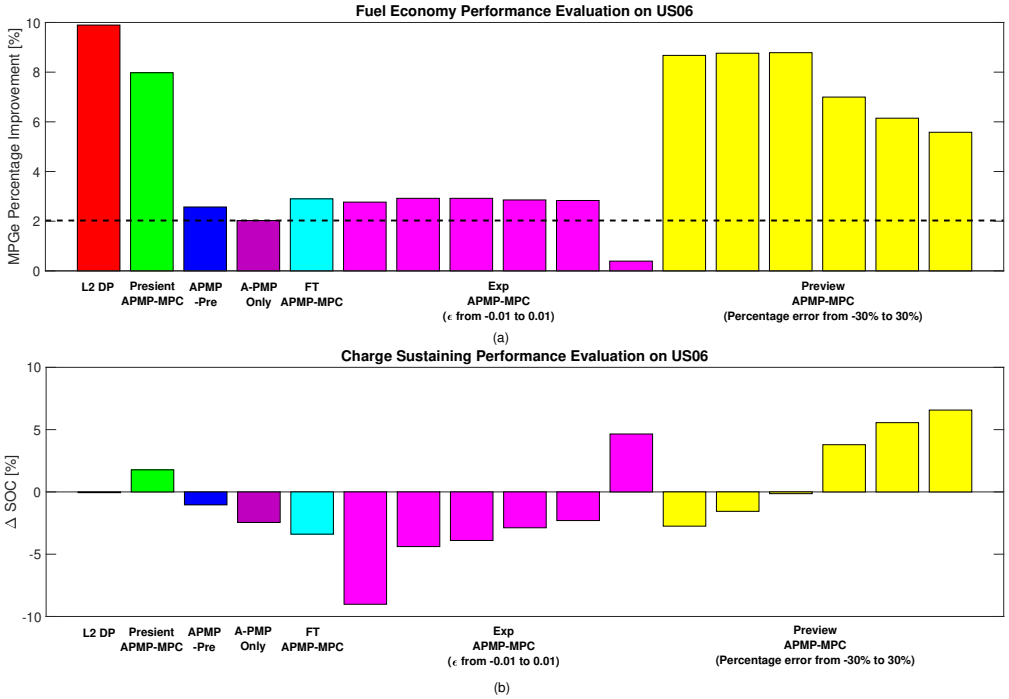

Figure 5.15: Performance evaluation on US06 driving cycle; (a) fuel economy performance (MPGe) of different algorithms comparing with rule-based algorithm (b) charge sustaining performance (ΔSOC) of different algorithms.

Fig. 5.15 and Fig. 5.16 provide the performance evaluation on US06 and UDDS driving cycles, respectively. For the US06 cycle shown in Fig. 5.15, the improvement is observed on almost all the prediction methods, even without any load preview. The FT APMP-MPC shows a 2.90% improvement over the rule-based algorithm. The Exp APMP-MPC shows a 2.92% improvement when ϵ equals -0.002 and the preview APMP-MPC shows a 8.76% improvement when the maximum percentage

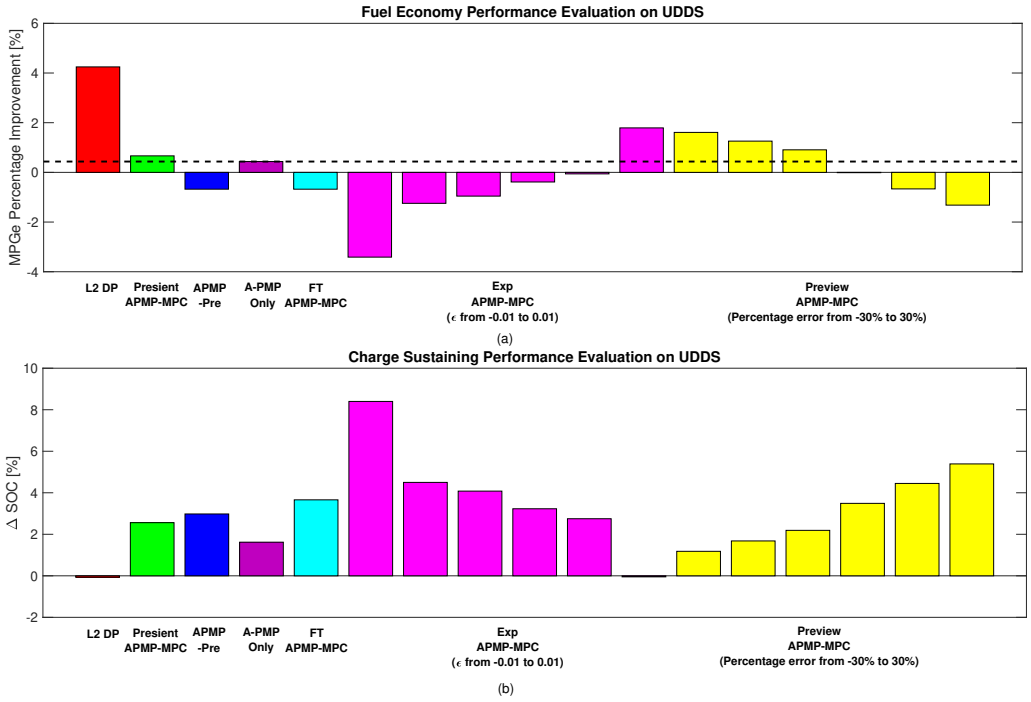

Figure 5.16: Performance evaluation on UDDS driving cycle; (a) fuel economy performance (MPGe) of different algorithms comparing with rule-based algorithm (b) charge sustaining performance (ΔSOC) of different algorithms.

error is -20%. However, the improvement for a city cycle like UDDS was decreased to less than 2% (Fig. 5.16). To better understand the simulation results, two metrics are used to assess the effects of load prediction error:

- Average root mean squared error (RMS error, m/s) of the predicted load over all of the control horizons.
- RMS error of the FCS output over the driving cycle comparing with Level 2 DP results.

The results are shown in Fig. 5.17(b) and (c), respectively. The MPGe percentage improvement of different APMP-MPC algorithms are shown in Fig. 5.17(a). The average RMS error of the predicted load provides a direct insights on how accurate the load predictor should be to have an affordable APMP-MPC algorithm. The results show that the magnitude of the RMS error is related to the performance degradation of fuel economy. The preview APMP-MPC results are a good reference. For city cycle like NYCC and UDDS, the RMS error needs to be less than $0.5kW$ in order to guarantee a good FE performance by using APMP-MPC algorithm. For more aggressive driving cycles like US06, the tolerance can be up to $1.1kW$. Further comparison is to view the RMS error of the FCS output trajectory. In the proposed APMP-MPC algorithm, three errors are combined to cause the FCS output trajectory error: the error of load predictor; the deviation of the A-PMP algorithm due to the estimation error of the co-state; the tracking error of the MPC because of the activation of constraints. Since all the errors are tangled together, the RMS error of the FCS output trajectory provides an baseline of a good APMP-MPC algorithm. For city cycle like NYCC and UDDS, the RMS error needs to be less than $1.2kW$ in order to guarantee a good FE performance by using APMP-MPC algorithm. For more aggressive driving cycles like US06, the tolerance can be up to $2.5kW$.

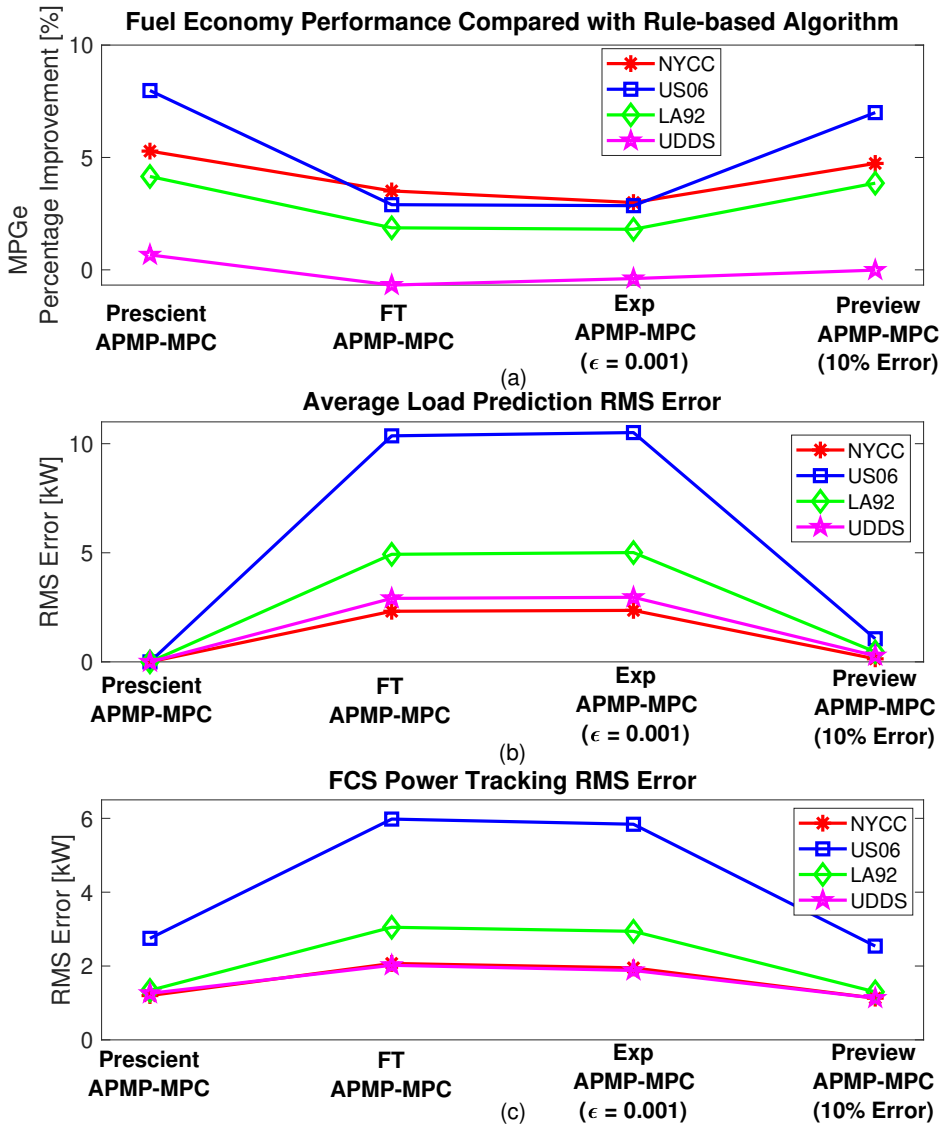

Figure 5.17: Effects of the load prediction error on fuel economy performance: (a)Fuel economy performance compared with rule-based algorithm, (b)average load prediction RMS error, (c) FCS power tracking RMS error. For Exp APMP-MPC, $\epsilon = 0.001$, for Preview APMP-MPC, maximum percentage error is 10%.

5.3.3 Effects of Implementing a Load Governor

One solution to improve the proposed APMP-MPC algorithm is to improve the performance of the load predictor by reducing the RMS prediction error. Additionally, one should also consider mechanisms that could reduce the effects of prediction error. In this subsection, such mechanisms are discussed. A load governor, which is simplified to a rate limiter is considered. To better understand the effects of imposing a load governor, the Level 1 DP is extended. There are two reasons to use DP in this study instead of A-PMP as the high level energy management algorithm. First, the proposed APMP-MPC estimates the co-state value online and includes an SOC governor to ensure charge sustaining performance. These two features are entangled with MPC algorithm as a feedback controller, where the co-state estimation error also affects the fuel economy, making it hard to separate from the load prediction error. Furthermore, designing an optimal A-PMP algorithm with load governor means to extend the system dynamics by adding another co-state value and is hard to guarantee the global optimal solutions. Thus, an extended Level 1 DP strategy is used as the reference trajectory for MPC, along with adding the same time varying percentage error to keep the evaluation consistent.

To impose a rate limiter into the Level 1 DP, the control input is modified. Instead of using the requested FCS power $P_{fc\_c}(k)$, as described in (2.3), the power command difference, which is defined as the changing rate of the power command, $\Delta P_{fc\_c}(k)$ is adopted. The state variable is further extended to two states, battery SOC and the FCS power command $P_{fc\_c}(k)$. Furthermore, one more equation needs to be added into the system dynamics:

$$P_{fc\_c}(k) = P_{fc\_c}(k-1) + \Delta P_{fc\_c}(k). \tag{5.22}$$

By modifying the minimum and maximum value of the new control input $\Delta P_{fc\_c}(k)$,

a rate limiter is imposed in the Level 1 DP formulation. The results are shown in Fig. 5.18 and Fig. 5.19. The fuel economy performance for UDDS driving cycle compared with Level 1 DP is presented in Fig. 5.20. When the rate limiter is set to $5kW/s$, the optimal fuel economy is very similar to that with no rate limiter. When the FE degradation tolerance is extended to 1.5%, the rate limiter can then be set to $1kW/s$.

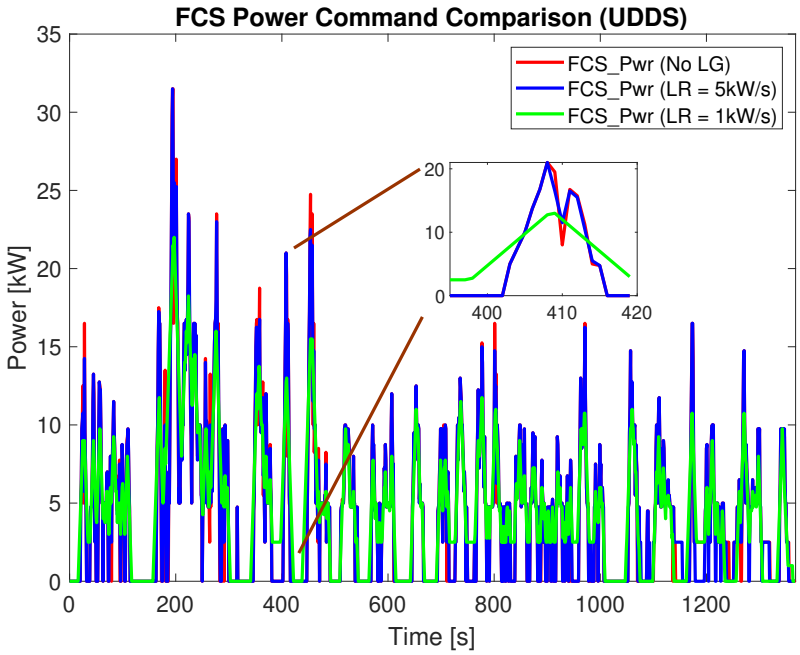

Figure 5.18: FCS output power trajectory comparison on different rate limitors for UDDS.

The effects of imposing a load governor are evaluated in the following process. The optimal Level 1 DP strategy with different rate limiter is implemented in the DP-MPC algorithm. The UDDS driving cycle is selected and the fuel economy performance is analyzed and shown in Fig. 5.21. Furthermore, the fuel economy results are compared with the optimal Level 1 DP results for each rate limiter. The sensitivity analysis is shown in Fig. 5.22. As can be seen, the drawbacks of having the load prediction errors can be mitigated by imposing a rate limiter. The MPGe degradation changes from 9% to 7% after implementing a rate limiter with the value set to be $1kW/s$.

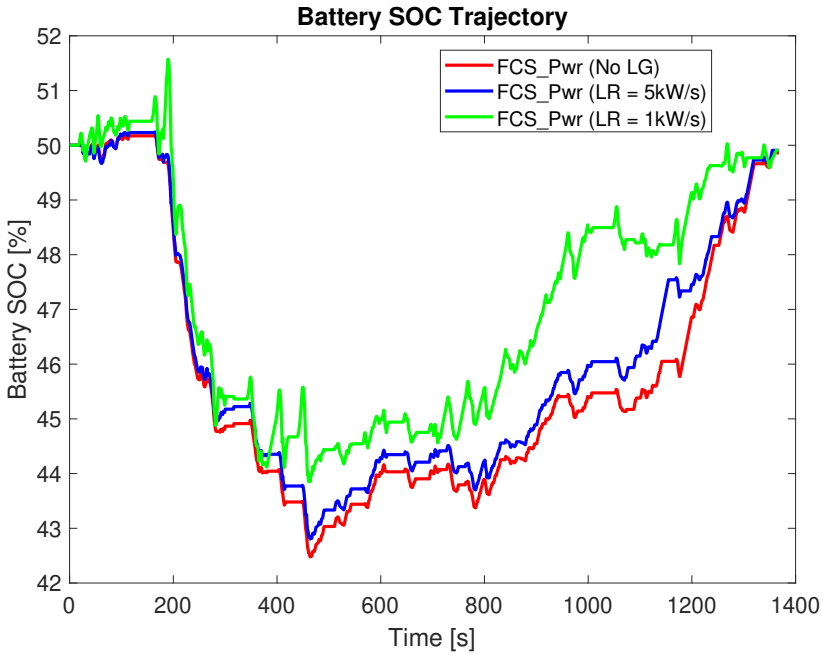

Figure 5.19: Battery SOC trajectory comparison on different rate limitor for UDDS.

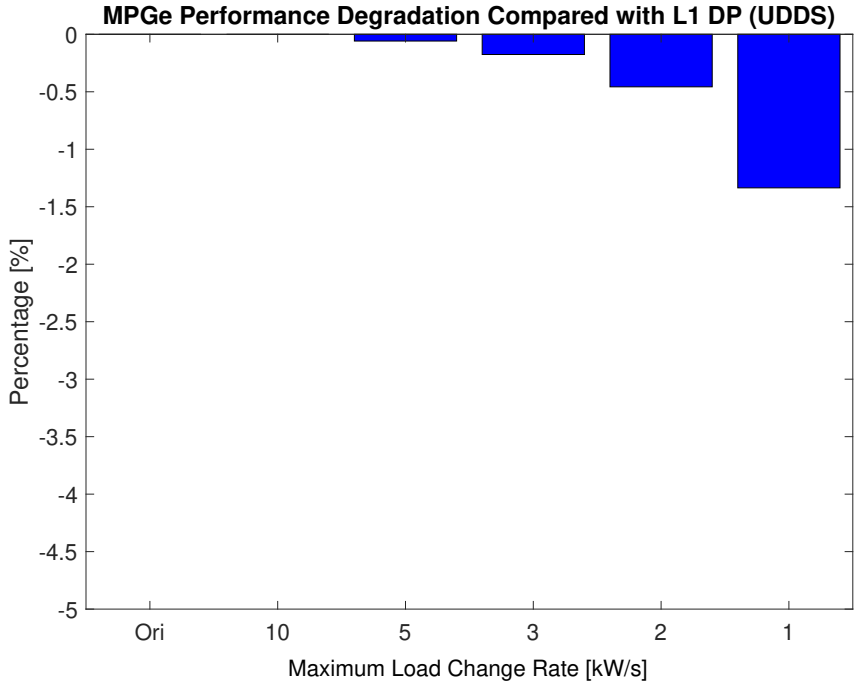

Figure 5.20: Fuel economy comparison on different rate limitor for UDDS.

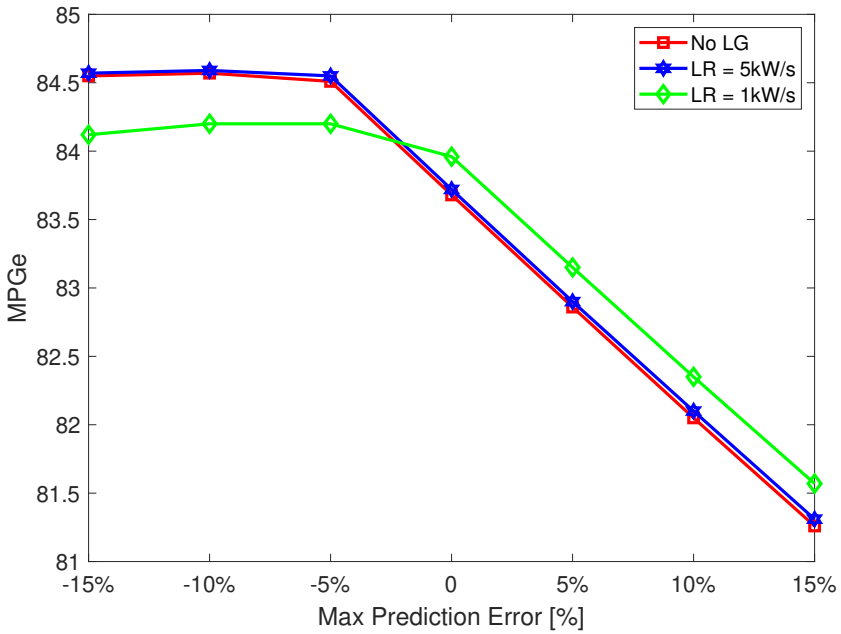

Figure 5.21: Fuel economy comparison using DP-MPC on different rate limitor for UDDS.

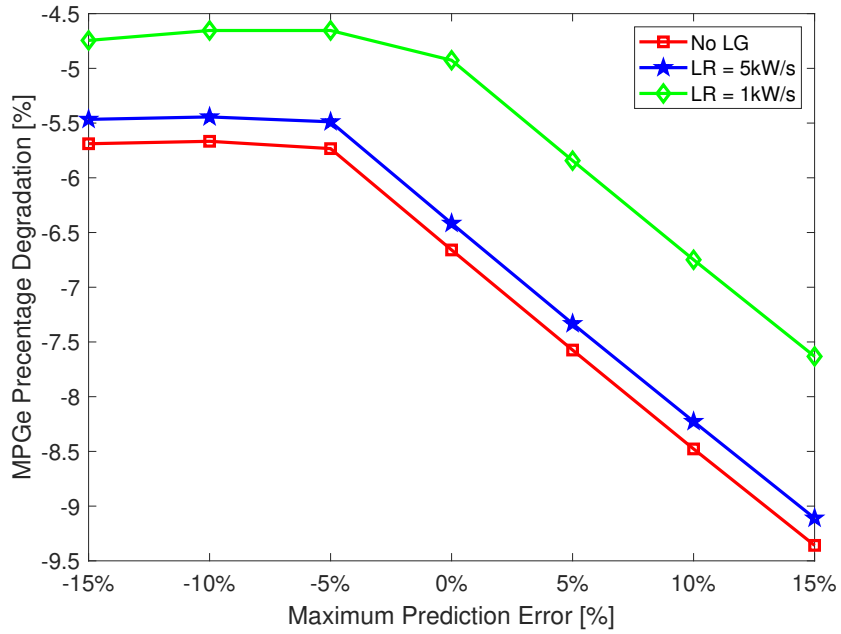

Figure 5.22: The effects of imposing a load governor to reduce the sensitivity of fuel economy on prediction error for UDDS driving cycle.

5.4 Conclusion

A real-time energy management algorithm, APMP-MPC, is proposed in this chapter to address the energy management problem while mitigating the effects of FCS transient power dynamics. The proposed algorithm shows potential improvements ranging from 0.23% to 5.95% on representative driving cycles with the assumption of prescient load information. Furthermore, a comparative study of four different load predictors for APMP-MPC based energy management in a FCV is presented. Results demonstrate that the simple FT-APMP-MPC can extract a better fuel economy on aggressive driving cycles, such as US06. To maintain the effectiveness of using the proposed APMP-MPC algorithm for FCVs energy management, the RMS prediction error has to be lower than $1.1kW$ throughout the entire driving cycle. The data-driven prediction methods need to by further developed to meet the criteria. From another point of view, the sensitivity of the prediction error on fuel economy can be attenuated by using a rate-limiter. This method can be considered as the second choice if a good prediction method is not available.

CHAPTER VI

Conclusions

6.1 Conclusions

In this thesis, a hierarchical control framework was presented for real-time energy management aiming at reducing the controller design and calibration effort for the FCVs powertrain controls. At the beginning, a systematic analysis framework was proposed to understand the dynamic effects of FCS on optimal energy management. Dynamic programming methods were used and two levels of DP approaches were adopted to derive optimal power split strategies. Level 1 DP ignored the FCS dynamics while Level 2 DP incorporated the FCS dynamics. Different evaluations were performed, such as evaluation of the linear filter time constant, zero-dynamics and model parameter variations. The results showed that substantial loss of performance could occur if the slow dynamics were not included in DP. The loss of fuel economy could be higher than 3% if the settling time of FCS power dynamics was more than $3s$, and the energy deficiency due to the nonminimum phase dynamics was higher than $2.5kJ$ for a unit step reference command.

Based on the analysis of the effects of FCS dynamics on optimal energy management, two real-time energy management strategies were developed and evaluated: A-PMP for fast FCS dynamics and APMP-MPC for slow FCS dynamics. By adopting the techniques from the optimal control, a modified Hamiltonian equation was

proposed and a novel adaption method was implemented to update the co-state in real-time, which brought the PMP method online. The A-PMP strategy only relied on the travel time as the trip information and can guarantee the charge sustaining performance. A representative powertrain model was built by adopting the configuration based on a Fusion Energi Hybrid Vehicle. The proposed A-PMP algorithm was implemented on both the simulation environment and the real workhorse vehicle. The numerical simulation on the simplified powertrain model successfully proved the effectiveness of the A-PMP strategy. The MPGe performance degradation was less than 1.7% compared with the optimal DP strategy for a $1.4hrs$ drive. The robustness of the strategy was also validated. The proposed algorithm was then further validated in a high fidelity powertrain. Numerical simulation showed improvements ranging from 1.1% to 7.0% with regen braking on representative driving cycles. Initial evaluations of the A-PMP on a testing vehicle was done. The HIL test and the vehicle test successfully proved the A-PMP could be implemented in real time. The validation results showed potential benefits of using the model-based optimization method on real-time energy management for FCVs.

To deal with the slow FCS dynamics, the hierarchical control framework, APMP-MPC strategies, was detailed and validated. The simulation results showed potential improvements ranging from 0.23% to 5.95% on representative driving cycles with assumption of prescient load information. The effects of load prediction error on the performance of APMP-MPC strategy were evaluated and analyzed. The conclusions showed that the leverage of FCV energy management was not as high as the other hybrid vehicles, such as HEVs and PHEVs. The prediction errors were critical to any predicted based energy management methods. For the proposed APMP-MPC structure, the RMS prediction error had to be less than $1.1kW$ over the entire driving cycle to render a better fuel economy.

6.2 Future Research Directions

The research presented in this thesis established potential work focusing on the collaborations of the vehicle level energy management design and the sub system controller design. It also leads to several proposed future research efforts:

6.2.1 Better Online Adaptation Methods for Co-state Variables

Although the proposed A-PMP showed the robustness on different driving cycles, the performance can be further improved if more advanced multi-parametric models will be explored to extract better co-state estimation. Furthermore, the online estimation of the optimal power split strategy should also have the ability to adapt to sudden change of the driving conditions to make the A-PMP more robust.

6.2.2 Robustness Validations on the Testing Vehicles

Further vehicle tests are required to evaluate the performance. The hierarchical APMP-MPC controller should also be tested in the HIL environment and implemented in the testing vehicle. Validation of the FCS dynamics models are important. Real-time system identification methods should be developed to assist the APMP-MPC in establishing robustness against the load prediction error and the model prediction error. The focus should be on maintaining the overall load prediction error at less than $1.1kW/s$ for the current powertrain, but all the analysis framework can be extended and adopted to different types of hybrid vehicles.

6.2.3 Advanced Load Prediction Methods Development

Data driven methods are not the focuses in our current research. However, combining the advanced data driven methods with the advantages of model-driven optimization may lead to the ultimate solution of the real-time energy management for HEVs. Model-based optimization will provide the structure and the essence of the

energy management, and more advanced load prediction methods will improve the robustness of the strategy.

6.2.4 Derivation of an Unified A-PMP Algorithm for HEV

A-PMP algorithm has already been proved to be effective in real-time energy management for FCVs. The methodology should also be implementable in traditional HEVs. An unified A-PMP algorithm suitable for different kinds of HEVs should be explored and validated.

BIBLIOGRAPHY

BIBLIOGRAPHY

[1] CC Chan. The state of the art of electric and hybrid vehicles. *Proceedings of the IEEE*, 90(2):247–275, 2002.

[2] Lorenzo Serrao, Simona Onori, and Giorgio Rizzoni. A comparative analysis of energy management strategies for hybrid electric vehicles. *Journal of Dynamic Systems, Measurement, and Control*, 133(3):031012, 2011.

[3] Alireza Khaligh and Zhihao Li. Battery, ultracapacitor, fuel cell, and hybrid energy storage systems for electric, hybrid electric, fuel cell, and plug-in hybrid electric vehicles: State of the art. *IEEE transactions on Vehicular Technology*, 59(6):2806–2814, 2010.

[4] Siang Fui Tie and Chee Wei Tan. A review of energy sources and energy management system in electric vehicles. *Renewable and Sustainable Energy Reviews*, 20:82–102, 2013.

[5] GJ Offer, D Howey, M Contestabile, R Clague, and NP Brandon. Comparative analysis of battery electric, hydrogen fuel cell and hybrid vehicles in a future sustainable road transport system. *Energy policy*, 38(1):24–29, 2010.

[6] Ching Chue Chan. The state of the art of electric, hybrid, and fuel cell vehicles. *Proceedings of the IEEE*, 95(4):704–718, 2007.

[7] James Larminie, Andrew Dicks, and Maurice S McDonald. *Fuel cell systems explained*, volume 2. J. Wiley Chichester, UK, 2003.

[8] Till Bunsen, Pierpaolo Cazzola, Marine Gorner, Leonardo Paoli, Sacha Scheffer, Renske Schuitmaker, Jacopo Tattini, and Jacob Teter. Global ev outlook 2018: Towards cross-modal electrification. 2018.

[9] California Air Resources Board Staff. Staff report: Initial statement of reasons advanced clean cars. Technical report, California Environmental Protection Agency, 2011.

[10] Paola Costamagna and Supramaniam Srinivasan. Quantum jumps in the pemfc science and technology from the 1960s to the year 2000: Part ii. engineering, technology development and application aspects. *Journal of power sources*, 102(1-2):253–269, 2001.

[11] MA Hannan, FA Azidin, and Azah Mohamed. Hybrid electric vehicles and their challenges: A review. *Renewable and Sustainable Energy Reviews*, 29:135–150, 2014.

[12] Chan-Chiao Lin, Soonil Jeon, Huei Peng, and Jang Moo Lee. Driving pattern recognition for control of hybrid electric trucks. *Vehicle System Dynamics*, 42(1-2):41–58, 2004.

[13] Sunita Satyapal. Hydrogen and fuel cell program overview. In *2018 Annual Merit Review, Fuel Cell Technology Program, Office of Energy Efficiency and Renewable Energy, US Department of Energy, Washington, DC*, 2018.

[14] Kai Wu, Ming Kuang, Milos Milacic, Xiaowu Zhang, and Jing Sun. Analysis of effects of fuel cell system dynamics on optimal energy management. In *ASME 2017 Dynamic Systems and Control Conference*, pages V003T43A001–V003T43A001. American Society of Mechanical Engineers, 2017.

[15] Jay Tawee Pukrushpan. *Modeling and control of fuel cell systems and fuel processors*. University of Michigan Ann Arbor, Michigan, USA, 2003.

[16] Suman Basu, Chao-Yang Wang, and Ken S Chen. Phase change in a polymer electrolyte fuel cell. *Journal of The Electrochemical Society*, 156(6):B748–B756, 2009.

[17] D Gerteisen, W Mérida, T Kurz, P Lupotto, M Schwager, and C Hebling. Spatially resolved voltage, current and electrochemical impedance spectroscopy measurements. *Fuel Cells*, 11(2):339–349, 2011.

[18] CZ Qin. *Numerical investigations on two-phase flow in polymer electrolyte fuel cells*. PhD thesis, UU Department of Earth Sciences, 2012.

[19] Meng Ni. Modeling of a planar solid oxide fuel cell based on proton-conducting electrolyte. *International Journal of energy research*, 34(12):1027–1041, 2010.

[20] Cheng Bao and Wolfgang G Bessler. Two-dimensional modeling of a polymer electrolyte membrane fuel cell with long flow channel. part i. model development. *Journal of Power Sources*, 275:922–934, 2015.

[21] T Berning and N Djilali. A 3d, multiphase, multicomponent model of the cathode and anode of a pem fuel cell. *Journal of the Electrochemical Society*, 150(12):A1589–A1598, 2003.

[22] Adam Z Weber and John Newman. Modeling transport in polymer-electrolyte fuel cells. *Chemical reviews*, 104(10):4679–4726, 2004.

[23] Dong Hao, Jianping Shen, Yongping Hou, Yi Zhou, and Hong Wang. An improved empirical fuel cell polarization curve model based on review analysis. *International Journal of Chemical Engineering*, 2016, 2016.

[24] Sabine Geiger-Gritsch, Bjoern Stollenwerk, Rebecca Miksad, Beate Guba, Claudia Wild, and Uwe Siebert. Safety of bevacizumab in patients with advanced cancer: a meta-analysis of randomized controlled trials. *The oncologist*, 15(11):1179–1191, 2010.

[25] S Fukuhara, Y Ait-Amirat, and M Becherif. Experimental validation of a pem fuel cell model.

[26] Jason B Siegel, Stanislav V Bohac, Anna G Stefanopoulou, and Serhat Yesilyurt. Nitrogen front evolution in purged polymer electrolyte membrane fuel cell with dead-ended anode. *Journal of the Electrochemical Society*, 157(7):B1081–B1093, 2010.

[27] Buz A McCain, Anna G Stefanopoulou, and Jason B Siegel. Controllability and observability analysis of the liquid water distribution inside the gas diffusion layer of a unit fuel cell model. *Journal of Dynamic Systems, Measurement, and Control*, 132(6):061303, 2010.

[28] Keith Promislow, Paul Chang, Herwig Haas, and Brian Wetton. Two-phase unit cell model for slow transients in polymer electrolyte membrane fuel cells. *Journal of The Electrochemical Society*, 155(7):A494–A504, 2008.

[29] SP Philipps and C Ziegler. Computationally efficient modeling of the dynamic behavior of a portable pem fuel cell stack. *Journal of Power Sources*, 180(1):309–321, 2008.

[30] Joshua Golbert and Daniel R Lewin. Model-based control of fuel cells::(1) regulatory control. *Journal of power sources*, 135(1-2):135–151, 2004.

[31] Faysal Tiss, Ridha Chouikh, and Amenallah Guizani. Dynamic modeling of a pem fuel cell with temperature effects. *International journal of hydrogen energy*, 38(20):8532–8541, 2013.

[32] Yaosuo Xue, Liuchen Chang, Sren Baekhj Kjaer, Josep Bordonau, and Toshihisa Shimizu. Topologies of single-phase inverters for small distributed power generators: an overview. *IEEE transactions on Power Electronics*, 19(5):1305–1314, 2004.

[33] Nashat Jalil, Naim A Kheir, and Mutasim Salman. A rule-based energy management strategy for a series hybrid vehicle. In *American Control Conference, 1997. Proceedings of the 1997*, volume 1, pages 689–693. IEEE, 1997.

[34] Mutasim Salman, Niels J Schouten, and Naim A Kheir. Control strategies for parallel hybrid vehicles. In *American Control Conference, 2000. Proceedings of the 2000*, volume 1, pages 524–528. IEEE, 2000.

[35] Antonio Sciarretta, Michael Back, and Lino Guzzella. Optimal control of parallel hybrid electric vehicles. *IEEE Transactions on control systems technology*, 12(3):352–364, 2004.

[36] Chan-Chiao Lin, Huei Peng, Jessy W Grizzle, and Jun-Mo Kang. Power management strategy for a parallel hybrid electric truck. *IEEE transactions on control systems technology*, 11(6):839–849, 2003.

[37] Dimitri P Bertsekas. *Dynamic programming and optimal control*, volume 1. Athena scientific Belmont, MA, 1995.

[38] Olle Sundström and Anna Stefanopoulou. Optimum battery size for fuel cell hybrid electric vehiclepart i. *Journal of fuel cell science and technology*, 4(2):167–175, 2007.

[39] Xiaowu Zhang, Chiao-Ting Li, Dongsuk Kum, and Huei Peng. Prius+ and volt-: Configuration analysis of power-split hybrid vehicles with a single planetary gear. *IEEE Transactions on Vehicular Technology*, 61(8):3544–3552, 2012.

[40] Min-Joong Kim and Huei Peng. Power management and design optimization of fuel cell/battery hybrid vehicles. *Journal of power sources*, 165(2):819–832, 2007.

[41] Thounthong Phatiphat, Stephane Rael, and Bernard Davat. Energy management of fuel cell/battery/supercapacitor hybrid power source for vehicle applications. *Journal of power sources*, 193(1):376–385, 2009.

[42] Sedghisigarchi Kourosh and Ali Feliachi. Dynamic and transient analysis of power distribution systems with fuel cells-part i: fuel-cell dynamic model. *IEEE transactions on energy conversion*, 19(2):423–428, 2004.

[43] Euh-Suh Koo, Hyeoun-Dong Lee, Seung-Ki Sul, and Joohn-Sheok Kim. Torque control strategy for a parallel hybrid vehicle using fuzzy logic. In *Industry Applications Conference, 1998. Thirty-Third IAS Annual Meeting. The 1998 IEEE*, volume 3, pages 1715–1720. IEEE, 1998.

[44] Niels J Schouten, Mutasim A Salman, and Naim A Kheir. Fuzzy logic control for parallel hybrid vehicles. *IEEE transactions on control systems technology*, 10(3):460–468, 2002.

[45] Namwook Kim, Sukwon Cha, and Huei Peng. Optimal control of hybrid electric vehicles based on pontryagin's minimum principle. *IEEE Transactions on Control Systems Technology*, 19(5):1279–1287, 2011.

[46] Jorge Moreno, Micah E Ortúzar, and Juan W Dixon. Energy-management system for a hybrid electric vehicle, using ultracapacitors and neural networks. *IEEE transactions on Industrial Electronics*, 53(2):614–623, 2006.

[47] Wei-Song Lin and Chen-Hong Zheng. Energy management of a fuel cell/ultracapacitor hybrid power system using an adaptive optimal-control method. *Journal of Power Sources*, 196(6):3280–3289, 2011.

[48] Rui Xiong, Jiayi Cao, and Quanqing Yu. Reinforcement learning-based real-time power management for hybrid energy storage system in the plug-in hybrid electric vehicle. *Applied Energy*, 211:538–548, 2018.

[49] Daniel F Opila, Xiaoyong Wang, Ryan McGee, and JW Grizzle. Real-time implementation and hardware testing of a hybrid vehicle energy management controller based on stochastic dynamic programming. *Journal of dynamic systems, measurement, and control*, 135(2):021002, 2013.

[50] Scott Jason Moura, Hosam K Fathy, Duncan S Callaway, and Jeffrey L Stein. A stochastic optimal control approach for power management in plug-in hybrid electric vehicles. *IEEE Transactions on control systems technology*, 19(3):545–555, 2011.

[51] Liangfei Xu, Minggao Ouyang, Jianqiu Li, Fuyuan Yang, Languang Lu, and Jianfeng Hua. Application of pontryagin's minimal principle to the energy management strategy of plugin fuel cell electric vehicles. *international journal of hydrogen energy*, 38(24):10104–10115, 2013.

[52] Cristian Musardo, Giorgio Rizzoni, Yann Guezennec, and Benedetto Staccia. A-ecms: An adaptive algorithm for hybrid electric vehicle energy management. *European Journal of Control*, 11(4-5):509–524, 2005.

[53] Pierluigi Pisu and Giorgio Rizzoni. A comparative study of supervisory control strategies for hybrid electric vehicles. *IEEE Transactions on Control Systems Technology*, 15(3):506–518, 2007.

[54] Chiao-Ting Li and Huei Peng. Optimal configuration design for hydraulic split hybrid vehicles. In *American Control Conference (ACC), 2010*, pages 5812–5817. IEEE, 2010.

[55] Lorenzo Serrao, Simona Onori, and Giorgio Rizzoni. Ecms as a realization of pontryagin's minimum principle for hev control. In *American Control Conference, 2009. ACC'09.*, pages 3964–3969. IEEE, 2009.

[56] Simona Onori and Lorenzo Serrao. On adaptive-ecms strategies for hybrid electric vehicles. In *Proceedings of the International Scientific Conference on Hybrid and Electric Vehicles, Malmaison, France*, pages 6–7, 2011.

[57] Lorenzo Serrao, Antonio Sciarretta, Olivier Grondin, Alexandre Chasse, Yann Creff, Domenico Di Domenico, Philippe Pognant-Gros, Carole Querel, and Laurent Thibault. Open issues in supervisory control of hybrid electric vehicles: A unified approach using optimal control methods. *Oil & Gas Science and Technology–Revue dIFP Energies nouvelles*, 68(1):23–33, 2013.

[58] Bo Gu and Giorgio Rizzoni. An adaptive algorithm for hybrid electric vehicle energy management based on driving pattern recognition. In *ASME 2006 International Mechanical Engineering Congress and Exposition*, pages 249–258. American Society of Mechanical Engineers, 2006.

[59] Ching Chuen Chan, Alain Bouscayrol, and Keyu Chen. Electric, hybrid, and fuel-cell vehicles: Architectures and modeling. *IEEE transactions on vehicular technology*, 59(2):589–598, 2010.

[60] N Sulaiman, MA Hannan, Azah Mohamed, EH Majlan, and WR Wan Daud. A review on energy management system for fuel cell hybrid electric vehicle: Issues and challenges. *Renewable and Sustainable Energy Reviews*, 52:802–814, 2015.

[61] Mehdi Ansarey, Masoud Shariat Panahi, Hussein Ziarati, and Mohammad Mahjoob. Optimal energy management in a dual-storage fuel-cell hybrid vehicle using multi-dimensional dynamic programming. *Journal of Power Sources*, 250:359–371, 2014.

[62] Jay T Pukrushpan, Anna G Stefanopoulou, and Huei Peng. Modeling and control for pem fuel cell stack system. In *Proceedings of the American Control Conference*, volume 4, pages 3117–3122, 2002.

[63] Gregory L Plett. Extended kalman filtering for battery management systems of lipb-based hev battery packs: Part 3. state and parameter estimation. *Journal of Power sources*, 134(2):277–292, 2004.

[64] Gray Tyler and Matthew Shirk. 2010 toyota prius vin 0462 hybrid electric vehicle battery test results. *The Idaho National Laboratory*, 2013.

[65] Simona Onori, Serrao Lorenzo, and Rizzoni Giorgio. *Hybrid electric vehicles: Energy management strategies*. Berlin Heidelberg: Springer, 2016.

[66] Manfred Morari and Zafiriou Evanghelos. *Robust process control*. Prentice Hall, 1989.

[67] Dimitri P Bertsekas, Dimitri P Bertsekas, Dimitri P Bertsekas, and Dimitri P Bertsekas. *Dynamic programming and optimal control*, volume 1. Athena scientific Belmont, MA, 2005.

[68] Zou Yuan, Liu Teng, Sun Fengchun, and Huei Peng. Comparative study of dynamic programming and pontryagins minimum principle on energy management for a parallel hybrid electric vehicle. *Energies*, 6(4):2305–2318, 2013.

[69] Namwook Kim and Aymeric Rousseau. Sufficient conditions of optimal control based on pontryagins minimum principle for use in hybrid electric vehicles. *Proceedings of the Institution of Mechanical Engineers, Part D: Journal of Automobile Engineering*, 226(9):1160–1170, 2012.

[70] Namwook Kim, Daeheung Lee, Suk Won Cha, and Huei Peng. Optimal control of a plug-in hybrid electric vehicle (phev) based on driving patterns. In *International battery, hybrid and fuel cell electric vehicle symposium*, pages 1–9, 2009.

[71] Martina Joševski and Dirk Abel. Multi-time scale model predictive control framework for energy management of hybrid electric vehicles. In *Decision and Control (CDC), 2014 IEEE 53rd Annual Conference on*, pages 2523–2528. IEEE, 2014.

[72] Chao Sun, Xiaosong Hu, Scott J Moura, and Fengchun Sun. Velocity predictors for predictive energy management in hybrid electric vehicles. *IEEE Trans. Contr. Sys. Techn.*, 23(3):1197–1204, 2015.

[73] Chao Sun, Scott Jason Moura, Xiaosong Hu, J Karl Hedrick, and Fengchun Sun. Dynamic traffic feedback data enabled energy management in plug-in hybrid electric vehicles. *IEEE Transactions on Control Systems Technology*, 23(3):1075–1086, 2015.

[74] Yanjun Huang, Hong Wang, Amir Khajepour, Hongwen He, and Jie Ji. Model predictive control power management strategies for hevs: A review. *Journal of Power Sources*, 341:91–106, 2017.

[75] Rui Wang and Srdjan M Lukic. Review of driving conditions prediction and driving style recognition based control algorithms for hybrid electric vehicles. In *Vehicle Power and Propulsion Conference (VPPC), 2011 IEEE*, pages 1–7. IEEE, 2011.

[76] Stefano Di Cairano, Daniele Bernardini, Alberto Bemporad, and Ilya V Kolmanovsky. Stochastic mpc with learning for driver-predictive vehicle control and its application to hev energy management. *IEEE Trans. Contr. Sys. Techn.*, 22(3):1018–1031, 2014.

[77] Harpreetsingh Banvait, Jianghai Hu, and Yaobin Chen. Energy management control of plug-in hybrid electric vehicle using hybrid dynamical systems. *IEEE Transactions on Intelligent Transportation Systems*, 2013.

[78] H Ali Borhan, Ardalan Vahidi, Anthony M Phillips, Ming L Kuang, and Ilya V Kolmanovsky. Predictive energy management of a power-split hybrid electric vehicle. In *American Control Conference, 2009. ACC'09.*, pages 3970–3976. IEEE, 2009.

[79] Yi Lu Murphey, Jungme Park, Zhihang Chen, Ming L Kuang, M Abul Masrur, and Anthony M Phillips. Intelligent hybrid vehicle power controlpart i: Machine learning of optimal vehicle power. *IEEE Transactions on Vehicular Technology*, 61(8):3519–3530, 2012.

[80] Pei Zhang, Fuwu Yan, and Changqing Du. A comprehensive analysis of energy management strategies for hybrid electric vehicles based on bibliometrics. *Renewable and Sustainable Energy Reviews*, 48:88–104, 2015.

[81] Y Zhang. *DIRECT algorithm and driving cycle recognition based optimization study for hybrid electric vehicle*. PhD thesis, Ph. D. Thesis, Dept. Mech. Eng., Beijing Inst. of Tech., Beijing, China, 2010.

[82] Thijs van Keulen, B De Jager, A Serrarens, and M Steinbuch. Optimal energy management in hybrid electric trucks using route information. *Oil & Gas Science and Technology–Revue de lInstitut Français du Pétrole*, 65(1):103–113, 2010.

[83] Mohd Azrin Mohd Zulkefli, Jianfeng Zheng, Zongxuan Sun, and Henry X Liu. Hybrid powertrain optimization with trajectory prediction based on inter-vehicle-communication and vehicle-infrastructure-integration. *Transportation Research Part C: Emerging Technologies*, 45:41–63, 2014.

[84] Abbas Fotouhi, Rubiyah Yusof, Rasoul Rahmani, Saad Mekhilef, and Neda Shateri. A review on the applications of driving data and traffic information for vehicles energy conservation. *Renewable and Sustainable Energy Reviews*, 37:822–833, 2014.